# CARBON BUDGETS IN COASTAL ESTUARIES OF THE NORTHWESTERN GULF OF MEXICO UNDER HYDROLOGIC CONTROL

A Dissertation

by

HONGMING YAO

BS, Hunan Agricultural University, 2010
MS, Ocean University of China, 2013

Submitted in Partial Fulfillment of the Requirements for the Degree of

DOCTOR of PHILOSOPHY

in

COASTAL & MARINE SYSTEM SCIENCE

Texas A&M University-Corpus Christi
Corpus Christi, Texas

August 2019

August 2019

# CARBON BUDGET IN COASTAL ESTUARIES OF THE NORTHWESTERN GULF OF MEXICO UNDER HYDROLOGIC CONTROL

A Dissertation

by

HONGMING YAO

This dissertation meets the standards for scope and quality of
Texas A&M University-Corpus Christi and is hereby approved.

Xinping Hu, PhD
Chair

Paul Montagna, PhD
Committee Member

Toshiaki Shinoda, PhD
Committee Member

Lei Jin, PhD
Committee Member

Zhanfei Liu, PhD
Committee Member

Philip Rhoades, PhD
Graduate Faculty Representative

August 2019

# ABSTRACT

Globally, estuaries are considered as important $CO_2$ sources to the atmosphere. However, previous studies on estuarine carbon fluxes have mostly focused on temperate and high latitude regions, leaving a significant knowledge gap in subtropical and tropical estuaries. In addition, the drivers that cause large spatiotemporal variability in estuarine inorganic and organic carbon fluxes remain insufficiently explored. In this dissertation, carbon budgets in four northwestern Gulf of Mexico (nwGOM) estuaries along a climatic gradient, Lavaca-Colorado Estuary (LCE), Guadalupe Estuary (GE), Mission-Aransas Estuary (MAE), and Nueces Estuary (NE), were evaluated. All these estuaries, with annual $CO_2$ emission ranging 2.7—35.9 $mol \cdot C \cdot m^{-2} \cdot y^{-1}$, are moderate to strong $CO_2$ sources. However, there was large spatiotemporal variability that corresponded to changes in hydrologic conditions. The two northern estuaries (LCE and GE), due to larger riverine discharges, had an order of magnitude higher $CO_2$ emissions than the southern estuaries (MAE and NE). In addition, episodic flooding made the entire regional $CO_2$ fluxes differ significantly under dry (-0.7—20.9 $mmol \cdot C \cdot m^{-2} \cdot d^{-1}$) and wet (11.6—170.0 $mmol \cdot C \cdot m^{-2} \cdot d^{-1}$) conditions. A mass balance model for carbon budget predicted lateral transport of total organic matter (TOC) and dissolved inorganic carbon (DIC) from tidal wetlands, which accounted for ~95% and 70% of total TOC and DIC inputs to the open estuarine water, respectively. However, the loss of coastal saltmarsh-mangrove habitats due to sea level rise could result in ~1% per year decline in estuarine $CO_2$ fluxes at the expense of decreasing lateral carbon transport. Finally, this dissertation suggested that the average estuarine $CO_2$ flux from nwGOM was about 8 times higher than previously estimated North America estuarine $CO_2$ flux. Additionally, flooding condition was estimated to elevate $CO_2$ emission and lateral fluxes by 10 times in this region.

# ACKNOWLEDGEMENTS

I would like to thank Texas A&M University-Corpus Christi (TAMU-CC), Harte Research Institute for Gulf of Mexico Studies at TAMU-CC, National Oceanic and Atmospheric Administration (NOAA) NOS National Center for Coastal Ocean Science (Contract No. NA15NOS4780185), National Science Foundation (OCE 1654232), Mission-Aransas National Estuarine Research Reserve (MANERR) from the Office Coastal Management, University of Texas Marine Science Institute, Texas Commission on Environmental Quality (TCEQ), Texas Water Development Board (TWDB) for their financial and research support.

Special thanks is given to my advisor, Dr. Xinping Hu, who spent an enormous amount of time guiding me from a student with almost no related background to now an independent writer that contributes to the scientific literature. Not only to my academic advancement, Dr. Hu is also very supportive to my personal life, as I am an international student who is far away from family and friends. I also appreciate all the support from my committee members, Drs. Paul Montagna, Zhanfei Liu, Lei Jin, Toshiaki Shinoda and Philip Rhoades. I have enjoyed every single field trip with Dr. Montagna's group. Similarly, I enjoyed the time getting along with Dr. Liu's lab members, both during fieldwork and while visiting their campus.

I appreciate all the great support from my lab mates and their friendship during my Ph.D. - Melissa McCutcheon, Cory Staryk, Hongjie Wang, Qiyuan Liu, Ouyang Zhangxian, Larissa Dias, and Corrie Clark. I enjoyed participating in all conferences with most of them along with Melissa, and countless number of field trips with Cory. Besides, I am deeply thankful to all the friends that I have met here, my Ph.D. life would have been much tougher without them.

TABLE OF CONTENTS

CONTENTS PAGE

ABSTRACT ..... v

ACKNOWLEDGEMENTS ..... vi

LIST OF TABLES ..... xi

LIST OF FIGURES ..... xii

CHAPTER I: INTRODUCTION ..... 1

1.1. The biogeochemical transition zone from land to ocean ..... 1

1.2. Carbon budget in estuarine systems ..... 2

1.3. Climatic change on estuarine systems ..... 3

References ..... 6

CHAPTER II: RESPONSES OF CARBONATE SYSTEM AND $CO_2$ FLUX TO EXTENDED DROUGHT AND INTENSE FLOODING IN A SEMIARID SUBTROPICAL ESTUARY ..... 10

2.1. Introduction ..... 11

2.2. Materials and methods ..... 13

2.2.1. Field sampling ..... 13

2.2.2. Chemical analyses ..... 15

2.2.3. Air-Water $CO_2$ flux calculation ..... 17

2.2.4. Thermal and non-thermal effects on $pCO_2$ variations ..... 19

2.2.5. Data analysis ..... 20

2.3. Results ..... 20

2.3.1. Hydrologic conditions....20
2.3.2. Carbonate chemistry....22
2.3.3. Air-water $CO_2$ flux....23
2.4. Discussion....24
2.4.1. DIC and TA dynamics during the dry-wet cycle....24
2.4.2. Controlling factors on the $pCO_{2,water}$ variations during the dry-wet cycle....27
2.4.3. Air-water $CO_2$ flux dynamics and controlling factors during the dry-wet cycle....29
2.5. Conclusions....31
References....33
CHAPTER III: HYDROLOGIC CONTROLS ON $CO_2$ CHEMISTRY AND FLUX IN SUBTROPICAL LAGOONAL ESTUARIES OF THE NORTHWESTERN GULF OF MEXICO....58
3.1. Introduction....60
3.2. Methods....61
3.2.1. Study sites....61
3.2.2. Chemical analyses....62
3.2.3. Air-Water $CO_2$ flux calculation....63
3.2.4. Statistical analysis....64
3.3. Results....65
3.3.1. River discharge....65
3.3.2. Salinity....65
3.3.3. Dissolved oxygen concentration....66
3.3.4. Estuarine carbonate system....66

3.3.5. Carbonate chemistry of river and ocean end-members....67
3.4. Discussion....68
3.4.1. DIC and TA variations under dry and wet conditions....68
3.4.2. River-borne, ocean-borne, and estuarine generated $CO_2$....72
3.4.3. Annual and seasonal $CO_2$ flux....75
3.5. Conclusions....78
References....79
CHAPTER IV: CARBON BUDGETS IN NORTHWESTERN GULF OF MEXICO COASTAL ESTUARIES: IMPLICATIONS FOR LATERAL TRANSPORT AND CHALLENGES OF FLOODING AND SEA LEVEL RISE....98
4.1. Introduction....99
4.2. Methods....101
4.2.1. Study sites....101
4.2.2. Field campaign and laboratory analyses....101
4.2.3. Carbon mass balance....102
4.2.4. River inflow....103
4.2.5. Atmospheric flux....103
4.2.6. Net ecosystem metabolism (NEM)....104
4.2.7. Burial....105
4.2.8. Export to the coastal ocean....105
4.2.9. Calcification....106
4.2.10. Lateral transport....106
4.3. Results....106

4.3.1. Carbon budgets ..... 106
4.3.2. River inflow ..... 106
4.3.3. Air-water $CO_2$ flux ..... 107
4.3.4. NEM ..... 107
4.3.5. Lateral transport ..... 108
4.3.6. Carbon burial in sediments ..... 108
4.3.7. Export to the coastal ocean ..... 108
4.3.8. Uncertainties ..... 109
4.4. Discussion ..... 109
4.4.1. Importance of lateral transport from tidal marshes and mangroves ..... 109
4.4.2. Hydrologic control on estuarine carbon budget ..... 112
4.4.3. Integrated carbon budget and future climate influence ..... 114
4.5. Implications ..... 116
References ..... 117
CHAPTER V: SUMMARY AND CONCLUSIONS ..... 136
APPENDICES ..... 139
Appendix 1. Estuarine air-water $CO_2$ fluxes along North America's Coast ..... 139
Appendix 2. Copyright of Chapter II ..... 141

LIST OF TABLES

TABLES PAGE

Table 2.1. Physical and chemical conditions of MAE during drought and flooding periods in MAE. D and F indicate drought and flooding period, respectively. ..... 42

Table 2.2. Temporal and spatial analysis of the carbonate system tested by two-way ANOVA. "√" denotes a significant main factor interaction between sampling time (i.e. drought-flooding cycle) and sampling location. ..... 43

Table 2.3. Salinity, DIC, and TA in the riverine and oceanic input endmembers. ..... 44

Table 2.4. Thermal vs non-thermal effects on $pCO_2$ variations in MAE. ..... 45

Table 2.5. Air-water $CO_2$ fluxes in different estuaries. ..... 46

Table 2.6. Estimated average air-water $CO_2$ flux ($mmol \cdot C \cdot m^{-2} \cdot d^{-1}$) distribution in the MAE..... 47

Table 3.1. Hydrologic and carbonate system parameters in four nwGOM estuaries (April 2014- February 2017). ..... 86

Table 3.2. Two-way ANOVA tests for different variables in estuarine hydrology and the carbonate system. The factors include hydrological conditions (wet vs. dry) and locations..... 87

Table 3.3. Estuarine parameters and carbonate system end-members for each estuary at dry (D) and wet (W) conditions. ..... 88

Table 3.4. Annual and seasonal air-water $CO_2$ fluxes in U.S. estuaries. ..... 89

Table 4.1. Hydrologic information in four nwGOM lagoons ..... 124

Table 4.2. Annual carbon fluxes in four nwGOM lagoons. (*Unit*: $mol \cdot C \cdot m^{-2} \cdot yr^{-1}$) ..... 125

Table 4.3. Estuarine carbonate system in different hydrologic periods. (*Unit*: $\mu mol \cdot kg^{-1}$ *for DIC*) ..... 126

Table 4.4. Lateral TOC and DIC transport from saltmarshes and mangroves ..... 127

LIST OF FIGURES

FIGURES PAGE

Figure 2.1. The map of the Mission-Aransas Estuary (MAE) and the five System Wide Monitoring Program stations. ..... 48

Figure 2.2. The difference between measured and calculated TA (from pH and DIC) and its relationship with salinity. ..... 49

Figure 2.3. Monthly freshwater discharges from two major rivers into the MAE from 05/2014 to 04/2015 (data source, USGS). ..... 50

Figure 2.4. Seasonal variations of temperature, dissolved oxygen, and salinity in the MAE. The gray and black lines indicate surface and bottom water conditions, respectively. ..... 51

Figure 2.5. Seasonal variations of pH (total scale), DIC, TA, $pCO_{2,water}$, and $\Omega_{ar}$ in MAE. The gray and black lines indicate surface and bottom water conditions, respectively, and the straight lines in the $pCO_2$ panels indicates $pCO_{2,air}$. ..... 52

Figure 2.6. Air-water $CO_2$ fluxes at the five stations and wind speed (location) from 05/2014 to 04/2015. ..... 53

Figure 2.7. DIC, TA vs. salinity during the drought period (05/2014-02/2015). The solid and dashed lines represent mixing lines between Aransas and Mission rivers and the Gulf of Mexico (GOM) coastal water, respectively, and the dotted line represents the evaporation line of the GOM coastal water. ..... 54

Figure 2.8. DIC, TA vs. salinity during the flooding period (03/2015-04/2015). The solid and dashed lines represent mixing lines between Aransas and Mission rivers and the Gulf of Mexico (GOM) coastal water, respectively, and the dotted line represents the evaporation line of the GOM coastal water. ..... 55

Figure 2.9. Seasonal variations of observed $pCO_{2,water}$ ($pCO_{2,obs}$), thermal $pCO_2$ ($pCO_{2,thermal}$), and non-thermal $pCO_2$ ($pCO_{2,non\text{-}thermal}$). The horizontal lines represent annual average values. . 56

Figure 2.10. TA/DIC ratio vs. salinity in the MAE. ..... 57

Figure 3.1. Map of sampling stations in the northwestern Gulf of Mexico estuaries and contributing rivers, "•"means estuary sampling stations; "▲" means river sampling stations; "×" means USGS monitoring gauges; "+" means NOAA monitoring stations. Estuary area is delineated with dashed lines on the map..... 90

Figure 3.2. River discharge (a) and air-water $CO_2$ flux (b) in studied estuaries, shaded area means stand deviation within 95% confidence. (units: $m^3 \cdot s^{-1}$ for river discharge, $mmol \cdot C \cdot m^{-2} \cdot d^{-1}$ for air-water $CO_2$ flux)..... 91

Figure 3.3. Average seasonal variations of carbonate system in studied estuaries, shaded area means standard deviation within 95% confidence. (units: $\mu mol \cdot kg^{-1}$ for DIC and TA, $\mu atm$ for $pCO_2$) ..... 92

Figure 3.4. DIC, TA and $CO_2$ flux variations during hydrologic changes, a. observed DIC in dry condition; b. observed TA in dry condition; c. calculated extra produced/consumed DIC by estuarine process in dry condition; d. calculated TA by estuarine process in dry condition; e. observed DIC in wet condition; f. observed TA in wet condition; g. calculated extra produced/consumed DIC by estuarine process in wet condition; h. calculated TA by estuarine process in wet condition; i. TA/DIC ratios in dry condition; j. TA/DIC ratios in wet conditions; k. air-water $CO_2$ flux in dry condition; l. air-water $CO_2$ flux in wet condition. Vertical dashed lines in panel a, c, e, g, i, k indicate for hypersalinity. (units: $\mu mol \cdot kg^{-1}$ for DIC, TA, $DIC_{estuarine}$, $TA_{estuarine}$, $mmol \cdot C \cdot m^{-2} \cdot d^{-1}$ for air-water $CO_2$ flux) ..... 93

Figure 3.5. ΔDIC vs. ΔTA in each estuary. Lines indicate different biogeochemical processes that will direct DIC and TA changes in fixed ratios (numbers in bracket indicate the ratios/slopes, Liu et al. 2017; Sippo et al. 2016). a. photosynthesis; b. hydrolysis; c. iron reduction; d. manganese reduction; e. calcium dissolution; f. sulfate reduction; g. denitrification; h. aerobic respiration; i. nitrification/sulfide oxidation; j. calcium precipitation; k. pure water dilution/evaporation. (unit: $\mu mol \cdot kg^{-1}$)..... 94

Figure 3.6. Area-weighted average categorized aqueous $CO_2$ concentrations ($[CO_2]_r$ ; $[CO_2]_o$ ; $[CO_2]_e$) in studied estuaries during sampling period. (unit: $\mu mol \cdot kg^{-1}$) ..... 95

Figure 3.7. Linearity between categorized $[CO_2]_x$ and air-water $CO_2$ flux in studied estuaries during hydrologic changes. D = dry condition, W = wet condition. (units: $\mu mol \cdot kg^{-1}$ for $[CO_2]_x$ ; $mmol \cdot C \cdot m^{-2} \cdot d^{-1}$ for air-water $CO_2$ flux)..... 96

Figure 3.8. Seasonality of air-water $CO_2$ flux and categorized $[CO_2]_x$ in studied estuaries. (units: $\mu mol \cdot kg^{-1}$ for $[CO_2]_x$ ; $mmol \cdot C \cdot m^{-2} \cdot d^{-1}$ for air-water $CO_2$ flux)..... 97

Figure 4.1. Sampling stations in northwestern GOM estuaries, a. estuary; b. river; c. sediment. ..... 128

Figure 4.3. Carbon fluxes (unit: $mmol \cdot C \cdot m^{-2} \cdot d^{-1}$) in four studied estuaries. a. riverine DIC inflows; b. lateral DIC inflows; c. averaged air-water $CO_2$ flux; d. riverine TOC inflows; e. lateral TOC inflows; f. averaged NEM. ..... 130

Figure 4.4. Correlations between different fluxes (unit: $mmol \cdot C \cdot m^{-2} \cdot d^{-1}$). a. lateral TOC vs. air-water $CO_2$ flux; b. lateral DIC vs. air-water $CO_2$ flux; c. lateral TOC vs. NEM; d. lateral DIC vs. NEM. ..... 131

Figure 4.5. Carbon fluxes (unit: $mmol \cdot C \cdot m^{-2} \cdot d^{-1}$) under different hydrologic conditions. The headings are D—drought; FR—flooding relaxation; F—flooding; H—hurricane..... 132

Figure 4.6. Estuarine air-water $CO_2$ fluxes (unit: $mol{\cdot}C{\cdot}m^{-2}{\cdot}yr^{-1}$, see more details in Appendix.1) in North America's coast. ..... 133

Figure 4.7. Carbon fluxes (unit: $mol{\cdot}C{\cdot}m^{-2}{\cdot}yr^{-1}$) from saltmarsh and mangrove, comparison between this study and other research (Borges et al. 2005; Bouillon et al. 2008; Sippo et al. 2016; Wang and Cai 2004; Wang et al. 2016)..... 134

Figure 4.8. Schematic representation of integrated carbon fluxes (unit: $mol{\cdot}C{\cdot}m^{-2}{\cdot}yr^{-1}$) in the nwGOM estuaries. (a) carbon fixation by saltmarshes and mangroves; (b) $CO_2$ evasion from saltmarshes and mangroves; (c) carbon sequestration within the saltmarsh and mangrove habitats; (d) lateral DIC transport; (e) lateral TOC transport; (f) riverine DIC; (g) riverine TOC; (h) air-water $CO_2$ flux; (i) pelagic and benthic mixed NEM; (j) organic carbon burial; (k) DIC export; (l) TOC export..... 135

# CHAPTER I: INTRODUCTION

## 1.1. The biogeochemical transition zone from land to ocean

Estuary is defined as a "semi-enclosed coastal body of water" within which seawater is diluted by freshwater derived from land drainage (Perillo 1995; Pritchard 1967). As the transitional region between the land and the ocean, the mixing between freshwater and seawater and subsequent biogeochemical reactions significantly influence estuarine biogeochemistry. For example, based on overall negative net ecosystem metabolism (NEM), community respiration surpasses gross primary production, indicating that estuarine systems are generally net heterotrophic. This heterotrophy is primarily driven by the respiration of riverine organic matter loading (Gattuso et al. 1998). On the other hand, maximum primary production in estuarine areas often occurs at intermediate salinities due to light and nutrients availability (Conley et al. 1995). Physical attributes including vertical stratification, longitudinal gradients, and water residence time can vary significantly among different estuaries. Estuaries, as extremely dynamic systems, are usually characterized by strong physicochemical gradients, enhanced biological activity, and intense sedimentation and resuspension (Gattuso et al. 1998). Such heterogeneity makes each estuary a unique and complex system of its own.

Lagoonal estuaries, i.e., the water body is separated from the coastal ocean by barrier island(s), account for 23% of the global estuarine area (Dürr et al. 2011). North America has 34% of lagoonal estuaries in the world, much greater than on other continents (Barnes 1980). These lagoonal estuaries are shallow (depth <5 m), and are influenced by freshwater input from upstream rivers or groundwater, open ocean tidal propagation, precipitation, and evaporation (Lécuyer et al. 2012; Stumpp et al. 2014). The Texas coast is located in the northwestern Gulf of Mexico (nwGOM) that has one of the world's largest subtropical lagoonal estuaries (Dürr et al.

2011). Distributed across a climatic gradient, these estuaries receive reduced freshwater inflow from northeast to southwest as a result of precipitation decrease and evaporation increase along with increasing temperature (Montagna et al. 2012). Thus, characterized by geomorphologic similarity yet climatic diversity, the nwGOM coastal area is ideal for studying climate change effects on estuarine carbon cycle.

1.2. Carbon budget in estuarine systems

Globally, it is estimated that estuaries receive 0.50±0.30 and 0.75±0.55 $Pg \cdot C \cdot yr^{-1}$ of inorganic and organic carbon combined from rivers and adjacent tidal wetland, and export 0.95±0.95 $Pg \cdot C \cdot yr^{-1}$ to continental shelves (Bauer et al. 2013). Overall the result of net heterotrophy suggests that 0.20±0.20 $Pg \cdot C \cdot yr^{-1}$ organic carbon would be respired/remineralized in estuaries (Bauer et al. 2013). Meanwhile, estuaries are viewed as places for carbon burial. The total organic carbon (TOC) burial in estuaries is about 0.10±0.05 $Pg \cdot C \cdot yr^{-1}$, which is nearly 20 times greater than carbon burial in the deep sea (Hopkinson et al. 2012). However, there is no consensus on carbon flux for global estuaries owing to various hydrologic and vegetation characteristics (Hopkinson et al. 2012).

Similar to the magnitude of heterotrophy, the global estuarine $CO_2$ emission is on the order of 0.10—0.25 $Pg \cdot C \cdot yr^{-1}$, which is on the same order of magnitude as continental shelf $CO_2$ uptake and is also equivalent to nearly 30% of riverine net total carbon input from the land (Bauer et al. 2013; Cai 2011; Laruelle et al. 2015; Zhai et al. 2007). However, the air-water $CO_2$ flux varies dramatically in global estuaries due to geomorphologic and climatic reasons. For example, Laruelle (2010) suggested that the global estuarine $CO_2$ flux range from 17.3±16.6 to 28.5±24.9 $mol \cdot m^{-2} \cdot yr^{-1}$ for lagoons and tidal embayments, respectively. Both are major global estuarine types. In addition, Chen (2013) suggested the lowest area-normalized $CO_2$ flux (~2.2

$mol \cdot m^{-2} \cdot yr^{-1}$) is from North American estuaries, the largest estuarine surface area on earth. Nevertheless, these large-scale data syntheses all suffer data gaps, signifying the importance of further studies on estuarine $CO_2$ flux studies.

1.3. Climatic change on estuarine systems

Coastal areas are the most vulnerable to climate change. The consensus in the scientific community is that changing climate will increase the risk of flooding, posing a great threat to the coastal areas (Hirabayashi et al. 2013; Milly et al. 2002; Mousavi et al. 2011). Estuarine hydrologic condition has received considerable attention in past decades because freshwater plays a fundamental role in estuarine functions. In riverine carbon fluxes to estuaries, DIC accounts for around 41%, and dissolved organic carbon (DOC) is about 22% (Meybeck 1993). Thus, estuarine metabolism is significantly influenced by riverine input. For example freshwater inflow can affect estuarine NEM by altering organic and inorganic load (Bianchi 2007; Montagna et al. 2002; Russell et al. 2006). Estuarine hydrology can have high spatial and temporal variability due to geomorphological and physical heterogeneity. With changing hydrologic conditions, riverine input plays a crucial but variable role in estuarine biogeochemistry (Sinha et al. 2017).

In addition to "regular" seasonal variations in river input, large scale weather event caused floods can increase estuarine $CO_2$ flux significantly as well. For example, a large flooding event in June 2011 increased water $pCO_2$ dramatically and switched the Mississippi Delta from a net $CO_2$ sink to source (Bianchi et al. 2013b). During Hurricane Joaquin in October 2015, stormy conditions elevated $CO_2$ fluxes by 8—15 times in New River Estuary (15.7 to 265.0 $mmol \cdot m^{-2} \cdot d^{-1}$) and Neuse River Estuary (7.7 to 62.0 $mmol \cdot m^{-2} \cdot d^{-1}$) in the North Carolina Coast (Van Dam et al. 2018). Given that riverine organic and inorganic carbon becomes more bioavailable in

flooding, enhanced heterotrophic activities and riverine $CO_2$ ventilation (Bianchi et al. 2013b; Borges et al. 2006) will be more conductive to $CO_2$ emission.

In general, the nwGOM is recognized as a region that would experience prolonged drought but punctuated by intense floods (Milliman et al. 2008; Montagna et al. 2012). First, previous long-lasting droughts prevented groundwater from being recharged, which placed an increased stress on its discharge to coastal areas (Hernandez and Uddameri 2014). On the other hand, flooding is equally serious as it can flush out the estuaries with freshwater and sometimes create freshwater lake conditions that maintain low salinity for a prolonged time, and these freshening events are caused by storm events and even hurricanes, for the latter eleven major hurricanes have made landfall along this coastline since 1950. In addition, under the periodical EI Nińo-Southern Oscillation influence, nwGOM estuaries receive extremely variable year-to-year inflows (Liu et al. 2019; Montagna et al. 2012). Beside hydrologic changes, measurable land subsidence and sea level rise have driven this area particularly vulnerable to high coastal surges based on model simulation (Mousavi et al. 2011). All these factors suggest that the nwGOM is one of the most dynamic regions that could be significantly affected by the climate change, and as a consequence, inorganic and organic carbon fluxes are probably subject to large variability in the long term. Therefore, research on carbon budget in nwGOM estuaries is needed to compare the magnitude of carbon fluxes in the context of global budget and identify the major contributing factor(s). Furthermore, due to an extreme range of hydrologic conditions from drought to flooding, examining estuarine carbon budgets under these conditions can improve our understanding of estuarine biogeochemistry, i.e. net ecosystem metabolism (NEM) and carbon fluxes, and explore possible changes in the context of climate change.

In this study, I investigated the air-water $CO_2$ fluxes and evaluated carbon budgets of different nwGOM estuaries that share geomorphological similarity but have hydrologic diversity. My research, with intensive field observations from 2014 to 2018, included an extreme hydrologic range from dry to complete flooding (i.e. hurricane). This study quantified nwGOM estuarine $CO_2$ fluxes and found moderate to strong $CO_2$ emission levels compared with other North American estuaries. I also found that hydrology exerted the primary control on inorganic and organic carbon processing. Estuarine $CO_2$ flux, in conjunction with riverine and internal biogeochemical processes, increased substantially under both hypersaline and flooding conditions. However, the overall autotrophy compensated flooding-driven $CO_2$ evasion during the flood relaxation period. My study also examined the contribution of tidal wetland (saltmarshes and mangroves) in nwGOM that led to large lateral inorganic and organic carbon transports that exceeded river input. Both lateral fluxes are important to maintain the high annual $CO_2$ emission and organic carbon burial in nwGOM estuaries.

References

Barnes, R. S. K. 1980. Coastal lagoons. Cambridge University Press.

Bauer, J. E., W. J. Cai, P. A. Raymond, T. S. Bianchi, C. S. Hopkinson, and P. A. Regnier. 2013. The changing carbon cycle of the coastal ocean. Nature **504:** 61-70.

Bianchi, T. S. 2007. Biogeochemistry of estuaries. Oxford University Press on Demand.

Bianchi, T. S. and others 2013. Enhanced transfer of terrestrially derived carbon to the atmosphere in a flooding event. Geophysical Research Letters **40:** 116-122.

Borges, A. V., L. S. Schiettecatte, G. Abril, B. Delille, and F. Gazeau. 2006. Carbon dioxide in European coastal waters. Estuarine, Coastal and Shelf Science **70:** 375-387.

Cai, W. J. 2011. Estuarine and coastal ocean carbon paradox: $CO_2$ sinks or sites of terrestrial carbon incineration? Annual review of marine science **3:** 123-145.

Chen, C. T. A., T. H. Huang, Y. C. Chen, Y. Bai, X. He, and Y. Kang. 2013. Air–sea exchanges of $CO_2$ in the world's coastal seas. Biogeosciences **10:** 6509-6544.

Conley, D. J., W. M. Smith, J. C. Cornwell, and T. R. Fisher. 1995. Transformation of particle-bound phosphorus at the land-sea interface. Estuarine, Coastal and Shelf Science **40:** 161-176.

Dürr, H. H., G. G. Laruelle, C. M. van Kempen, C. P. Slomp, M. Meybeck, and H. Middelkoop. 2011. Worldwide typology of nearshore coastal systems: Defining the estuarine filter of river inputs to the oceans. Estuaries and Coasts **34:** 441-458.

Gattuso, J.-P., M. Frankignoulle, and R. Wollast. 1998. Carbon and Carbonate Metabolism in Coastal Aquatic Ecosystems. Annual Review of Ecology and Systematics.

Hernandez, E. A., and V. Uddameri. 2014. Standardized precipitation evaporation index (SPEI)-based drought assessment in semi-arid south Texas. Environmental earth sciences **71:** 2491-2501.

Hirabayashi, Y. and others 2013. Global flood risk under climate change. Nature Climate Change **3:** 816–821.

Hopkinson, C. S., W.-J. Cai, and X. Hu. 2012. Carbon sequestration in wetland dominated coastal systems—a global sink of rapidly diminishing magnitude. Current Opinion in Environmental Sustainability **4:** 186-194.

Laruelle, G. G., H. H. Dürr, C. P. Slomp, and A. V. Borges. 2010. Evaluation of sinks and sources of $CO_2$ in the global coastal ocean using a spatially-explicit typology of estuaries and continental shelves. Geophysical Research Letters **37**.

Laruelle, G. G., R. Lauerwald, J. Rotschi, P. A. Raymond, J. Hartmann, and P. Regnier. 2015. Seasonal response of air–water $CO_2$ exchange along the land–ocean aquatic continuum of the northeast North American coast. Biogeosciences **12:** 1447-1458.

Lécuyer, C., A. M. Bodergat, F. Martineau, F. Fourel, K. Gürbüz, and A. Nazik. 2012. Water sources, mixing and evaporation in the Akyatan lagoon, Turkey. Estuarine, Coastal and Shelf Science **115:** 200-209.

Liu, N., C. Liu, and T. Lavigne. 2019. The Variation of the Intensity, Height, and Size of Precipitation Systems with El Niño–Southern Oscillation in the Tropics and Subtropics. Journal of Climate **32:** 4281-4297.

Meybeck, M. 1993. C, N, P and S in rivers: from sources to global inputs, p. 163-193. Interactions of C, N, P and S Biogeochemical cycles and global change. Springer.

Milliman, J. D., K. L. Farnsworth, P. D. Jones, K. H. Xu, and L. C. Smith. 2008. Climatic and anthropogenic factors affecting river discharge to the global ocean, 1951–2000. Global and Planetary Change **62:** 187-194.

Milly, P. C. D., R. T. Wetherald, K. Dunne, and T. L. Delworth. 2002. Increasing risk of great floods in a changing climate. Nature **415:** 514.

Montagna, P., T. A. Palmer, and J. Pollack. 2012. Hydrological Changes and Estuarine Dynamics Springer Science & Business Media.

Montagna, P. A., M. Alber, P. Doering, and M. S. Connor. 2002. Freshwater inflow: science, policy, management. Estuaries **25:** 1243-1245.

Mousavi, M. E., J. L. Irish, A. E. Frey, F. Olivera, and B. L. Edge. 2011. Global warming and hurricanes: the potential impact of hurricane intensification and sea level rise on coastal flooding. Climatic Change **104:** 575-597.

Perillo, G. M. 1995. Definitions and geomorphologic classifications of estuaries. Developments in Sedimentology **53:** 17-47.

Pritchard, D. W. 1967. What is an estuary: physical viewpoint. American Association for the Advancement of Science.

Russell, M. J., P. A. Montagna, and R. D. Kalke. 2006. The effect of freshwater inflow on net ecosystem metabolism in Lavaca Bay, Texas. Estuarine, Coastal and Shelf Science **68:** 231-244.

Sinha, E., A. Michalak, and V. Balaji. 2017. Eutrophication will increase during the 21st century as a result of precipitation changes. Science **357:** 405-408.

Stumpp, C., A. Ekdal, I. E. Gönenc, and P. Maloszewski. 2014. Hydrological dynamics of water sources in a Mediterranean lagoon. Hydrology and Earth System Sciences **18:** 4825-4837.

Van Dam, B. R., J. R. Crosswell, and H. W. Paerl. 2018. Flood-driven $CO_2$ emissions from adjacent North Carolina estuaries during Hurricane Joaquin (2015). Marine Chemistry **207:** 1-12.

Zhai, W., M. Dai, and X. Guo. 2007. Carbonate system and $CO_2$ degassing fluxes in the inner estuary of Changjiang (Yangtze) River, China. Marine Chemistry **107:** 342-356.

# CHAPTER II: RESPONSES OF CARBONATE SYSTEM AND $CO_2$ FLUX TO EXTENDED DROUGHT AND INTENSE FLOODING IN A SEMIARID SUBTROPICAL ESTUARY


## Abstract

Globally, estuaries are considered important $CO_2$ sources to the atmosphere. However, estuarine water carbonate chemistry and $CO_2$ flux studies have focused on temperate and high latitude regions, leaving a significant data gap in subtropical estuaries. This study examined water column carbonate system and air-water $CO_2$ flux in the Mission-Aransas Estuary (MAE), a subtropical semiarid estuary in the northwestern Gulf of Mexico (GOM), by collecting samples at five System Wide Monitoring Program stations from 05/2014 to 04/2015. The carbonate system parameters (total alkalinity - TA, dissolved inorganic carbon - DIC, pH, $CO_2$ partial pressure - $pCO_2$, and carbonate saturation state with respect to aragonite - $\Omega_{Ar}$) and air-water $CO_2$ flux all displayed substantial seasonal and spatial variations. Based on freshwater inflow conditions, a drought period occurred between 05/2014 and 02/2015, while a flooding period occurred from 03/2015 to 04/2015. Average DIC was 2194.7±156.8 and 2132.5±256.8 $\mu mol \cdot kg^{-1}$, TA was 2497.6±172.1 and 2333.4±283.1 $\mu mol \cdot kg^{-1}$, $pCO_2$ was 477±94 and 529±251 µatm, and $CO_2$ flux was 28.3±18.0 $mmol \cdot C \cdot m^{-2} \cdot d^{-1}$ and 51.6±83.9 $mmol \cdot C \cdot m^{-2} \cdot d^{-1}$ in the drought and flooding period, respectively. Integrated annual air-water $CO_2$ flux during our studied period was estimated to be 12.4±3.3 $mol \cdot C \cdot m^{-2} \cdot y^{-1}$, indicating that this estuary was a net $CO_2$ source. High wind speed, warm climate, riverine input, and estuarine biogeochemical processes all contributed to the high $CO_2$ efflux despite the modest $pCO_2$ levels year round.

## 2.1. Introduction

Human activities have significantly increased atmospheric $CO_2$ concentration since the Industrial Revolution. Although occupying a small area (~0.3%) of the global ocean , estuaries play a disproportionately important role in the global $CO_2$ budget (Bauer et al. 2013). In general, estuaries are a net $CO_2$ source due to net heterotrophy. For example, Frankignoulle (1998) suggested that $CO_2$ efflux from European estuaries represents 5%-10% of anthropogenic $CO_2$ emissions throughout Europe. Global estuarine $CO_2$ emissions could reach an approximate rate of 0.1-0.25 $Pg \cdot C \cdot yr^{-1}$, which is on the same order of magnitude as continental shelf $CO_2$ uptake and equivalent to as much as 30% of total riverine carbon export (Bauer et al. 2013; Cai 2011; Chen et al. 2013; Laruelle et al. 2015; Regnier et al. 2013b; Zhai et al. 2007). Large $CO_2$ release from estuaries could be attributed to hydrologic conditions (i.e., due to higher dissolved inorganic carbon to alkalinity ratio in river waters than the receiving seawater) and intensive biological activities. For example, Joesoef et al. (2015) found that more $CO_2$ is released into the atmosphere in the upper Delaware estuary than the lower estuary, and Guo et al. (2009) reported that $CO_2$ flux in the Pear River Estuary is dominated by aerobic remineralization of organic matter.

There are many uncertainties in estimating $CO_2$ flux in an estuary. A major reason for such uncertainty is temporal variation of riverine fluxes (Abril et al. 2004; Crosswell et al. 2014) that are not easily captured in estuarine studies, which tend to have low temporal sampling resolution. On the other hand, despite that lagoonal estuaries are generally recognized as important $CO_2$ sources particularly in tropical and temperate areas (Laruelle et al. 2010), whether the existing global estimate in those studied areas can represent all estuarine types is unknown given the drastically different hydrologic conditions of these estuaries. As one of the world's largest

subtropical lagoonal estuary systems (Dürr et al. 2011), the northwestern Gulf of Mexico (GOM) estuaries lack data for studying the $CO_2$ source/sink issue. Located in a semiarid subtropical region, south Texas has been experiencing prolonged drought with intense flooding occurring intermittently, thus estuaries in this area receive generally low riverine inflows, punctuated by large storms (Milliman et al. 2008; Mooney and McClelland 2012).How the changing hydrologic state alters $CO_2$ flux and its magnitude is unclear.

In an estuary, carbonate system parameters are usually controlled by mixing and biogeochemical processes. An estuary that receives variable nutrient and organic matter input from a river will have altered metabolic processes, which will affect the carbonate system (Doney et al. 2009; Feely et al. 2010). For example, in the Chwaka Bay of Tanzania, due to the presence of seagrass, pH increases and total dissolved inorganic carbon (DIC) decreases through enhanced photosynthesis and calcification (Semesi et al. 2009); while in the Long Island Sound, significant pH reduction could occur when enhanced respiration in subsurface water is coupled with $CO_2$ production (Wallace et al. 2014). In estuaries with significant freshwater influence, carbonate saturation state with respect to aragonite ($\Omega_{Ar}$) is strongly correlated with salinity. For example, in Glacier Bay in the eastern Gulf of Alaska, low total alkalinity (TA) concentration, resulting from glacier discharge, decreases $\Omega_{Ar}$ substantially to below aragonite undersaturation (Reisdorph and Mathis 2014). The carbonate system parameters in high latitude estuaries have large fluctuations due to significant seasonal changes in freshwater flux, nutrient delivery, and light intensity (Cross et al. 2013; Reisdorph and Mathis 2014). Even in a single estuary, carbonate system parameters could change quickly because of varying riverine input and strength of biological activities, as well as weather conditions (Mooney and McClelland 2012).

In this study, we characterized carbonate chemistry and $CO_2$ flux in the Mission-Aransas Estuary (MAE). Our primary goals were to understand how the carbonate system in MAE responded to freshwater input, and to study the air-water $CO_2$ flux in this estuary and understand its control(s).

## 2.2. Materials and methods

### 2.2.1. Field sampling

MAE is a shallow lagoonal estuary located along the south Texas coast (Fig. 2.1). It consists of three connected water bodies: Aransas Bay is a defined as a primary bay and is connected to the Gulf of Mexico (GOM) via the Aransas ship channel; Copano and Mesquite are secondary bays closer to riverine input (Kim and Montagna 2012). Copano Bay receives freshwater inflows directly from the Mission and Aransas Rivers, the two major freshwater sources for the entire estuary. Mesquite Bay receives inflow from adjacent San Antonio Bay during flooding periods.

Five long-term System Wide Monitoring Program (SWMP) stations were established in the MAE by the Mission-Aransas National Estuarine Research Reserve (MA-NERR) in 2007 (Fig. 2.1, https://sites.cns.utexas.edu/manerr). The SWMP program is a nationally coordinated and standardized program and is used for tracking short-term variability and long-term changes in a host of biological, physical, and chemical parameters. The five stations were designed to represent key estuarine conditions that range from freshwater inflow (station CW in Fig. 2.1) to hydrologic connection between the estuary and the GOM (SC; Evans et al. 2015). Water depths at these sampling stations ranged from 1.2 m (MB) to 6.2 m (SC).

Surface and bottom water samples were taken by a Van Dorn water sampler during the 05/2014 – 04/2015 period following the standard protocol for ocean $CO_2$ studies (Dickson et al. 2007). From 11/2014 to 03/2015, samples were taken monthly, and sampling occurred biweekly

during the warmer months in the rest of our sampling year. All field samplings were done between 9:00 AM and 2:00 PM. Briefly, 250 mL narrow-neck borosilicate glass bottles were used to collect water samples for TA, DIC, and pH analyses. 100 µL of saturated $HgCl_2$ was added to the water sample to arrest biological activity. The samples were stored at 4°C in the dark until analysis, usually within 2-3 weeks of sample collection. 125 mL polypropylene bottles were used to collect $Ca^{2+}$ samples. In the study by Bockmon (2014), filtration for coastal water carbonate system characterization was recommended. However, we did not find significant difference between filtered and unfiltered samples in this estuary (also see Hu et al. 2015), thus we used unfiltered samples for this study. A calibrated YSI 6600 V2 data sonde was used to obtain *in situ* temperature, pressure, and dissolved oxygen (DO) concentration at each station.

To examine the effect of freshwater inflow on the estuarine carbonate system, we imported daily discharge data from the United States Geological Survey (USGS) real-time stream flow record (http://waterdata.usgs.gov/tx/nwis/rt) that located at the river mouth of Mission (USGS #08189500) and Aransas Rivers (USGS #08189700), then calculated monthly riverine discharge. Wind speed and barometric pressure were obtained every 30 minutes from the weather station at Copano East (CE) (http://lighthouse.tamucc.edu/pq), and daily mean wind speed was applied to sampling days. Wind speed data collected from the weather station (3 m) was converted to 10 m above the water surface using the wind profile power law,

$$\frac{U_1}{U_2} = \left(\frac{z_1}{z_2}\right)^P \qquad (1)$$

here $u_2$ is the wind speed at height $z_2$ = 10 m, $u_1$ is the collected wind speed data at height $z_1$ = 3 m, the exponent P (0.11) around GOM area is extracted by Hsu et al. (P = 0.11; 1994).

2.2.2. Chemical analyses

All water samples were analyzed for DIC, TA, pH, and salinity. $Ca^{2+}$ was analyzed for surface water only. For DIC analysis, 0.5 mL water sample was acidified by 0.5 mL 10% $H_3PO_4$ using a 2.5 mL syringe pump. The released $CO_2$ was analyzed on an AS-C3 DIC analyzer (Apollo SciTech). To analyze TA, 25 mL water sample was titrated with a 0.1 M HCl solution (in 0.5 M NaCl) using an AS-ALK2 alkalinity titrator (Apollo SciTech). Temperature of the titration vessel was maintained at 22±0.1°C using a water-jacketed circulation system. Certified Reference Material (Dickson et al. 2003) was used to construct the standard curve for the DIC analysis and to calibrate the acid used for TA titration. DIC and TA analyses had a precision of ±0.1%.

A spectrophotometric method (Carter et al. 2013) using purified m-cresol purple (mCP) obtained from Dr. Robert Byrne's lab (University of South Florida) was used for pH analysis on total scale (Liu et al. 2011). The indicator was adjusted to pH 7.92±0.01 every time before sample analysis with the aid of a calibrated Orion™ Ross™ glass electrode. A 10-cm water-jacketed absorbance cell used for pH measurements (Carter et al. 2013) was kept at 25±0.01°C. The dye effect was corrected via duplicate runs of each sample by adding two volumes (30 µL and 60 µL) of mCP following the procedure in Clayton and Byrne (1993). This method had a precision of ±0.0004 pH unit. Because of salinity limitations of the spectrophotometric method (20-40, Liu et al., 2011), for lower salinity samples we used the calibrated pH electrode to measure pH at 25˚C. All pH values obtained using the potentiometric method were converted to total scale using temperature and salinity (Millero 2001).

Salinity was measured using a benchtop salinometer (Orion Star™ A12, Thermo Scientific), which was calibrated using MilliQ water and known salinity CRM seawater each time before

sample analysis. The salinomter was also regularly calibrated with 0.5 M KCl at 25°C. $Ca^{2+}$ concentration was determined by potentiometric titration (Kanamori and Ikegami 1980) using EGTA as the titrant. The end-point was detected using a Metrohm® calcium-selective electrode on a semi-automated titration system. This method had a precision of ±0.5% for estuarine waters.

Water $pCO_2$ and $\Omega_{ar}$ at field conditions were calculated using the program CO2SYS (Lewis et al. 1998) based on DIC and lab measured pH. We used measured pH and DIC as input variables instead of the pH/TA combination to calculate $pCO_{2,water}$ to avoid possible errors that were resulted from organic alkalinity component (Abril et al. 2015). In fact, we found that the difference between titration alkalinity and calculated alkalinity (with pH and DIC) showed strong salinity dependence in the MAE (Fig. 2.2). Although calculated $pCO_{2,water}$ was subject to some degree of uncertainty, previous studies showed an 1:1 linear relationship between measured and calculated $pCO_{2,water}$ over a range of 300 to 4000 µatm in estuarine and coastal waters (Frankignoulle and Borges 2001).

Calculated $\Omega_{ar}$ from CO2SYS output was corrected using measured $Ca^{2+}$ concentration, which was a near perfect linear function of salinity throughout the year ($r^2 = 0.99$, data not shown). Carbonic acid dissociation constants (K1, $K_2$) in Millero (2010), bisulfate dissociation constant in Dickson (1990) were used in this calculation. In the MAE (http://missionaransas.org/science/download-data), the soluble reactive phosphorous concentration was on the order of ~ 2.0 µmol $kg^{-1}$ or less, and silicate concentration was on the order of ~ 200 µmol $kg^{-1}$. The effect of nutrients on calculated $\Omega_{ar}$ and $pCO_2$ was minimal. For example, $pCO_2$ would only differ by 0.2 µatm with or without nutrients in the CO2SYS program. Because not all water samples that were characterized for carbonate chemistry had concurrent nutrient information, nutrients were omitted in all carbonate speciation calculations.

2.2.3. Air-Water $CO_2$ flux calculation

The air-water flux of $CO_2$ was calculated using the following equation:

$$F = kK_0(pCO_{2,water} - pCO_{2,air}) \quad (2)$$

where k ($m \cdot d^{-1}$) is the gas transfer velocity calculated from wind speed, $K_0$ ($mol \cdot m^{-3} \cdot atm^{-1}$) is the gas solubility at measured *in situ* temperature and salinity (Weiss 1974), $pCO_{2,water}$ and $pCO_{2,air}$ are partial pressure of $CO_2$ in surface water and the atmosphere, respectively. Positive F value means $CO_2$ degassing to the atmosphere. $pCO_{2,air}$ can be calculated from:

$$pCO_{2,air} = xCO_{2,air} \times (P_b - P_w) \quad (3)$$

Here $P_b$ (atm) is the barometric pressure, which was downloaded from the weather station at Copano East (CE), $P_w$ (atm) is the water vapor pressure calculated using salinity and temperature (Weiss and Price 1980), and $xCO_{2,air}$ (ppm) is the mole fraction atmospheric $CO_2$ in dry air. We did not measure air $xCO_2$ directly but chose to download monthly averaged $xCO_2$ data from http://www.esrl.noaa.gov/gmd/ccgg/trends. We recognized the spatial difference in $xCO_2$ on the global scale. However, compared to the $xCO_2$ data from a coastal $CO_2$ monitoring site in eastern GOM (https://www.pmel.noaa.gov/co2/story/Coastal+MS), monthly average $xCO_2$ is no more than 15 ppm greater in the GOM than the Mauna Loa site in winter and the two $xCO_2$ records generally agree with each other to within ±2 ppm in summer. Therefore the subsequently calculated $CO_2$ flux would differ by a few percent using either $xCO_2$ record (or the actual $xCO_2$ at MAE). Given that the GOM site does not have a continuous dataset, we elected the Mauna Loa data for our calculation.

Gas transfer velocity (k) would differ depending on wind speed, tidal current, and bottom topography (Raymond and Cole 2001; Wanninkhof 1992). Unfortunately, there is no widely accepted k formulation in shallow estuary regions, and the carbon cycle community still has to

rely on wind speed dependence to estimate gas exchange rates. Because the equation in Raymond and Cole (2001) was mainly based on relatively low wind speed (<7 $m \cdot s^{-1}$) estuarine data, here we used the equation in Jiang et al. (2008), which covered larger amount of high wind speed data (up to 12 $m \cdot s^{-1}$) and was more appropriate to our studied area:

$$k = (0.314 \cdot U^2 - 0.436 \cdot U + 3.99) \times (Sc_{SST}/600)^{-0.5} \quad (4)$$

where $U$ is the wind speed at 10-m height ($m \cdot s^{-1}$), $Sc_{SST}$ indicates Schmidt number of $CO_2$ at the *in situ* temperature from the freshwater (flooding period) and seawater (drought period) equations, respectively (Wanninkhof 1992). This equation has also been adopted in recent estuarine studies (Bozec et al. 2012; Crosswell et al. 2012).

The total surface area of Aransas and Copano bays is 452 $km^2$ based on Texas Water Development Board (TWDB) record. Aransas Bay occupies 181 $km^2$ with estimated 10% of its area in the Aransas Ship Channel where the station SC is located, and Copano Bay is 271 $km^2$. There is no published record on the area of Mesquite Bay. We estimated its area using a closet rectangle on Google Earth® and calculated its area as 75 $km^2$. Due to relatively limited sampling stations, we decided to use area-weighted average method to calculate $CO_2$ flux in the MAE instead of taking arithmetic mean of the individual stations. Our results showed that the difference between these two methods for each trip was 2.5±7.0 $mmol \cdot C \cdot m^{-2} \cdot d^{-1}$, and integrated annual $CO_2$ flux is 12.4 $mol \cdot C \cdot m^{-2} \cdot y^{-1}$, compared with 11.4 $mol \cdot C \cdot m^{-2} \cdot y^{-1}$ using the arithmetic mean. We first calculated area-weighted $CO_2$ flux using $CO_2$ flux values at the five sampling stations and the respective areas above. Then to estimate seasonally (drought and flooding periods) or annually averaged $CO_2$ flux, we used the following equation:

$$F_{avg} = \frac{\sum F_i \times d_i}{\sum d_i} \quad (5)$$

$F_{avg}$ is area-weighted $CO_2$ flux and has a unit of mmol·C ·$m^{-2}$·$d^{-1}$ or mol·C ·$m^{-2}$·$y^{-1}$, $F_i$ is air-water $CO_2$ flux of each sampling trip, $d_i$ indicates days in between two consecutive trips. Note in our $CO_2$ flux calculations we did not consider diel effect. Given that our sampling always took place during the middle of the day (9:00 AM - 2:00 PM) when $pCO_2$ was likely the lowest due to photosynthesis, calculated fluxes may represent lower estimates of the actual values (Baumann et al. 2014).

2.2.4. Thermal and non-thermal effects on $pCO_2$ variations

Thermal and non-thermal effects on $pCO_{2,water}$ variations were evaluated using the method in Takahashi et al. (Eqaution 5 to 9; 2002). To remove the temperature effect, we normalized $pCO_{2,water}$ to annual mean temperature of 23.0°C ($T_{mean}$, Eq. 6). In surface seawater $pCO_2$ doubles for every 16°C increase in the oceanic waters ($\partial \ln pCO_2/\partial T = 0.0423$; Takahashi et al. 1993). However, the average $\partial \ln pCO_2/\partial T$ of MAE water was calculated to be slightly lower (0.0411±0.0068) than open ocean water. To evaluate the effect of temperature change on $pCO_2$, we used Eq. (7).

$$pCO_{2,non-thermal} = pCO_{2,obs} \times \exp[\delta \times (T_{mean} - T_{obs})] \quad (6)$$

$$pCO_{2,thermal} = pCO_{2,mean} \times \exp[\delta \times (T_{obs} - T_{mean})] \quad (7)$$

where δ is $\partial \ln pCO_2/\partial T$, subscripts *mean* and *obs* stand for annual mean and observed values, respectively.

To understand relative contributions of thermal and non-thermal effects on temporal $pCO_2$ changes, we applied the following equations:

$$\Delta pCO_{2,\mathrm{thermal}} = \mathrm{Max}\left(pCO_{2,\mathrm{thermal}}\right) - \mathrm{Min}\left(pCO_{2,\mathrm{thermal}}\right) \quad (8)$$

$$\Delta pCO_{2,\mathrm{non-thermal}} = \mathrm{Max}\left(pCO_{2,\mathrm{non-thermal}}\right) - \mathrm{Min}\left(pCO_{2,\mathrm{non-thermal}}\right) \quad (9)$$

$$T/B = \Delta pCO_{2,\mathrm{thermal}}/\Delta pCO_{2,\mathrm{non-thermal}} \quad (10)$$

Both $\Delta pCO_{2,thermal}$ and $\Delta pCO_{2,non\text{-}thermal}$ were calculated from the difference between the maximum and the minimum $pCO_2$ effects during either the drought or the flooding period. The T/B ratio illustrated the relative importance of thermal vs. non-thermal effects. In MAE, non-thermal effect indicated the combination of biogeochemical processes and physical mixing. Thermal effect on surface $pCO_{2,water}$ would exceed non-thermal if T/B ratio was greater than 1; conversely, non-thermal effect would dominate if T/B ratio was less than 1.

2.2.5. Data analysis

A two-factor analysis of variance (ANOVA) was used to test the effects of hydrologic condition and sampling locations on carbonate variables and $CO_2$ fluxes. Probabilities (P) of $<0.05$ were considered as significant. Normality and homogeneity of variance were ensured before ANOVA was conducted and there was no need to transform the data.

2.3. Results

2.3.1. Hydrologic conditions

During our sampling year, the drought period (05/2014-02/2015, 18 trips in total) was much longer than the flooding period (03/2015-04/2015, 4 trips in total; Fig. 2.3). Annual discharge for Mission River was $8.29 \times 10^7$ $m^3 \cdot y^{-1}$ while discharge for Aransas River was $1.88 \times 10^7$ $m^3 \cdot y^{-1}$. Aransas River had more discharge during the drought period (07/2014-02/2015), in which the month with the least discharge was recorded in August 2014 for Aransas and Mission Rivers ($97.40 \times 10^3$ and 0 $m^3$ $month^{-1}$, respectively). However, Mission River had more freshwater input during the flooding period (03/2015-04/2015). The MAE was affected by two strong storms in late 03/2015 and 04/2015 (Fig. 2.3). During this period, Mission River discharge was almost twice as much as Aransas River. The highest discharge from Aransas River (51.25 $m^3 \cdot s^{-1}$) was

recorded in 03/2015 and discharge from Mission River was the highest (118.93 $m^3 \cdot s^{-1}$) in 04/2015.

The average values of all physical and chemical parameters for the five stations during the drought and the flooding periods are listed on Table 2.1 and Fig. 2.4. The average water temperature during our study period was 23.0±6.3°C (N=216), with the highest temperature (average 29.3±0.7°C; N=20) observed in 08/2014 and the lowest (average 10.0±1.0°C; N=10) in 01/2015. High temperatures (>25°C) lasted from mid-spring to fall (05/2014 – 10/2014), a period much longer than low temperature conditions (<15°C, 11/2014, 01/2015 – early 03/2015). Temperature fluctuated between 15 and 25°C for the remainder of the sampling period (12/2014, late 03/2015 – 04/2015).

During the entire sampling period, average DO concentration was 212.5±33.7 $\mu mol \cdot kg^{-1}$ (N=216, Fig. 2.4). Higher DO concentrations occurred during cold months (11/2014 ~ 02/2015). Slight DO stratification occurred in Copano Bay (CW and CE) mostly in spring and summer. In particular, there was a sharp decrease in DO (from 249.8 to 70.4 $\mu mol \cdot kg^{-1}$) in CW bottom waters after the first storm event in late 03/2015.

Average salinity was 33.0±5.4 (N=216, Fig. 2.4) during our sampling period. During the drought period there was a gradient from lowest salinity (33.6±2.2, SC; N=35) in the lower primary bay to highest salinity (36.9±2.4, CW; N=36) in the upper secondary bays. Hypersaline conditions (S>36.4) occurred at all five stations from 06/2014-09/2014, and persisted particularly long at CW (late 06/2014-01/2015). In early 09/2014, the average salinity of the entire estuary was 38.7±0.8 (N=9), which was the highest during our study period. On the contrary, during the flooding period, there was a salinity gradient (surface and bottom average) across the estuary from the lowest (18.9±10.4, CW; N=8) to the highest (29.0±3.2, SC; N=8). Salinity stratification

was only observed in Copano Bay. Salinity decreased sharply at CW after the flood (from 30.1 to 5.1 for surface water).

2.3.2. Carbonate chemistry

All carbonate system parameters displayed significant spatial (station) and temporal differences (between the drought and flooding periods) with two-way ANOVA p values <0.001 for all cases (Table 2.2). Average pH in MAE was 8.017±0.096 (N=216) with relatively small seasonal and spatial variations than many estuarine studies to date. Nevertheless, pH was generally lower (average 7.983±0.064; N=49) when the temperature was high from late 07/2014 to 09/2014, during hypersaline conditions . Higher pH values (average 8.114±0.046; N=50) were observed at low temperature conditions from 11/2014 to early 03/2015, although pH decreased when the estuary switched from the drought to the flooding period, and a very sharp decline of pH at CW (Δ=-0.536 pH units) occurred right after the late 03/2015 storm event.

Annual DIC concentration averaged at 2183.2±180.4 $\mu mol \cdot kg^{-1}$ (N=216, Fig. 2.5). Average DIC concentration was 2194.7±156.8 $\mu mol \cdot kg^{-1}$ (N=176) during the drought period, and was lower from summer to early fall (2106.8±100.6 $\mu mol \cdot kg^{-1}$, 06/2014-10/2014; N=109) but higher in winter (2230.6±96.0 $\mu mol \cdot kg^{-1}$, 11/2014-02/2015; N=40). CW had the highest DIC concentration and SC had the lowest in drought condition. DIC concentrations during the flooding period (with an average of 2132.5±256.8 $\mu mol \cdot kg^{-1}$; N=40) were lower than the drought period. There was a large decrease in the surface waters at CW after the first storm event in late 03/2015 with DIC concentrations decreasing from 2239.4 (prior to the storm) to 1227.3 $\mu mol \cdot kg^{-1}$ (after the storm). During the flooding period, MB had the highest DIC concentration, CW the lowest. Along with salinity stratification in Copano Bay during the flooding period, DIC concentration was lower in surface waters than the bottom water.

TA followed a temporal pattern similar to DIC (Fig. 2.5). Average TA concentration was 2467.2±206.7 μmol·kg$^{-1}$ (N=216) across the five stations during the entire sampling period. Average TA concentration was 2497.6±172.1 μmol·kg$^{-1}$ (N=176) and 2333.4±283.1 μmol·kg$^{-1}$ (N=40) during the drought and the flooding period, respectively.

For the entire estuary, average $pCO_{2,water}$ was 487±138 μatm (N=216, Fig. 2.5). It was 477±94 μatm (N=176) during the drought period, and 529±251 μatm (N=40) during the flooding period. During the drought period, the highest average $pCO_{2,water}$ occurred at CE (542±105 μatm, N=36) and lowest at SC (423±70 μatm, N=35). During the flooding period, $pCO_{2,water}$ in most stations increased, and CW had the highest average $pCO_{2,water}$, and SC had the lowest. At the same time, calculated $pCO_{2,air}$ in MAE area during our study period averaged at 391±6 μatm using observed monthly $xCO_{2,air}$ at the Mauna Loa site.

Annual average $\Omega_{ar}$ was 3.2±0.7 in the MAE (N=216; Fig. 2.5). Average $\Omega_{ar}$ first increased (Δ=0.7) and then decreased (Δ=-1.4) in drought season, with both the highest (3.8±0.9 at CW, N=36) and lowest (2.9±0.3 at CE, N=36) average $\Omega_{ar}$ values observed in Copano Bay. Average $\Omega_{ar}$ decreased significantly during the transition from the drought period (average 3.3±0.6; N=176) to the flooding period (average 2.4±0.7; N=40). During the latter period, SC had the highest $\Omega_{ar}$ (2.9±0.2, N=8) value and CW had the lowest (1.5±0.8, N=8).

2.3.3. Air-water $CO_2$ flux

Average wind speed in the MAE was 6.2±2.6 m·s$^{-1}$ (N=17520, Fig. 2.6) during our sampled period. The highest average (9.7±0.9 m·s$^{-1}$; N=48) was observed in 08/2014 and lowest (2.1±0.8 m·s$^{-1}$; N=48) was observed in 01/2015. During our study period, higher wind speed was recorded in summer (06/2014-08/2014, average 7.1±2.3 m·s$^{-1}$; N=288) and winter had relatively lower wind speed (12/2014-02/2015, average 3.4±1.6 m·s$^{-1}$; N=143).

Overall, annual average air-water $CO_2$ flux was 12.4±3.3 $mol \cdot C \cdot m^{-2} \cdot y^{-1}$ (N=110, Fig. 2.6), and the entire estuary released $CO_2$ during most of our sampled period. Further, the air-water $CO_2$ flux pattern displayed significant seasonal and spatial variations ($p < 0.05$ tested by two-way ANOVA; Fig. 2.6). Throughout the drought period, air-water $CO_2$ flux varied between -13.5±7.6 and 109.4±71.3 $mmol \cdot C \cdot m^{-2} \cdot d^{-1}$ (02/2015 and 08/2014, respectively; N=5 for each average value). The estuary was a $CO_2$ source in the drought period during warm months (05/2014-10/2014) and was a sink during cold months (11/2014-02/2015). Moreover, there was an overall increase in $CO_2$ efflux from the drought to the flooding period mostly due to large increase of $CO_2$ emission at CW. In particular, there was a 100-fold increase (from 3.4 to 380.3 $mmol \cdot C \cdot m^{-2} \cdot d^{-1}$) at CW in late 03/2015 right after the first storm event.

## 2.4. Discussion

### 2.4.1. DIC and TA dynamics during the dry-wet cycle

Many Texas rivers have high levels of bicarbonate ion ($HCO_3^-$) as a result of high weathering rates of the drainage basins (Zeng et al. 2011) and generally high evaporation rates in the area (http://www.twdb.texas.gov/surfacewater/conditions/evaporation/). To unravel the factors that contributed to estuarine DIC and TA variations, we used the water chemistry data to construct two-endmember mixing diagrams for DIC and TA in the MAE during the drought and flooding periods, respectively (Figs. 2.7 and 2.8); we also investigated the effect of precipitation and evaporation. Note for the river endmembers, we did not take river endmember during the 2014-2015 boat trips. Since we did not have concurrent river chemistry data during our estuarine sampling period, to best estimate the river chemistry during the flooding and drought conditions, we collected river samples at Mission and Aransas rivers bimonthly between December 2015

and December 2016 (Table 2.3). Six trips were conducted during a drought period, and one trip was conducted at the end of May 2016 after significant flooding in south Texas.

As discussed in Hu et al. (2015), along a river-ocean mixing line, the lowest solute to salinity ratio (i.e., the slope of the evaporation line) would be at the ocean endmember if there were no reactions that consumed this solute. Clearly, all the data points to the right of the dotted line (i.e. the precipitation-evaporation line for seawater endmember, Fig. 2.7) during the drought period reflected net removal of DIC (panels a, b, and c) and TA (panels d, e, and f), and the Copano Bay stations (CE and CW) also showed larger extent of DIC and TA consumption under hypersaline conditions (panels a and d). Furthermore, because the Mission River had higher DIC and TA concentrations than the Aransas River (Table 2.3), the mixing line between the Mission River (the dashed line in Fig. 2.7) and the ocean water endmember (values in Table 2.3) should have a slightly steeper slope than that between the Aransas River and the ocean endmember (the solid line in Fig. 2.7). Therefore, all the data points that are bracketed by the river-ocean mixing lines and the left of the precipitation-evaporation line (to the lower of the plot) also indicated removal.

Normally in an estuarine mixing zone, data points that appear above a mixing line would indicate *in situ* production as many estuarine studies have indicated (Raymond et al. 2000). However, for lagoonal estuaries with prolonged residence time under drought conditions (Montagna et al. 2012), significant evaporation could increase solute concentration and salinity simultaneously based on the original river-ocean mixing line (see Hu et al. 2015 for a detailed discussion). Therefore, it is likely that evaporation may have played an important role in the water chemistry during the drought period (Fig. 2.7a&d). Our results could not rule out *in situ* production of DIC and TA in Copano Bay, although as one moves to Aransas Bay, consumption clearly dominated DIC and TA changes (Fig. 2.7b&e).

In the literature, alkalinity reduction has not been commonly reported in coastal estuaries (other than in coral reefs). Instead, alkalinity production due to net anaerobic reactions (pyrite burial and net denitrification) is often suggested as an important process (Dollar et al. 1991; Hu and Cai 2011; Smith et al. 1991). Alkalinity consumption due to calcification clearly is a possible mechanism as the MAE has abundant oyster reefs, representing the southernmost location for viable commercial production (Pollack et al. 2012). While not directly observed in the MAE, sulfate concentration in the adjacent Corpus Christi Bay immediately to the south of the MAE appeared to show excess relative to a conservative mixing during the drought period (D. Murgulet, personal comm.), indicating possible external reduced sulfur contribution that was oxidized to sulfuric acid. In addition, Benoit et al. (1994) also observed high levels suspended matter that contains Fe in San Antonio Bay and Corpus Christi Bay, both of which 'bracket' the MAE. It is known that oxidation of reduced sulfur and iron would produce $H^+$ that titrates TA (Chen 2002). Given the shallow depth of the MAE and windy conditions in this area, significant benthic contribution (i.e., reoxidation of reduced sedimentary compounds) is likely, especially during high wind conditions that could cause abundant sediment resuspension. More detailed studies, such as examining sulfur and metal dynamics under different hydrologic conditions, are needed.

During the flooding period, DIC and TA concentrations in the river endmembers decreased (Table 2.3) presumably due to the dilution effect. Apparently, it became more difficult to explain the DIC and TA variations using the simple mixing lines derived from the local rivers. However, a closer examination of the CW station data suggested that both surface (TA and DIC) and bottom waters (TA only) showed excellent mixing behavior while DIC in the bottom water showed slight respiration signal during the 2-month floodwater-dominated period. For example,

intercepts of TA-salinity regressions were 1207 μmol $kg^{-1}$ ($r^2$ = 0.95) for surface and 1449 μmol $kg^{-1}$ ($r^2$ = 0.99) for bottom water respectively; those of DIC-salinity regressions were 1123 μmol $kg^{-1}$ ($r^2$ = 0.98) for surface and 1374 μmol $kg^{-1}$ ($r^2$ = 0.89) for bottom water, respectively (Fig. 2.8a and d, regression lines not shown). Therefore, the stagnant endmember values (Table 2.3) were likely not accurate during the high freshwater inflow season, and the different regression intercepts between the surface and bottom waters may reflect changing freshwater endmember compositions (Cifuentes et al. 1990). Furthermore, Mesquite Bay (MB) (surface and bottom) and the Aransas Bay (bottom) showed "excess" DIC and TA compared to the river mixing line (Fig. 2.8b, c, e, and f). This was likely caused by overflow of high alkalinity San Antonio River (up to 5500 μmol $kg^{-1}$, Hu, unpublished data) water through Mesquite Bay (Evans et al. 2015) during the flooding period. This high alkalinity water influence decreased from Mesquite Bay to Aransas Bay.

2.4.2. Controlling factors on the $pCO_{2,water}$ variations during the dry-wet cycle

Carbonate system speciation in estuarine waters is controlled by various factors such as temperature, biological processes (primary production, calcification, etc.), and river-ocean mixing (Bozec et al. 2012; Hu and Cai 2013; Hunt et al. 2013; Joesoef et al. 2015). Here we evaluated the effect of temperature and riverine inputs during the drought and flooding periods.

During the drought period, the mean amplitude of thermal effect on water $pCO_2$ ($pCO_{2,thermal}$ - $pCO_{2,water}$) was ~190 μatm, which was partially compensated (~100 μatm) by counteractive non-thermal effect ($pCO_{2,non\text{-}thermal}$ - $pCO_{2,water}$), thus a net ~100 μatm of seasonal amplitude on $pCO_{2,water}$ was observed when there was a warming effect from spring to summer or a cooling effect from summer to winter (Fig. 2.9). During the flooding period however, mean thermal effect declined to ~90 μatm as water temperature increased slightly in 03/2015, whereas there

was a large fluctuation of non-thermal effect in 03/2015 - 04/2015. In particular, sharp increases in $pCO_{2,water}$ was observed in Copano Bay (CW and CE, respectively, Fig. 2.9), and $pCO_{2,non\text{-}thermal}$ reached its highest concentration (1211 μatm) when the first storm came in late 03/2015. These increases indicated that the storm event caused a dramatic increase in non-thermal $pCO_2$ (biological and/or mixing). According to Bruesewitz et al. (2013), community respiration in Copano Bay would greatly increase following a storm (thus increasing $pCO_2$). In addition, high river inflow resulted from storm event also brought in high $pCO_2$ water. The appearance of peak $pCO_{2,non\text{-}thermal}$ (715 μatm, early 04/2015) was delayed at CE compared to CW (Fig. 2.9) and the value was lower, indicating that the non-thermal effect became less pronounced with freshwater inflow propagating along the estuary.

Overall, thermal effect dominated the drought period from 05/2014 to 02/2015 for all stations except in AB (Table 2.4), where thermal and non-thermal effect were about the same. However, during the flooding period, Copano and Mesquite Bay had much lower T/B ratio, indicating that non-thermal effect played a dominant role in controlling $pCO_{2,water}$ variation, consistent with the discussion above. In addition, AB and SC exhibited similar T/B ratios across the dry/wet cycle, indicating that hydrologic state probably did not have a significant effect on the relative importance of thermal vs. non-thermal effect, at least during our sampled time. Considering that station AB is located in the primary bay that has direct exchange with the open Gulf through the ship channel, and that both AB and SC had smaller salinity variations during the annual cycle (Table 2.1), these stations clearly were less influenced by river inflow but more by exchange with the GOM.

2.4.3. Air-water $CO_2$ flux dynamics and controlling factors during the dry-wet cycle

Although accounting for 41% of world's estuarine area, average $CO_2$ flux in North American estuaries accounts for only 12% of global estuarine $CO_2$ emission, at a moderate value of 2.2 $mol \cdot C \cdot m^{-2} \cdot y^{-1}$, according to a recent synthesis (Chen et al. 2013). However, the average annual air-water $CO_2$ flux from MAE reached 12.4±3.3 $mol \cdot C \cdot m^{-2} \cdot y^{-1}$ based on our study. Even though this flux was consistent with results obtained in a limited number of tropical lagoons (Laruelle et al. 2010), it was significantly higher than many other North American estuaries and even some macrotidal estuaries in Europe (Table 2.5).

As an important factor that determines gas transfer velocity (Eq. 4), wind speed plays an important role in estuarine $CO_2$ flux. According to Chen et al. (2013), the mean air-water $pCO_2$ gradient of European estuaries is only about one third of those in Asian estuaries, whereas the mean air-water $CO_2$ flux from European estuaries doubled that in Asia due to much higher wind speed. Similarly, despite a relatively low average $pCO_{2,water}$ (487±138 μatm) in MAE compared with much higher $pCO_{2,water}$ in European and Asian estuaries (1600 and 4000 μatm, respectively; Chen et al. , 2013), high mean wind speed (5.4±2.3 $m \cdot s^{-1}$, compared with approximately 4 and 1.6 $m \cdot s^{-1}$ on European and Asian coasts, respectively; Chen et al. 2013) contributed to a relatively high $CO_2$ efflux in this estuary. Therefore, it is desirable to further investigate the role of other low latitude regions, not only within the estuaries, but coastal ocean, in estuarine $CO_2$ budget calculations.

Similar to many other estuaries, air-water $CO_2$ flux in MAE displayed strong temporal changes during our studied period (Tables 2.2 and 2.6). During the drought period, $CO_2$ emission from the estuary was the highest in summer and early fall (06/2014-09/2014, Fig. 2.6). This is likely a result of high wind speed (in average 6.0±2.4 $m \cdot s^{-1}$) and high water temperature, and the

later could enhance community respiration and evaporation, as more concentrated seawater holds less $CO_2$. For example, a simulation using CO2SYS suggests that for a seawater with salinity 35, total alkalinity 2270 μmol $kg^{-1}$, total dissolved inorganic carbon (DIC) 1977 μmol $kg^{-1}$, $pCO_2$ of this seawater would be 400 μatm at 25˚C. Then allowing the water evaporate to salinity 40 (hypersaline condition in Copano Bay), $pCO_2$ would increase to 494 μatm (Fig. 2.3). If allowing all "excess" $CO_2$ to degas and reach equilibrium with the 400 μatm atmosphere, a degassing process that may take only a few days given the shallow water depth here, this evaporation-concentrated water would hold ~50 μmol $kg^{-1}$ less DIC than the 'concentrated' original seawater. With additional alkalinity reduction, regardless its cause, prolonged water residence time would lead to even more $CO_2$ loss to the atmosphere. Indeed, TA/DIC ratio in all stations increased with increasing salinity (i.e., average TA/DIC increased from 1.116±0.012 to 1.172±0.024, along with the increase of average salinity from 31.6±1.0 to 38.7±0.8, N=10; Fig. 2.10). Part of the TA/DIC increase can be attributed to higher TA/DIC ratio in the ocean endmember, and then further depletion of DIC relative to TA toward hypersaline conditions indicated that evaporation contributed to a net $CO_2$ loss.

Toward the end of the drought period, $pCO_{2,water}$ started to decline with decreasing temperature, and the entire estuary became a weak $CO_2$ sink from late fall to winter (11/2014-02/2015). Particularly in 02/2015, at all five stations surface water was undersaturated for $CO_2$ (average $pCO_{2,water}$ = 341±49 μatm). This could be attributed to low riverine input and lower water temperature (Hunt et al. 2013). Note this period also had lower wind speed (average 3.7±0.9 $m \cdot s^{-1}$) thus $CO_2$ uptake was modest.

$CO_2$ efflux also displayed spatial variations during our sampling period (Table 2.6). There was a decreasing trend of average $CO_2$ emission (46.2 to 8.1 $mmol \cdot C \cdot m^{-2} \cdot d^{-1}$) from the

secondary bays (Copano and Mesquite) to the primary bay (Aransas). Mean air-water $CO_2$ flux at the ship channel (SC) was the lowest (8.1±34.2 $mmol \cdot C \cdot m^{-2} \cdot d^{-1}$; N=22). This spatial distribution agrees with other estuarine studies as $CO_2$ efflux typically decreases toward the ocean (Crosswell et al. 2012; Hunt et al. 2013; Joesoef et al. 2015). However, higher $CO_2$ emission was observed at mid-estuary (CE and MB) especially in the drought period. This was possibly due to more intense remineralization reactions (Table. 2.1; Fig. 2.5), which was in favor of $CO_2$ production. In flooding season, enhanced non-thermal effect dramatically increased (Section 4.1.1) air-water $CO_2$ flux at CW, whereas $CO_2$ degassing was maintained at similar level or even decreased in other part of this estuary, due presumably to nutrient-enhanced primary production (Reyna et al. 2017).

## 2.5. Conclusions

Both carbonate chemistry and $CO_2$ flux demonstrated substantial temporal and spatial variations in the subtropical MAE, which was affected by strong interannual changes in estuarine hydrologic states. There was a gradient for carbonate variables and $CO_2$ flux from the secondary bays to the primary bay. We observed significant TA and DIC removal during the drought period and mixing dominated distribution in the flooding season, although detailed mechanisms for the alkalinity loss still await further investigation.

Overall, the MAE was a $CO_2$ source with an annual average air-water $CO_2$ flux 12.4±3.3 $mol \cdot C \cdot m^{-2} \cdot y^{-1}$. High wind speed played an important role for this high $CO_2$ efflux despite the relatively small air-water $pCO_2$ gradient. This estimate is much higher than existing, yet scarce, estimates in other subtropical estuaries. During the drought and warm period, $CO_2$ emission was enhanced by increased temperature (hence increased respiration) and evaporation, and highest $CO_2$ emission (74.5±41.1 $mmol \cdot m^{-2} \cdot d^{-1}$; N=30) was found in summer in the drought period.

However, lower temperature in winter would turn the entire estuary into a weak $CO_2$ sink (-8.9±5.1 $mmol \cdot m^{-2} \cdot d^{-1}$; N=15). In the flooding period, storm events briefly yet significantly enhanced air-water $CO_2$ flux at CW due to much elevated $pCO_2$ level there. Overall, our work suggests that global estuarine $CO_2$ flux estimates need to be improved by incorporating new studies that focus on subtropical and/or windy estuaries.

References

Abril, G. and others 2015. Technical Note: Large overestimation of $pCO_2$ calculated from pH and alkalinity in acidic, organic-rich freshwaters. Biogeosciences **12:** 67-78.

Abril, G., M. V. Commarieu, D. Maro, M. Fontugne, F. Guérin, and H. Etcheber. 2004. A massive dissolved inorganic carbon release at spring tide in a highly turbid estuary. Geophysical Research Letters **31:** doi:10.1029/2004GL019714.

Bauer, J. E., W. J. Cai, P. A. Raymond, T. S. Bianchi, C. S. Hopkinson, and P. A. Regnier. 2013. The changing carbon cycle of the coastal ocean. Nature **504:** 61-70.

Benoit, G., S. D. Oktay-Marshall, A. Cantu, Hood, E. M.,, C. H. Coleman, M. O. Corapcioglu, and P. H. Santschi. 1994. Partitioning of Cu, Pb, Ag, Zn, Fe, Al, and Mn between filter-retained particles, colloids, and solution in six Texas estuaries. Marine Chemistry **45:** 307-336.

Bockmon, E. E., and A. G. Dickson. 2014. A seawater filtration method suitable for total dissolved inorganic carbon and pH analyses. Limnology and Oceanography: Methods **12:** 191-195.

Bozec, Y., T. Cariou, E. Macé, P. Morin, D. Thuillier, and M. Vernet. 2012. Seasonal dynamics of air-sea $CO_2$ fluxes in the inner and outer Loire estuary (NW Europe). Estuarine, Coastal and Shelf Science **100:** 58-71.

Bruesewitz, D. A., Wayne S. Gardner, Rae F. Mooney, Lindsey Pollard, and E. J. Buskey. 2013. Estuarine ecosystem function response to flood and drought in a shallow, semiarid estuary: Nitrogen cycling and ecosystem metabolism. Limnology and Oceanography **58:** 2293-2309.

Burdige, D. J. 2006. Geochemistry of marine sediments. Princeton University Press Princeton.

Cai, W. J. 2011. Estuarine and coastal ocean carbon paradox: $CO_2$ sinks or sites of terrestrial carbon incineration? Annual review of marine science **3:** 123-145.

Carter, B. R., J. A. Radich, H. L. Doyle, and A. G. Dickson. 2013. An automated system for spectrophotometric seawater pH measurements. Limnology and Oceanography: Methods **11:** 16-27.

Chen, C. T. A. 2002. Shelf-vs. dissolution-generated alkalinity above the chemical lysocline. Deep Sea Research Part II: Topical Studies in Oceanography **49:** 5365-5375.

Chen, C. T. A., T. H. Huang, Y. C. Chen, Y. Bai, X. He, and Y. Kang. 2013. Air–sea exchanges of $CO_2$ in the world's coastal seas. Biogeosciences **10:** 6509-6544.

Cross, J. N., J. T. Mathis, N. R. Bates, and R. H. Byrne. 2013. Conservative and non-conservative variations of total alkalinity on the southeastern Bering Sea shelf. Marine Chemistry **154:** 100-112.

Crosswell, J. R., M. S. Wetz, B. Hales, and H. W. Paerl. 2012. Air-water $CO_2$ fluxes in the microtidal Neuse River Estuary, North Carolina. Journal of Geophysical Research: Oceans **117:** doi:10.1029/2012jc007925.

Crosswell, J. R., M. S. Wetz, B. Hales, and H. W. Paerl. 2014. Extensive $CO_2$ emissions from shallow coastal waters during passage of Hurricane Irene (August 2011) over the Mid-Atlantic coast of the U.S.A. Limnology and Oceanography **59:** 1651-1665.

de la Paz, M., X. A. Padín, A. F. Ríos, and F. F. Pérez. 2010. Surface $fCO_2$ variability in the Loire plume and adjacent shelf waters: High spatio-temporal resolution study using ships of opportunity. Marine Chemistry **118:** 108-118.

Dickson, A. G. 1990. Standard potential of the reaction: AgCl(s)+ $12H_2(g)$= Ag(s)+ HCl(aq), and and the standard acidity constant of the ion $HSO_4^-$ in synthetic sea water from 273.15 to 318.15 K. The Journal of Chemical Thermodynamics **22:** 113-127.

Dickson, A. G., J. D. Afghan, and G. C. Anderson. 2003. Reference materials for oceanic $CO_2$ analysis: a method for the certification of total alkalinity. Marine Chemistry **80:** 185-197.

Dickson, A. G., C. L. Sabine, and J. R. Christian. 2007. Guide to Best Practices for Ocean $CO_2$ Measurements.

Dollar, S. J., S. V. Smith, S. M. Vink, S. Obrebski, and J. T. Hollibaugh. 1991. Annual cycle of benthic nutrient fluxes in Tomales Bay, California, and contribution of the benthos to total ecosystem metabolism. Marine ecology progress series. Oldendorf **79:** 115-125.

Doney, S. C. and others 2009. Mechanisms governing interannual variability in upper-ocean inorganic carbon system and air–sea $CO_2$ fluxes: Physical climate and atmospheric dust. Deep Sea Research Part II: Topical Studies in Oceanography **56:** 640-655.

Dürr, H. H., G. G. Laruelle, C. M. van Kempen, C. P. Slomp, M. Meybeck, and H. Middelkoop. 2011. Worldwide typology of nearshore coastal systems: Defining the estuarine filter of river inputs to the oceans. Estuaries and Coasts **34:** 441-458.

Evans, A., Kiersten Madden, and S. Palmer. 2015. The Ecology and Sociology Of The Mission-Aransas Estuary: An Estuarine and Watershed Profile.

Fagan, K. E., and F. T. Mackenzie. 2007. Air–sea $CO_2$ exchange in a subtropical estuarine-coral reef system, Kaneohe Bay, Oahu, Hawaii. Marine Chemistry **106:** 174-191.

Feely, R. A. and others 2010. The combined effects of ocean acidification, mixing, and respiration on pH and carbonate saturation in an urbanized estuary. Estuarine, Coastal and Shelf Science **88:** 442-449.

Frankignoulle, M. and others 1998. Carbon dioxide emission from European estuaries. Science **282:** 434-436.

Frankignoulle, M., and A. V. Borges. 2001. Direct and indirect $pCO_2$ measurements in a wide range of $pCO_2$ and salinity values (the Scheldt estuary). Aquatic Geochemistry **7:** 267-273.

Guo, X., M. Dai, W. Zhai, W.-J. Cai, and B. Chen. 2009. $CO_2$ flux and seasonal variability in a large subtropical estuarine system, the Pearl River Estuary, China. Journal of Geophysical Research **114:** doi:10.1029/2008jg000905.

Hsu, S. A., Eric A. Meindl., and D. B. Gilhousen. 1994. Determining the power-law wind-profile exponent under near-neutral stability conditions at sea. Journal of Applied Meteorology **33:** 757-765.

Hu, X., and W.-J. Cai. 2013. Estuarine acidification and minimum buffer zone-A conceptual study. Geophysical Research Letters **40:** 5176-5181.

Hu, X., and W. J. Cai. 2011. An assessment of ocean margin anaerobic processes on oceanic alkalinity budget. Global Biogeochemical Cycles **25:** doi:10.1029/2010GB003859.

Hu, X., J. B. Pollack, M. R. McCutcheon, P. A. Montagna, and Z. Ouyang. 2015. Long-term alkalinity decrease and acidification of estuaries in northwestern Gulf of Mexico. Environmental Science & Technology **49:** 3401-3409.

Hunt, C. W., J. E. Salisbury, and D. Vandemark. 2011. Contribution of non-carbonate anions to total alkalinity and overestimation of $pCO_2$ in New England and New Brunswick rivers. Biogeosciences **8:** 3069-3076.

Hunt, C. W., J. E. Salisbury, and D. Vandemark. 2013. $CO_2$ input dynamics and air–sea exchange in a large New England estuary. Estuaries and Coasts **37:** 1078-1091.

Jiang, L. Q., W. J. Cai, and Y. Wang. 2008. A comparative study of carbon dioxide degassing in river- and marine-dominated estuaries. Limnology and Oceanography **53:** 2603-2615.

Joesoef, A., W. J. Huang, Y. Gao, and W. J. Cai. 2015. Air–water fluxes and sources of carbon dioxide in the Delaware Estuary: spatial and seasonal variability. Biogeosciences **12:** 6085-6101.

Kanamori, S., and H. Ikegami. 1980. Computer-processed potentiometric titration for the determination of calcium and magnesium in sea water. Journal of the Oceanographical Society of Japan **36:** 177-184.

Kim, H.-C., and P. A. Montagna. 2012. Effects of climate-driven freshwater inflow variability on macrobenthic secondary production in Texas lagoonal estuaries: A modeling study. Ecological Modelling **235-236:** 67-80.

Koczy, F. F. 1956. The specific alkalinity. Deep Sea Research (1953) **3:** 279-288.

Kratz, T., J. Schindler, D. Hope, J. Riera, and C. Bowser. 1997. Average annual carbon dioxide concentrations in eight neighboring lakes in northern Wisconsin, USA. Verhandlungen-Internationale Vereinigung für theoretische und angewandte Limnologie **26:** 335-338.

Laruelle, G. G., H. H. Dürr, C. P. Slomp, and A. V. Borges. 2010. Evaluation of sinks and sources of $CO_2$ in the global coastal ocean using a spatially-explicit typology of estuaries and continental shelves. Geophysical Research Letters **37:** doi:10.1029/2010gl043691.

Laruelle, G. G., R. Lauerwald, J. Rotschi, P. A. Raymond, J. Hartmann, and P. Regnier. 2015. Seasonal response of air–water $CO_2$ exchange along the land–ocean aquatic continuum of the northeast North American coast. Biogeosciences **12:** 1447-1458.

Lewis, E., D. Wallace, and L. J. Allison. 1998. Program Developed for $CO_2$ System Calculations. Carbon Dioxide Information Analysis Center, managed by Lockheed Martin Energy Research Corporation for the US Department of Energy Tennessee.

Liu, X., M. C. Patsavas, and R. H. Byrne. 2011. Purification and characterization of meta-cresol purple for spectrophotometric seawater pH measurements. Environmental Science & Technology **45:** 4862-4868.

Longley, W. L. 1994. Freshwater inflows to Texas bays and estuaries: ecological relationships and methods for determination of needs. Texas Water Development Board and Texas Parks and Wildlife Department.

Millero, F. J. 2001. The Physical Chemistry of Natural Waters: by Frank J. Millero. Wiley-Interscience.

Millero, F. J. 2010. Carbonate constants for estuarine waters. Marine and Freshwater Research **61:** 139-142.

Millero, F. J., W. T. Hiscock, F. Huang, M. Roche, and J. Z. Zhang. 2001. Seasonal variation of the carbonate system in Florida Bay. Bulletin of Marine Science **68:** 101-123.

Milliman, J. D., K. L. Farnsworth, P. D. Jones, K. H. Xu, and L. C. Smith. 2008. Climatic and anthropogenic factors affecting river discharge to the global ocean, 1951–2000. Global and Planetary Change **62:** 187-194.

Montagna, P., T. A. Palmer, and J. Pollack. 2012. Hydrological Changes and Estuarine Dynamics Springer Science & Business Media.

Mooney, R. F., and J. W. McClelland. 2012. Watershed Export Events and Ecosystem Responses in the Mission–Aransas National Estuarine Research Reserve, South Texas. Estuaries and Coasts **35:** 1468-1485.

Natchimuthu, S., I. Sundgren, M. Gålfalk, L. Klemedtsson, and D. Bastviken. 2017. Spatiotemporal variability of lake $pCO_2$ and $CO_2$ fluxes in a hemiboreal catchment. Journal of Geophysical Research: Biogeosciences **122:** 30-49.

Pollack, J. B., A. Cleveland, T. A. Palmer, A. S. Reisinger, and P. A. Montagna. 2012. A restoration suitability index model for the eastern oyster (Crassostrea virginica) in the Mission-Aransas Estuary, TX, USA. PLoS One **7:** e40839.

Raymond, P. A., J. E. Bauer, and J. J. Cole. 2000. Atmospheric $CO_2$ evasion, dissolved inorganic carbon production, and net heterotrophy in the York River estuary. Limnology and Oceanography **45:** 1707-1717.

Raymond, P. A., and J. J. Cole. 2001. Gas exchange in rivers and estuaries: Choosing a gas transfer velocity. Estuaries and Coasts **24:** 312-317.

Raymond, P. A., Nina F. Caraco, and J. J. Cole. 1997. Carbon dioxide concentration and atmospheric flux in the Hudson River. Estuaries **20:** 381-390.

Regnier, P. and others 2013. Anthropogenic perturbation of the carbon fluxes from land to ocean. Nature Geoscience **6:** 597-607.

Reisdorph, S. C., and J. T. Mathis. 2014. The dynamic controls on carbonate mineral saturation states and ocean acidification in a glacially dominated estuary. Estuarine, Coastal and Shelf Science **144:** 8-18.

Reyna, N. E., Amber Hardison, and Z. Liu. 2017. Influence of major storm events on the quantity and composition of particulate organic matter and the phytoplankton community in a subtropical estuary, Texas. Frontiers in Marine Science **4:** doi:10.3389/fmars.2017.00043.

Russell, M. J., and P. A. Montagna. 2007. Spatial and Temporal Variability and Drivers of Net Ecosystem Metabolism in Western Gulf of Mexico Estuaries. Estuaries and Coasts **30:** 137–153.

Sarma, V. V. S. S. and others 2012. Carbon dioxide emissions from Indian monsoonal estuaries. Geophysical Research Letters **39:** doi:10.1029/2011gl050709.

Semesi, I. S., S. Beer, and M. Björk. 2009. Seagrass photosynthesis controls rates of calcification and photosynthesis of calcareous macroalgae in a tropical seagrass meadow. Marine Ecology Progress Series **382:** 41-48.

Smith, S. V., J. T. Hollibaugh, S. J. Dollar, and S. Vink. 1991. Tomales Bay Metabolism: C-N-P Stoichiometry and Ecosystem Heterotrophy at the Land-Sea Interface. Estuarine, Coastal and Shelf Science **33:** 223-257.

Souza, M. F., V. R. Gomes, S. S. Freitas, R. C. Andrade, and B. Knoppers. 2009. Net ecosystem metabolism and nonconservative fluxes of organic matter in a tropical mangrove estuary, Piauí River (NE of Brazil). Estuaries and Coasts **32:** 111-122.

Takahashi, T., J. Olafsson, J. G. Goddard, D. W. Chipman, and S. Sutherland. 1993. Seasonal variation of $CO_2$ and nutrients in the high-latitude surface oceans: a comparative study. Global Biogeochemical Cycles **7:** 843-878.

Takahashi, T. and others 2002. Global sea–air $CO_2$ flux based on climatological surface ocean $pCO_2$, and seasonal biological and temperature effects. Deep-Sea Research II **49:** 1601-1622.

Wallace, R. B., H. Baumann, J. S. Grear, R. C. Aller, and C. J. Gobler. 2014. Coastal ocean acidification: The other eutrophication problem. Estuarine, Coastal and Shelf Science **148:** 1-13.

Wanninkhof, R. 1992. Relationship between wind speed and gas exchange. Journal of Geophysical Research **97:** 7373-7382.

Weiss, R. F. 1974. Carbon dioxide in water and seawater: the solubility of a non-ideal gas. Marine Chemistry **2:** 203-215.

Weiss, R. F., and B. A. Price. 1980. Nitrous oxide solubility in water and seawater. Marine Chemistry **8:** 347-359.

Wolf-Gladrow, D. A., R. E. Zeebe, C. Klaas, A. Körtzinger, and A. G. Dickson. 2007. Total alkalinity: The explicit conservative expression and its application to biogeochemical processes. Marine Chemistry **106:** 287-300.

Zeng, F.-W., C. A. Masiello, and W. C. Hockaday. 2010. Controls on the origin and cycling of riverine dissolved inorganic carbon in the Brazos River, Texas. Biogeochemistry **104:** 275-291.

Zhai, W., and M. Dai. 2009. On the seasonal variation of air – sea $CO_2$ fluxes in the outer Changjiang (Yangtze River) Estuary, East China Sea. Marine Chemistry **117:** 2-10.

Zhai, W., M. Dai, and X. Guo. 2007. Carbonate system and $CO_2$ degassing fluxes in the inner estuary of Changjiang (Yangtze) River, China. Marine Chemistry **107:** 342-356.

Table 2.1. Physical and chemical conditions of MAE during drought and flooding periods in MAE. D and F indicate drought and flooding period, respectively.

| Station | Period | Temp (°C) | Sal | DO ($\mu mol \cdot kg^{-1}$) | DO% | pH | DIC ($\mu mol \cdot kg^{-1}$) | TA ($\mu mol \cdot kg^{-1}$) | $pCO_{2,water}$ ($\mu atm$) | $\Omega_{ar}$ |
|---|---|---|---|---|---|---|---|---|---|---|
| Total | D | 23.6±6.6 | 34.7±2.9 | 208.0±31.8 | 97.2±5.23 | 8.018±0.080 | 2194.7±156.8 | 2497.6±172.1 | 477±49 | 3.3±0.6 |
| | F | 20.4±4.3 | 24.5±6.6 | 232.3±34.8 | 95.1±12.1 | 8.013±0.149 | 2132.5±256.8 | 2333.4±283.1 | 529±251 | 2.4±0.7 |
| CW | D | 23.4±6.9 | 36.9±2.4 | 207.2±29.3 | 97.9±4.3 | 8.046±0.042 | 2271.3±199.3 | 2626.2±234.5 | 450±62 | 3.8±0.9 |
| | F | 20.6±4.3 | 18.9±10.4 | 221.4±65.0 | 87.3±23.7 | 7.909±0.269 | 1870.9±390.0 | 2012.4±414.6 | 709±481 | 1.5±0.8 |
| CE | D | 23.7±6.9 | 35.0±2.4 | 206.9±31.7 | 97.2±5.5 | 7.960±0.084 | 2157.9±180.2 | 2429.2±174.8 | 542±105 | 2.9±0.3 |
| | F | 20.9±4.7 | 23.7±5.4 | 231.9±28.8 | 97.2±8.8 | 7.990±0.112 | 2056.4±136.6 | 2239.1±134.1 | 529±180 | 2.2±0.4 |
| AB | D | 23.6±6.6 | 34.4±2.6 | 205.5±32.3 | 95.9±4.8 | 8.034±0.044 | 2193.4±94.6 | 2506.8±77.9 | 453±50 | 3.4±0.7 |
| | F | 20.3±4.6 | 26.1±3.8 | 235.2±24.4 | 96.8±5.0 | 8.018±0.064 | 2237.3±88.4 | 2445.5±107.6 | 507±88 | 2.6±0.4 |
| SC | D | 23.9±5.5 | 33.6±2.2 | 206.5±28.3 | 96.3±5.9 | 8.051±0.069 | 2103.9±54.5 | 2402.4±47.4 | 423±70 | 3.4±0.4 |
| | F | 19.2±4.2 | 29.0±3.2 | 243.3±18.6 | 98.7±6.2 | 8.109±0.048 | 2091.0±25.1 | 2342.6±36.7 | 368±48 | 2.9±0.2 |
| MB | D | 23.6±7.3 | 33.6±3.5 | 214.4±38.2 | 98.9±5.4 | 7.998±0.109 | 2248.8±149.6 | 2522.7±157.5 | 521±110 | 3.2±0.3 |
| | F | 20.9±4.5 | 24.5±4.2 | 230.1±21.1 | 95.7±4.2 | 8.038±0.086 | 2407.0±52.2 | 2627.4±50.7 | 530±106 | 2.8±0.3 |

Table 2.2. Temporal and spatial analysis of the carbonate system tested by two-way ANOVA. "√" denotes a significant main factor interaction between sampling time (i.e. drought-flooding cycle) and sampling location.

| Parameter | Significant Interaction | df | *F* | *p* |
|---|---|---|---|---|
| pH | √ | 4 | 5.522 | <0.001 |
| DIC | √ | 4 | 12.124 | <0.001 |
| TA | √ | 4 | 18.060 | <0.001 |
| $pCO_{2,water}$ | √ | 4 | 6.430 | <0.001 |
| $\Omega_{ar}$ | √ | 4 | 11.953 | <0.001 |

Both main factors (drought vs. flooding, sample stations) were significant.

Table 2.3. Salinity, DIC, TA in the riverine and oceanic input endmembers.

| | GOM * | Aransas River | | Mission River | |
|---|---|---|---|---|---|
| | | Drought (N=6) | Flooding | Drought (N=6) | Flooding |
| Salinity | 36.4±0.3 | 0.7±0.1 | 0.1 | 0.7±0.2 | 0.1 |
| DIC ($\mu mol \cdot kg^{-1}$) | 2063.4±11.4 | 4345.1±509.2 | 1841.7 | 4856.7±761.5 | 2291.3 |
| TA ($\mu mol \cdot kg^{-1}$) | 2424.6±12.7 | 4450±542.0 | 1832.9 | 4843.1±798.8 | 2265.0 |

* Gulf of Mexico endmember was the average of the upper 30 m water column on the Texas shelf (N=106; Hu, unpublished data); river end member was decided by our survey between December 2015 and December 2016, in which 6 trips were taken in drought periods and 1 trip was taken in wet period with similar water discharge condition based on the USGS gages data.

Table 2.4. Thermal vs non-thermal effects on $pCO_2$ variations in MAE.

| Bay | Station | $\Delta pCO_{2,thermal}$ (µatm) | | $\Delta pCO_{2,non\text{-}thermal}$ (µatm) | | T/B | |
|---|---|---|---|---|---|---|---|
| | | Drought | Flooding | Drought | Flooding | Drought | Flooding |
| Copano Bay | CW | 371 | 194 | 335 | 991 | 1.11 | 0.20 |
| | CE | 379 | 206 | 309 | 361 | 1.23 | 0.57 |
| Aransas Bay | AB | 399 | 185 | 391 | 180 | 1.02 | 1.02 |
| | SC | 339 | 181 | 221 | 101 | 1.53 | 1.79 |
| Mesquite Bay | MB | 389 | 208 | 277 | 245 | 1.40 | 0.85 |

Table 2.5. Air-water $CO_2$ fluxes in different estuaries.

| Estuary | Average air-water $CO_2$ flux (*unit*: mol·C·m$^{-2}$·y$^{-1}$ for annual; mmol· C·m$^{-2}$·d$^{-1}$ for seasonal) | | | | | Latitude | Reference |
|---|---|---|---|---|---|---|---|
| | Annual | Spring (Mar-May) | Summer (Jun-Aug) | Fall (Sep-Nov) | Winter (Dec-Feb) | | |
| [a]Kennebec (US) | 3.5±1.0 | 31.7 | | | -11.5 | 44°48′ N | (Hunt et al. 2011) |
| [a]Delaware (US) | 2.4±4.8 | -13.7±16.4 | 13.4±22.2 | 2.7±6.6 | 15.6±5.2 | 38°42′- 39°18′ N | (Joesoef et al. 2015) |
| [a]Neuse River (US) | 4.7 | 1.73 | -0.84 | 38.4 | 12.1 | 34°40′- 35°30′N | (Crosswell et al. 2012) |
| [b]Florida Bay (US) | 1.7 | | | | | 25°N | (Millero et al. 2001) |
| [b]Kaneohe Bay (US) | 1.5 | | | | | 21°24′N | (Fagan and Mackenzie 2007) |
| [b]Loire (FR) | 8.3±15.5 | | | | | 46°30′- 47°30′ N | (de la Paz et al. 2010) |
| [b]Changjiang (CN) | -1.9±1.3 | -8.8±5.8 | -4.9±4.0 | 2.9±2.5 | -10.4±2.3 | 29°30′- 32°30′ N | (Zhai and Dai 2009) |
| [b]Pearl River (CN) | 6.9±2.6 | 12.2~79.4 | 5.3~108.2 | 15.4~24.9 | -1.09~22.6 | 21°30′- 23°30′ N | (Guo et al. 2009) |
| [b]Chalakudi (IN) | 4.7 | | 12.86 | | | 10°41′N | (Sarma et al. 2012) |
| [b]Piaui River estuary (BR) | 15.0 | | | | | 11°30′S | (Souza et al. 2009) |
| [a]Mission-Aransas (US) | 12.4±3.3 | 41.8±35.0 | 74.5±41.1 | 23.8±16.4 | -8.9±5.1 | 27°50′- 28°08′ N | This study |

* Superscripts a,b indicate different tidal types, a - microtidal estuary and b - macrotidal estuary.

Table 2.6. Estimated average air-water $CO_2$ flux ($mmol \cdot C \cdot m^{-2} \cdot d^{-1}$) distribution in the MAE.

| | Copano Bay | | Aransas Bay | | Mesquite Bay | Average |
|---|---|---|---|---|---|---|
| | CW | CE | AB | SC | MB | |
| Drought | 18.2±24.2 | 47.0±53.2 | 18.7±24.4 | 11.7±34.5 | 45.7±64.4 | 28.3±18.0 |
| Flooding | 147.9±218.4 | 40.9±69.3 | 28.7±19.5 | -15.1±20.3 | 55.7±36.0 | 51.6±83.9 |
| Annual | 35.7±144.8 | 46.2±86.0 | 20.0±37.7 | 8.1±45.5 | 47.1±76.4 | 33.8±9.0 |

* Two-way ANOVA suggests that both "dry-flooding cycle" and "stations" had significant effect on $CO_2$ flux, and the interaction effects were significant ($df = 4$, $F = 2.538$, $P<0.05$).

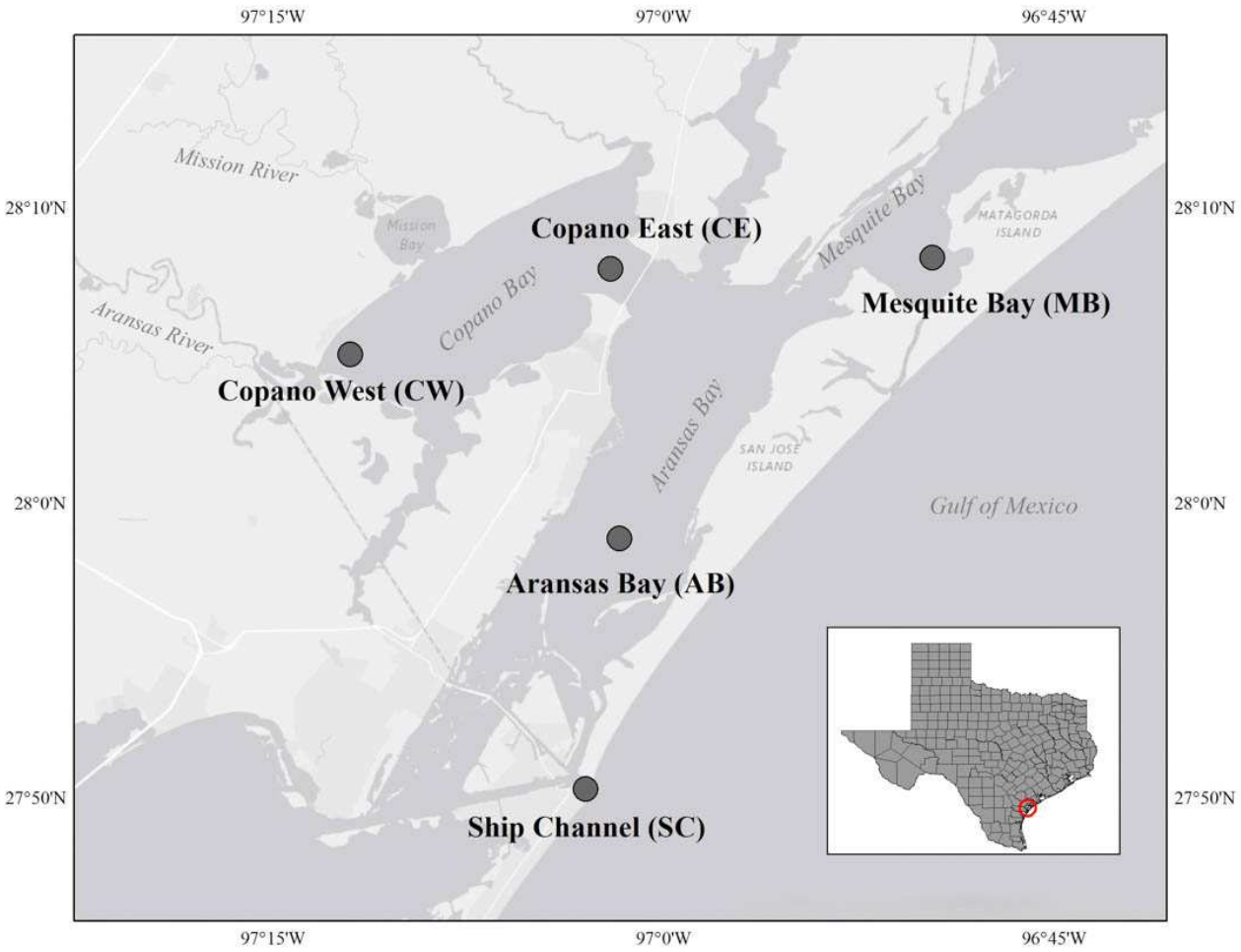


Figure 2.1. The map of the Mission-Aransas Estuary (MAE) and the five System Wide Monitoring Program stations.

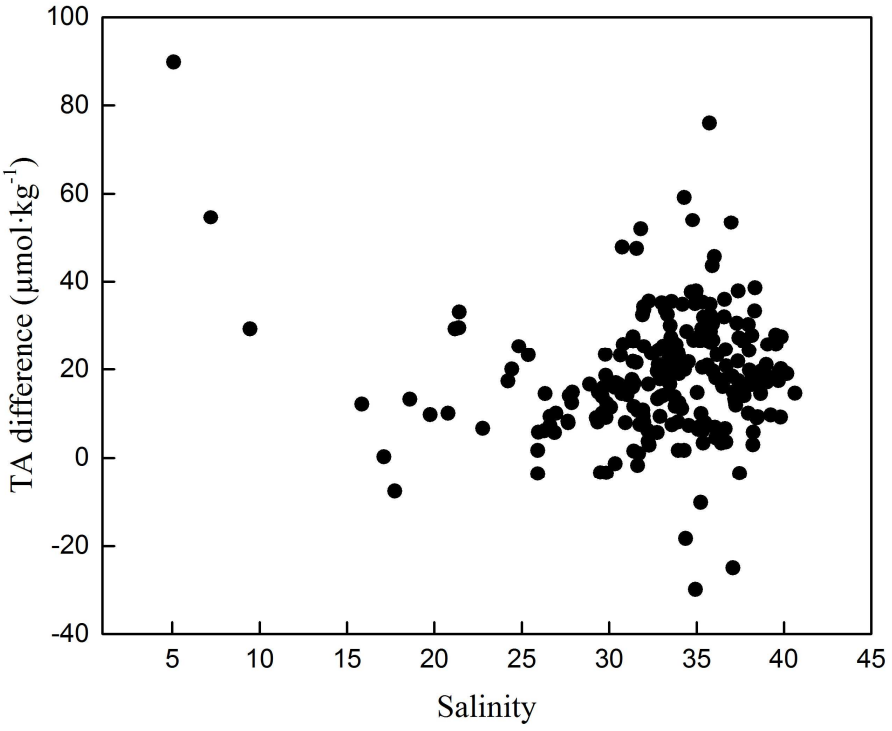


Figure 2.2. The difference between measured and calculated TA (from pH and DIC) and its relationship with salinity.

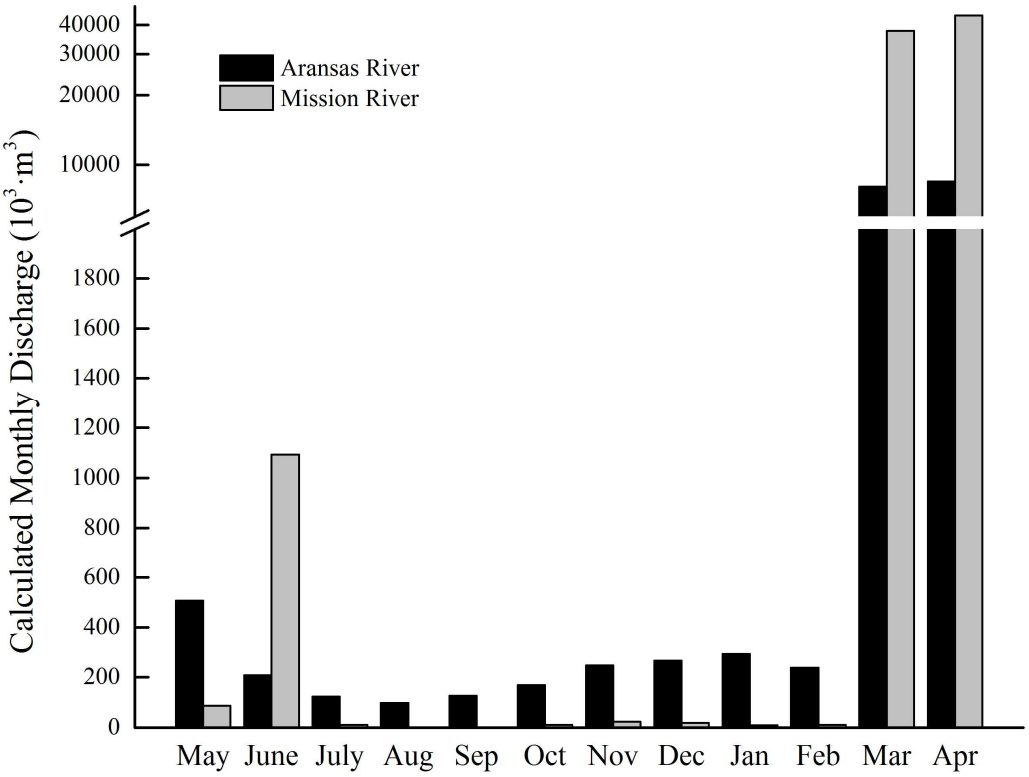


Figure 2.3. Monthly freshwater discharges from two major rivers into the MAE from 05/2014 to 04/2015 (data source, USGS).

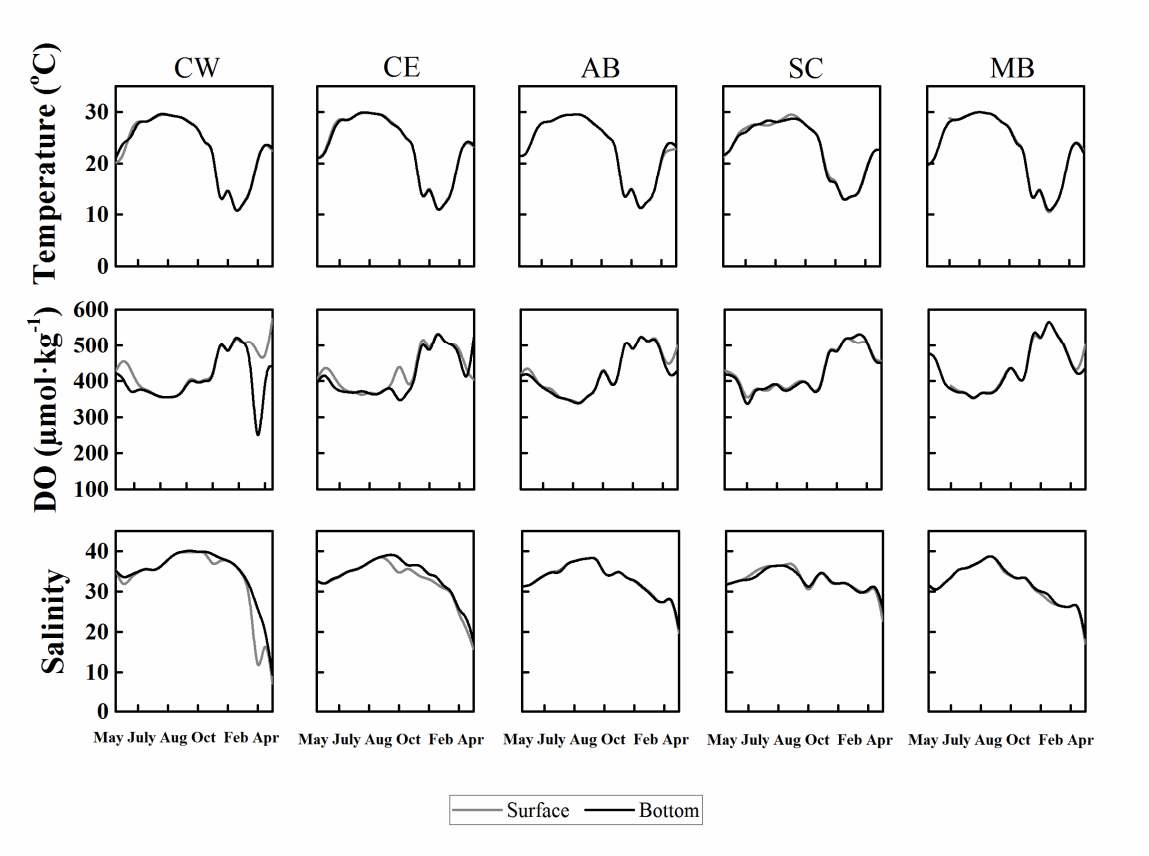


Figure 2.4. Seasonal variations of temperature, dissolved oxygen, and salinity in the MAE. The gray and black lines indicate surface and bottom water conditions, respectively.

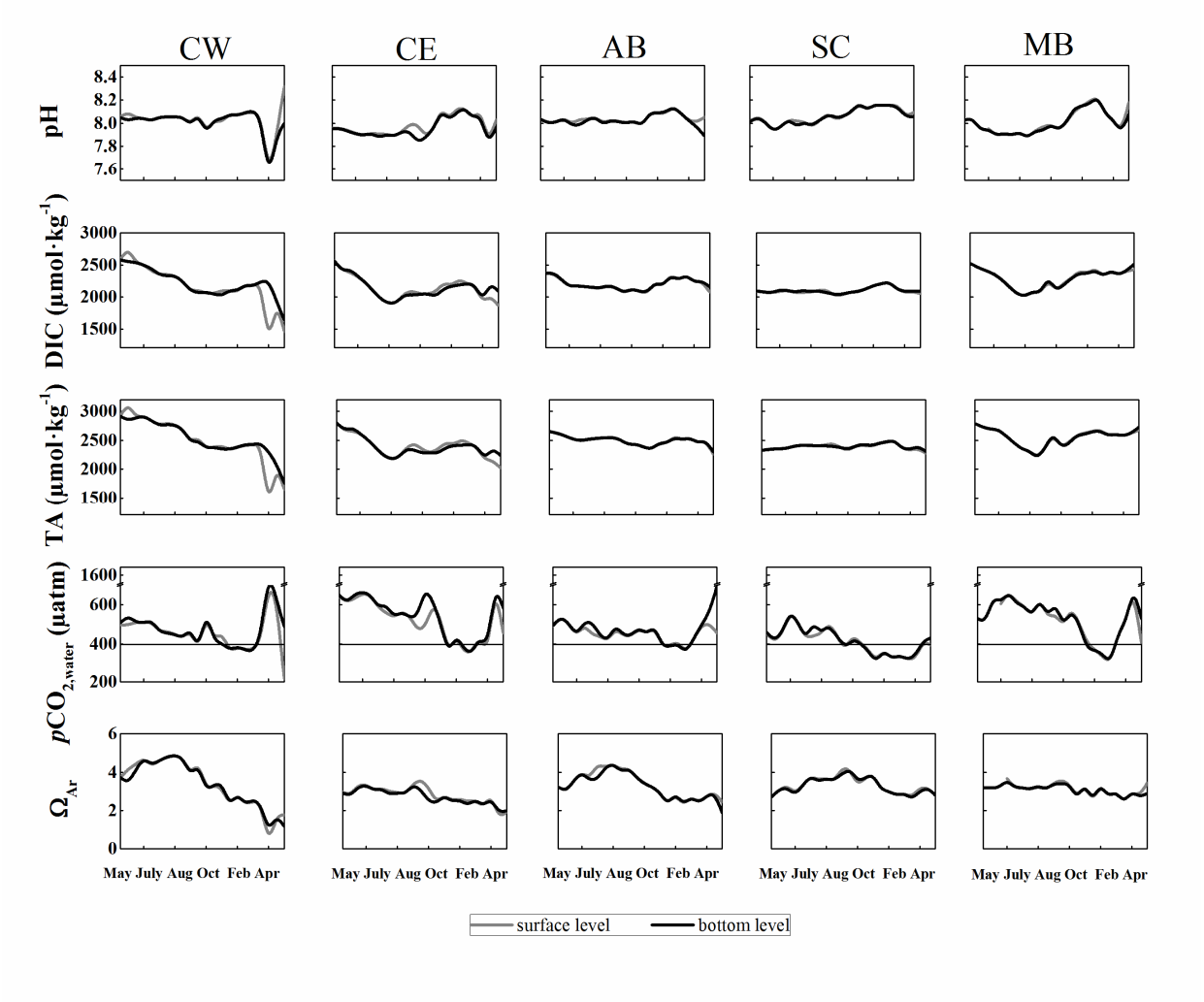


Figure 2.5. Seasonal variations of pH (total scale), DIC, TA, $pCO_{2,water}$, and $\Omega_{ar}$ in MAE. The gray and black lines indicate surface and bottom water conditions, respectively, and the straight lines in the $pCO_2$ panels indicates $pCO_{2,air}$.

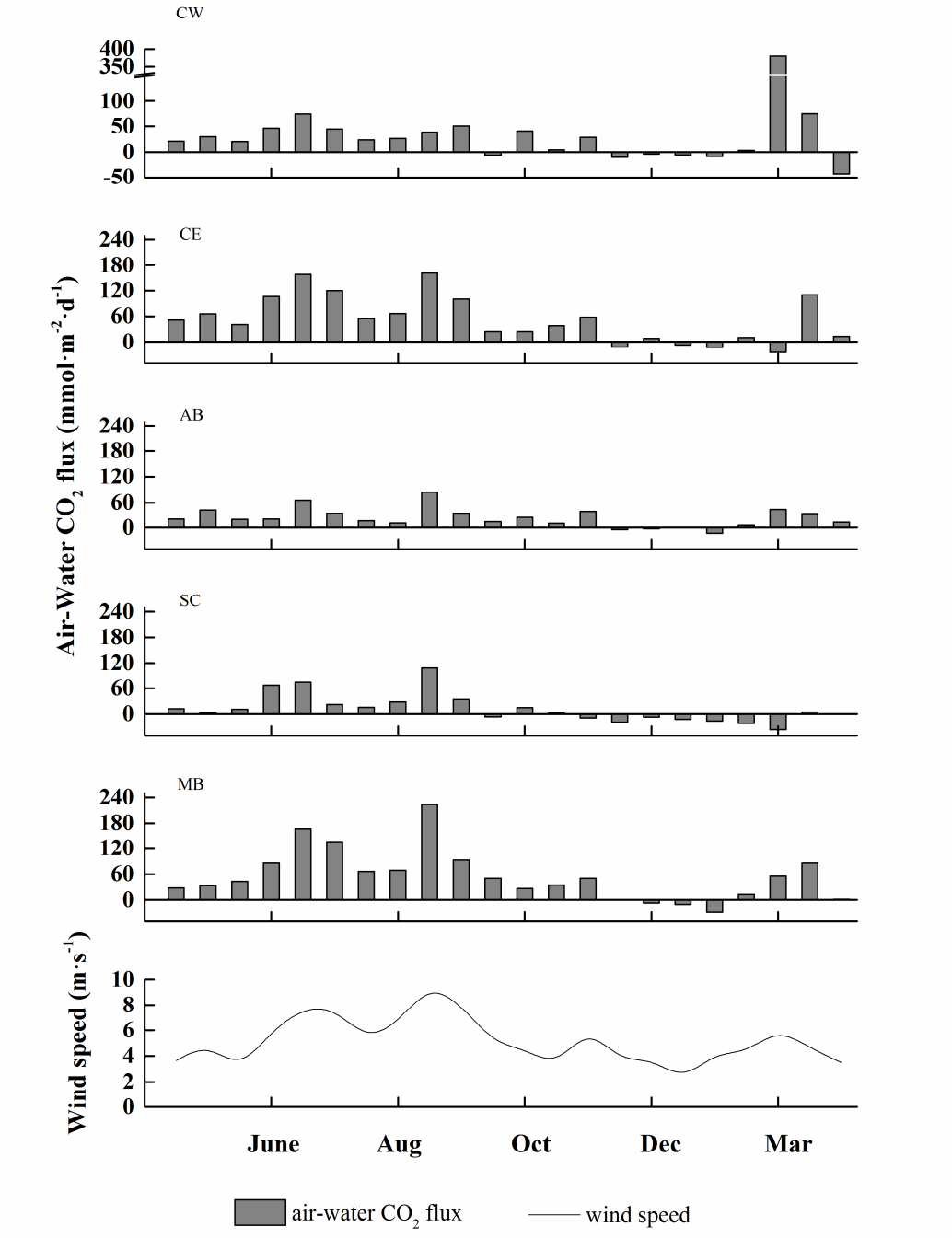


Figure 2.6. Air-water $CO_2$ fluxes at the five stations and wind speed (location) from 05/2014 to 04/2015.

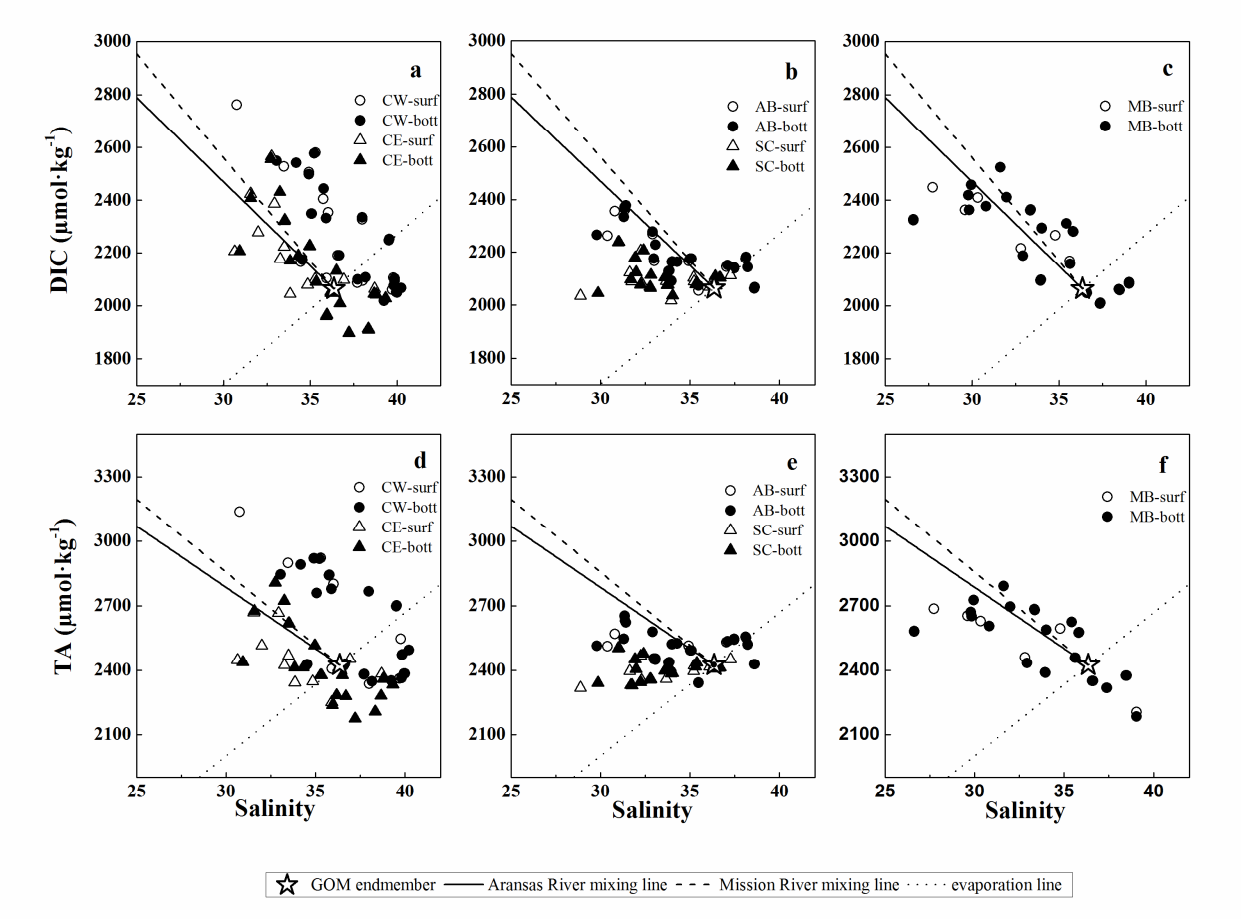


Figure 2.7. DIC, TA vs. salinity during the drought period (05/2014-02/2015). The solid and dashed lines represent mixing lines between Aransas and Mission rivers and the Gulf of Mexico (GOM) coastal water, respectively, and the dotted line represents the evaporation line of the GOM coastal water.

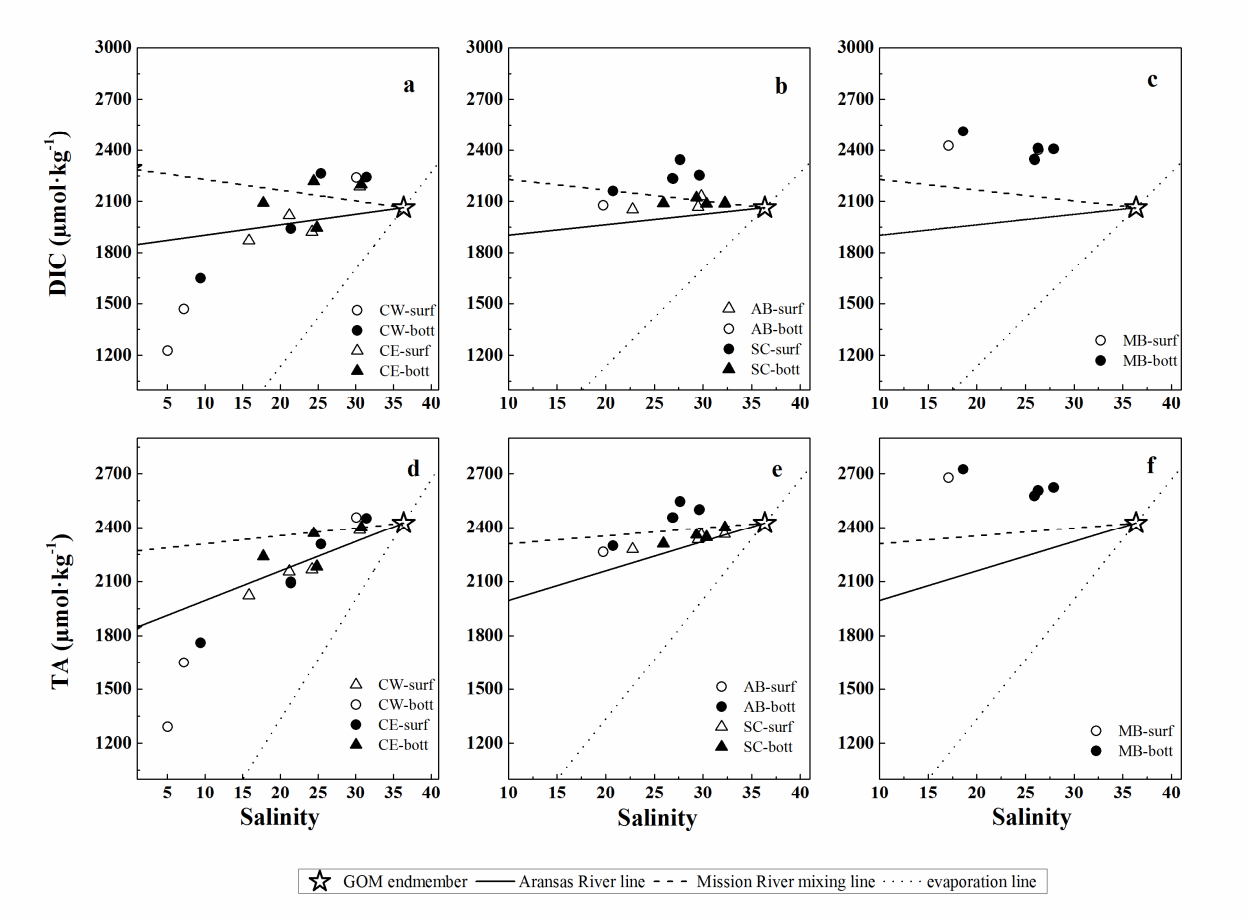


Figure 2.8. DIC, TA vs. salinity during the flooding period (03/2015-04/2015). The solid and dashed lines represent mixing lines between Aransas and Mission rivers and the Gulf of Mexico (GOM) coastal water, respectively, and the dotted line represents the evaporation line of the GOM coastal water.

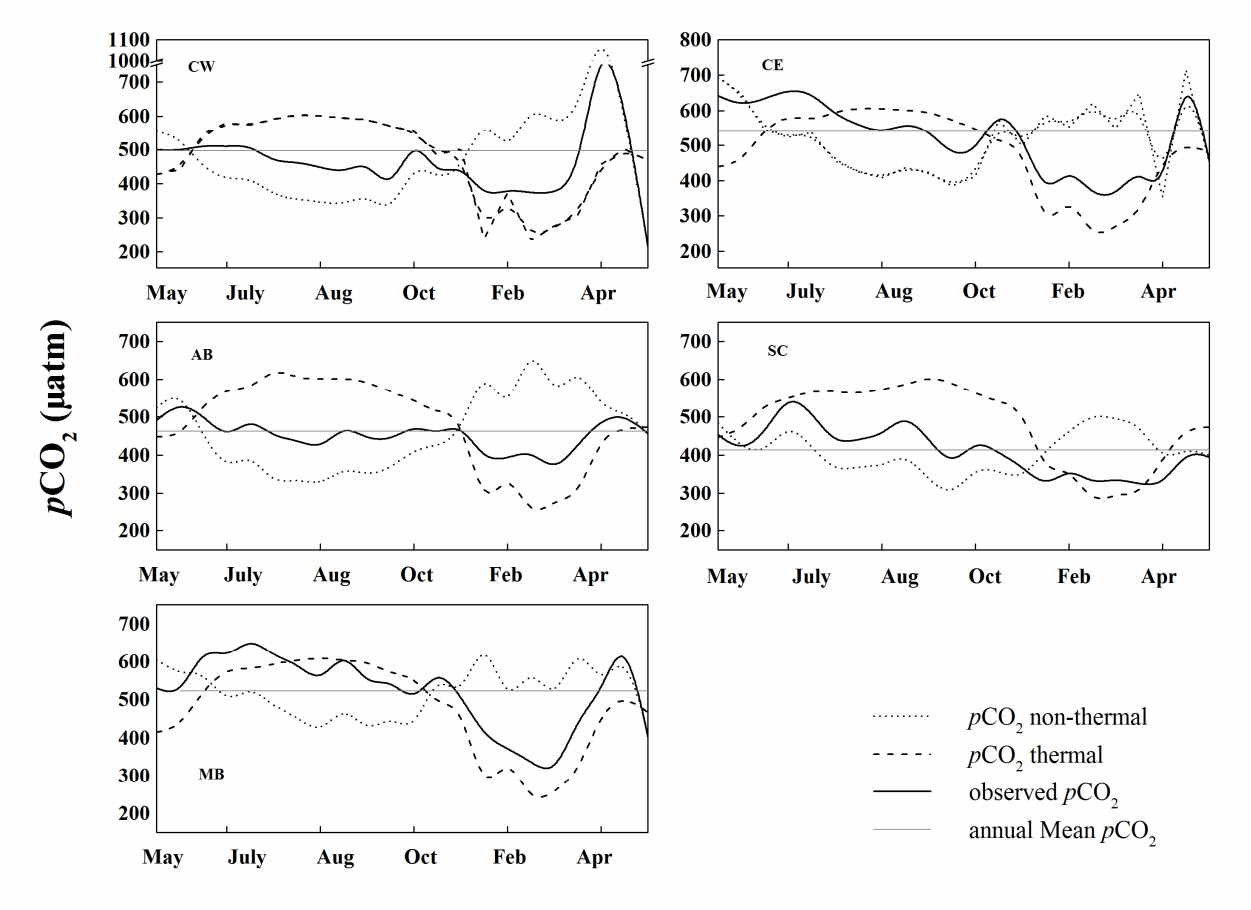


Figure 2.9. Seasonal variations of observed $pCO_{2,water}$ ($pCO_{2,obs}$), thermal $pCO_2$ ($pCO_{2,thermal}$), and non-thermal $pCO_2$ ($pCO_{2,non\text{-}thermal}$). The horizontal lines represent annual average values.

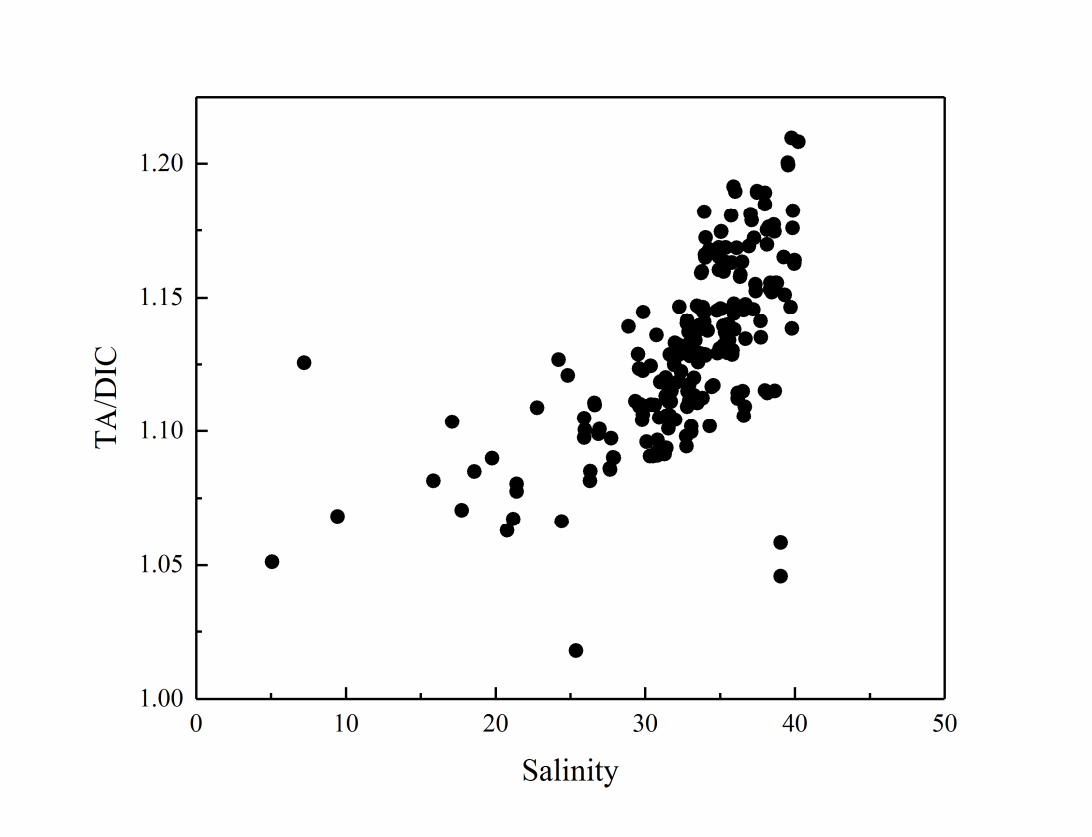


Figure 2.10. TA/DIC ratio vs. salinity in the MAE.

# CHAPTER III: HYDROLOGIC CONTROLS ON $CO_2$ CHEMISTRY AND FLUX IN SUBTROPICAL LAGOONAL ESTUARIES OF THE NORTHWESTERN GULF OF MEXICO


## Abstract

Estuaries are considered $CO_2$ source to the atmosphere, but with significant uncertainties in the magnitude of $CO_2$ flux and knowledge gaps in understanding its controlling factors for different estuarine systems. The study examined the role of hydrologic conditions on estuarine $CO_2$ system based on four northwest Gulf of Mexico (nwGOM) estuaries with extreme hydrologic conditions during April 2014—February 2017. Annual air-water $CO_2$ flux ranged 2.7—35.9 $mol \cdot C \cdot m^{-2} \cdot y^{-1}$, with approximately an order of magnitude decline from north to south where river discharge diminished. Episodic flooding made $CO_2$ flux differ significantly between dry (-0.7—20.9 $mmol \cdot C \cdot m^{-2} \cdot d^{-1}$) and wet (11.6—170.0 $mmol \cdot C \cdot m^{-2} \cdot d^{-1}$) conditions. Under the wet condition, increases in dissolved inorganic carbon (DIC) and total alkalinity (TA) significantly elevated $CO_2$ emission. Further, ventilation of river-borne $CO_2$ strengthened the emission when estuary became overwhelmingly river-dominated. During flood relaxation, all estuaries had DIC and TA consumption in moderate salinity range (10—30) as strong evidence of primary productivity. Such productivity balanced previous $CO_2$ emission from floods and yielded smaller $CO_2$ efflux on an annual scale. However, this consumption weakened during drought period when salinity increased toward ocean end-member (S=36.5 in the Gulf of Mexico). When prolonged drought occurred as represented by hypersalinity (S>36.5), both DIC and TA consumption and $CO_2$ degassing were enhanced because of both biogeochemical and evaporative effects. Due to flooding and windy conditions, spring and summer had strong $CO_2$ emission. Relaxation of flooding in fall changed these estuaries into a weak $CO_2$ source or sink.

Low temperatures in winter further depressed $CO_2$ efflux unless there was a pulse in freshwater input, which would increase the $CO_2$ flux.

## 3.1. Introduction

In the highly dynamic transition zone where the land meets the ocean, estuaries are usually a $CO_2$ source, due to net heterotrophy, but with substantial spatiotemporal variations in $CO_2$ flux (Chen et al. 2013; Laruelle et al. 2010). As a major estuarine type, coastal lagoons are generally shallow (<5 m) and have limited exchange with the adjacent ocean (Boynton et al. 1996). The estimated $CO_2$ flux (17.3±16.6 $mol \cdot C \cdot yr^{-1} \cdot m^{-2}$) from coastal lagoons is almost the same as that from the world's largest estuarine type - fjords (17.5±14.0 $mol \cdot C \cdot yr^{-1} \cdot m^{-2}$), and together they account for two thirds of total global estuarine area (the former accounts for 23.6%, the later accounts for 42.7%; Bauer et al. 2013; Laruelle et al. 2010). North America has 34% of the world's lagoonal estuaries (Cromwell 1971), most of which are located in the Gulf of Mexico (Dürr et al. 2011). Yao and Hu (2017) suggested that Mission-Aransas Estuary in the northwestern Gulf of Mexico (nwGOM) is a moderate to strong $CO_2$ source with an estimated $CO_2$ flux at 12.3±3.3 $mol \cdot C \cdot m^{-2} \cdot y^{-1}$. The lack of data for the rest of the northwestern Gulf of Mexico region makes it difficult to accurately quantify regional estuarine $CO_2$ flux, especially given that the region is subject to a strong latitudinal climatic gradient.

There are seven major lagoonal estuary systems with similar geomorphic structure and physiography along the 600 km of Texas coastline in the nwGOM (Longley 1994). The secondary bay (upper estuary in this study) in each estuary directly receives inflow from at least one major river while the larger primary bay (lower estuary in this study) has restricted connection to the nwGOM due to the barrier island chain. Despite the similarity, these estuaries are remarkably diverse hydrologically due to the presence of a climatic gradient (Montagna et al. 2012). This gradient (wetter in northeast and drier in southwest) causes large freshwater export variations in these estuaries, decreasing almost two orders of magnitude from northeast to

southwest (Longley 1994; Montagna et al. 2012). Both recorded data (Texas Water Development Board, http://www.twdb.texas.gov) and a climate projection (Milliman et al. 2008) indicate that these estuaries are subject to prolonged periods of drought punctuated by periods of intense flooding, resulting in extreme changes in hydrologic conditions in a relatively short period (weeks to months). The fast and intense transitions make the nwGOM coast an ideal place to study hydrologic influence on estuarine $CO_2$ chemistry and flux.

To fill in the data gap in the nwGOM lagoonal systems, we characterized $CO_2$ chemistry and flux based on a three-year dataset (2014-2017) in four estuaries. We examined spatial and temporal variations in $CO_2$ flux and identified main controls on both carbonate chemistry and $CO_2$ flux.

## 3.2. Methods

### 3.2.1. Study sites

Four nwGOM estuaries (Fig. 3.1) —Lavaca-Colorado Estuary (LCE), Guadalupe Estuary (GE), Mission-Aransas Estuary (MAE), and Nueces Estuary (NE)—were sampled between April 2014 and February 2017. These shallow estuaries (1—5 m in depth) are located in the middle of the nwGOM coast along a freshwater inflow gradient (Russell and Montagna 2007). We sampled LCE, GE, NE seasonally in April, July, October, and January of each year from 2014 to 2017, with the exception of 2017, when we sampled in February instead of January. These sampling months represent spring, summer, fall, and winter, respectively. Sampling occurred more frequently (monthly to bimonthly) in MAE (Yao and Hu 2017). River samples were collected bimonthly between October 2015 and June 2017, with additional field campaigns right after flooding events. Carbonate chemistry of river end-members for these estuaries were then derived from average of corresponding riverine data (Fig. 3.1).

Our sampling stations spanned from the river mouth(s) to tidal inlet in each estuary. Samples were taken from the surface and the bottom of the water column in estuaries (and from the surface only in the rivers) using a Van Dorn water sampler. Samples were preserved following the standard protocol for ocean $CO_2$ studies (Dickson et al. 2007). All field sampling was done during the daytime. *In-situ* data (temperature, pressure, and dissolved oxygen) were obtained using a calibrated YSI 6600 V2 data sonde.

Monthly river discharge data were obtained from the United States Geological Survey (USGS) real-time streamflow record (http://waterdata.usgs.gov/tx/nwis/rt). Hourly wind speed and barometric pressure data were obtained from National Oceanic and Atmospheric Administration's (NOAA) weather stations along the coast (https://tidesandcurrents.noaa.gov/stations.html). Daily mean wind speed and barometric pressure were calculated for the sampling days. Wind speed from anemometers that were typically installed at ~3 m height above water was converted to wind speed at 10 m height using the wind profile power law (Hsu et al. 1994).

3.2.2. Chemical analyses

Water samples were analyzed for carbonate system parameters—total alkalinity (TA), dissolved inorganic carbon (DIC), and pH. Briefly, DIC and TA were both analyzed at 22±0.1°C. DIC was determined by acidifying 0.5 mL of sample with 10% phosphoric acid and quantifying the extracted $CO_2$ on an AS-C3 DIC analyzer (Apollo SciTech). TA was determined using the Gran Titration (Gran 1952) on an AS-ALK2 alkalinity titrator (Apollo SciTech). Both DIC and TA analyses had a precision of ±0.1%. Certified Reference Material (CRM Batch#142, 156, 159; Dickson et al. 2003) was used throughout our analyses for data quality control and assurance.

pH was measured using either a spectrophotometric method (with precision of ±0.004 when salinity > 20, 25±0.1°C; Carter et al. 2013) or an Orion$^{TM}$ Ross pH electrode (when salinity<20, at 25±0.1°C, calibrated with NBS buffers at 4.01, 7.0, 10.01). pH measurements had a precision of ±0.004 for the spectrophotometric method and ±0.01 for the electrode. All potentiometric pH values were converted to total scale using the measured pH (at NBS scale). Salinity was measured using a benchtop salinometer calibrated with MilliQ water and known salinity CRM.

$pCO_{2,water}$ and pH at *in-situ* temperature were calculated using the program CO2SYS (Lewis et al. 1998) based on DIC concentration and lab measured pH at 25°C. We used the DIC/pH combination as the input variables to avoid possible errors associated with non-carbonate alkalinity when TA is used in the speciation calculations (Abril et al. 2015). Carbonic acid dissociation constants ($K_1$, $K_2$) from Millero (2010a) and the bisulfate dissociation constant from Dickson (1990) were used. In our previous study (Yao and Hu, 2017), a salinity dependent ΔTA (i.e., $TA_{measured} - TA_{calculated}$) was observed. Orr et al. (2018) analyzed 2.6—3.2% uncertainty in $pCO_2$ when pairing DIC/pH for calculations in CO2SYS, which equated to approximately 8-16 μatm error in $pCO_2$ in this study (by applying annual average $pCO_2$ range from those estuaries). In addition, our calculated $pCO_{2,water}$ matched well (±20 μatm) with real-time monitoring values using a calibrated $CO_2$ sensor (McCutcheon et al., in prep).

3.2.3. Air-Water $CO_2$ flux calculation

We used equation (1) to calculate the air-water $CO_2$ flux:

$$F = kK_0\left(pCO_{2,water} - pCO_{2,air}\right) \quad (1)$$

where k ($m \cdot d^{-1}$) is the gas transfer velocity as a function of wind speed, $K_0$ ($mol \cdot m^{-3} \cdot atm^{-1}$) is the gas solubility at measured *in-situ* temperature and salinity (Weiss 1974); $pCO_{2,water}$ represents surface water value, and $pCO_{2,air}$ can be calculated from:

$$pCO_{2,air} = xCO_{2,air} \times (P_b - P_w) \quad (2)$$

where $P_b$ (atm) is the barometric pressure from NOAA weather stations (Fig. 3.1), $P_w$ (atm) is the water vapor pressure calculated using salinity and temperature (Weiss and Price 1980), and $xCO_{2,air}$ (ppm) is the mole fraction of atmospheric $CO_2$ in dry air. $xCO_{2,air}$ data was obtained from a $CO_2$ buoy at the Mississippi Coast (https://www.pmel.noaa.gov/co2/story/Coastal+MS).

A positive flux (F value) means that $CO_2$ is degassing to the atmosphere. Gas transfer velocity k was a parameterized using wind speed and the equation from Jiang et al. (2008), which was derived from Raymond and Cole (2001) based on a larger amount of data in higher wind speed (>6 $m \cdot s^{-1}$):

$$k = (0.314 \cdot U^2 - 0.436 \cdot U + 3.99) \times (Sc_{SST}/600)^{-0.5} \quad (3)$$

where $U$ is the wind speed at 10 m height ($m \cdot s^{-1}$). $Sc_{SST}$ is Schmidt number of $CO_2$ at *in-situ* temperature (Wanninkhof 1992).

Area-weighted annual average $CO_2$ flux was calculated in each estuary following the equation:

$$F_{avg} = \frac{\sum F_i \times d_i}{\sum d_i} \quad (4)$$

$F_{avg}$ is annual average $CO_2$ flux and has a unit of $mmol \cdot m^{-2} \cdot d^{-1}$ or $mol \cdot m^{-2} \cdot y^{-1}$, $F_i$ is area-weighted $CO_2$ flux of sampling trip $i$, $d_i$ indicates interval days in between two consecutive trips from $i$ to $i$+1 (Yao and Hu 2017).

3.2.4. Statistical analysis

Two-way ANOVA was conducted to test estuarine carbonate system in response to the interaction between hydrologic and spatial variations. Wet/dry condition was chosen as a variable to test the significance of hydrologic change, location (four estuaries) was chosen to test

the spatial change significance. Probabilities ($p$) of <0.05 were considered significant, assumptions of normality and homogeneity were met before two-way ANOVA.

3.3. Results

3.3.1. River discharge

During each month of field campaigns, cumulative monthly mean riverine discharge of each estuary was imported from USGS water gauges (Fig. 3.2a). During our study period, a significant increase in river discharge was recorded in response to major storms in spring-summer 2015; spring-summer 2016; winter-spring 2017, respectively. According to the river discharge and corresponding estuarine salinity behavior (i.e. in LCE average river discharge increased ~250% and salinity decreased ~50% from wet to dry), time periods were categorized into two hydrologic conditions—dry and wet. Wet periods in LCE and GE averaged river discharge rates of 117.4±111.2 and 69.6±13.4 $m^3 \cdot s^{-1}$, respectively, which were about three times discharge rates during dry periods (i.e. 41.9±37.7 and 19.9±9.3 $m^3 \cdot s^{-1}$, respectively). Although total discharge was much less in MAE and NE, these estuaries also experienced spikes in discharge that could be categorized into the same dry and wet seasons, with increases from 0.5 ±0.6 to 10.7±11.6 $m^3 \cdot s^{-1}$ and 4.9±3.5 to 25.0±34.5 $m^3 \cdot s^{-1}$, respectively.

A freshwater inflow gradient was observed, with approximately one order of magnitude decline from northern (annual discharge 116.4±143.7 $m^3 \cdot s^{-1}$ for LCE) to southern (annual discharge 9.9±19.2 $m^3 \cdot s^{-1}$ for NE) estuaries (Fig. 3.2a).

3.3.2. Salinity

Large temporal and spatial differences in salinity were observed in these estuaries because of differences in freshwater inflow (Tables 3.1&3.2). Consistent with the freshwater discharge, salinity was lower in the north (19.1±8.4 in LCE and 15.3±9.6 in GE) and higher in the south

(24.6±9.6 in MAE and 31.2±4.3 in NE). In addition, the fall season had the highest average salinity for the entire area, possibly because of low freshwater inflow and relatively high evaporation. Hypersalinity (salinity greater the ocean end-member salinity 36.5) occurred in upper MAE and NE between summer and fall 2014, which marked the end of a multiyear drought.

3.3.3. Dissolved oxygen concentration

No hypoxia was observed during our study period. The water column from all estuaries had the highest DO (316.2±110.1 μmol·kg$^{-1}$; n=139) in winter and the lowest average (207.1±37.7 μmol·kg$^{-1}$; n=139) in summer. In addition, DO concentration decreased from northern (254.4± 88.5 μmol·kg$^{-1}$ in LCE annually) to southern estuaries (lowest 223.1±33.9 μmol·kg$^{-1}$ for NE annually).

3.3.4. Estuarine carbonate system

TA and DIC showed strong seasonal and spatial variations in the studied estuaries (Table 3.1, Fig. 3.3a—b). For example, GE had the highest TA and DIC (annual average 3053.6±354.3 μmol·kg$^{-1}$ and 2733.1±391.7 μmol·kg$^{-1}$, respectively), whereas LCE had the lowest TA and DIC (annual average 2418.3±444.4 μmol·kg$^{-1}$ and 2178.6±388.5 μmol·kg$^{-1}$). Strong interaction of hydrology:location ($p$<0.001, Table 3.2) reflected different responses to flooding condition in these estuaries. In LCE and MAE, TA and DIC decreased ~200 μmol·kg$^{-1}$ after the flood. In GE, however, both TA and DIC increased ~400 μmol·kg$^{-1}$ after the flood. In NE, neither of these parameters showed substantial changes (Table 3.1).

Highest and lowest pH of the entire studied area were found in winter (8.22±0.26) and summer (8.04±0.14), respectively. pH in GE was higher than other estuaries, with an

exceptionally high level 8.50±0.27 observed in winter. LCE and GE experienced large variations in pH between dry and wet conditions, with pH decreasing after a flood by an average of 0.13 (LCE) and 0.05 (GE), respectively. In contrast, pH remained stable in MAE and NE despite changed in hydrologic condition.

A decreasing trend in $pCO_2$ was observed from northern to southern estuaries, with the highest annual mean in LCE (595.1±559.8 μatm) and lowest annual in NE (419.8±106.5 μatm). Despite various temporal TA and DIC changes in different estuaries, $pCO_2$ displayed a consistent seasonality throughout the studied estuaries, higher in spring (567.0±427.8 μatm) and summer (584.6±270.6 μatm), lower in fall (424.8±96.4 μatm) and winter (390.0±236.1 μatm). There was clear hydrologic and spatial interaction on $pCO_2$ in these estuaries (Table 3.2). From dry to wet condition, average $pCO_2$ almost doubled in LCE and GE (Table 3.1), while it increased only ~100 μatm in MAE and showed no substantial change in NE. Thus, $pCO_2$ in LCE and GE had larger temporal variations than MAE and NE (Fig. 3.3c).

3.3.5. Carbonate chemistry of river and ocean end-members

Carbonate chemistry data of the river end-member came from river campaigns, while ocean end-member data came from TCEQ quarterly field campaigns. Both TA and DIC displayed spatiotemporal variability in river and ocean end-members (Table 3.3). For example, TA and DIC concentrations were exceptionally high (3000—4500 $\mu mol \cdot kg^{-1}$) at all river mouths in dry conditions. In contrast, riverine TA and DIC concentrations substantially declined in wet conditions (both decreased 1500—3500 $\mu mol \cdot kg^{-1}$). The only exception was NE, in which minor change (~200 $\mu mol \cdot kg^{-1}$ lower) in riverine TA and DIC were observed under wet conditions. Compared to the river endmembers, the ocean endmember had little fluctuation in TA and DIC, with ~200 $\mu mol \cdot kg^{-1}$ decrease in wet conditions.

Higher (7.85—8.06) and lower (7.37—7.89) pH ranges were observed from river endmembers during dry and wet periods, respectively, whereas pH in the ocean end-member showed slight increase, i.e., from 8.05±0.07 in dry conditions to 8.14±0.09 in wet conditions.

3.3.6. Air-water $CO_2$ flux

Annual mean air-water $CO_2$ flux decreased by one order of magnitude moving from north to south, i.e., 25.6±28.9 $mol \cdot C \cdot m^{-2} \cdot y^{-1}$ in LCE and 2.7±8.1 $mol \cdot C \cdot m^{-2} \cdot y^{-1}$ in NE (Fig. 3.2b). In addition, $CO_2$ flux closely followed river discharge patterns (Fig. 3.2a&b). Especially in LCE and GE, $CO_2$ flux was greatly elevated by increased riverine inflow. LCE, MAE and NE had similar $CO_2$ fluxes in dry condition (~20 $mmol \cdot C \cdot m^{-2} \cdot d^{-1}$) but varied largely when it was wet. There were significant hydrologic and spatial differences in $pCO_2$, and there was also significant interaction between hydrologic and spatial controls ($p<0.001$, Table 3.2). LCE and GE both experienced large increases in $CO_2$ flux from dry to wet conditions (18.3±54.1 to 167.1±369.1 $mmol \cdot C \cdot m^{-2} \cdot d^{-1}$ and -0.7±42.5 to 167.1±369.1 $mmol \cdot C \cdot m^{-2} \cdot d^{-1}$, respectively). In comparison, $CO_2$ flux in MAE showed smaller increase from dry to wet conditions (16.9±34.5 to 40.1±72.0 $mmol \cdot C \cdot m^{-2} \cdot d^{-1}$), and $CO_2$ flux in NE barely changed (17.8±67.2 to 20.2±62.3 $mmol \cdot C \cdot m^{-2} \cdot d^{-1}$).

3.4. Discussion

3.4.1. DIC and TA variations under dry and wet conditions

Our sampling period started during a drought period in 2014 with limited river discharge until the drought ended in spring 2015, when the estuaries experienced a large increase in river discharge (Fig. 3.2a). For the remainder of the sampling period, the entire area fluctuated between wet and dry conditions intermittently.

Rivers in this semiarid area have been studied as potentially important DIC and $CO_2$ sources (Butman and Raymond 2011; Zeng et al. 2011), and our study further illustrated temporal and spatial variations of riverine inputs (Fig. 3.4). Riverine DIC of LCE was 3174.5±340.6 $\mu mol \cdot kg^{-1}$ in dry conditions (Table 3.3), close to the value reported in another study in this area (~2800 in Zeng et al. 2011). All rivers were enriched in DIC and TA compared to downstream estuaries and their ocean endmember, presumably due to high bedrock weathering and evaporation in this region (Stets et al. 2014; Zeng et al. 2011). However, during the wet period, intense flooding strongly diluted riverine DIC and TA (Table 3.3; Fig. 3.4b&f), which agreed with other studies in this region (Montagna et al. 2018; Mooney and McClelland 2012). This dilution effect varied significantly across this entire region, from the strongest in MAE (both TA and DIC were diluted more than half, ~2800 $\mu mol \cdot kg^{-1}$), to the weakest in NE (decreased 200 $\mu mol \cdot kg^{-1}$). Therefore, riverine inflow might contribute to estuarine carbonate chemistry differently between estuaries and hydrologic regimes and should be further examined in future estuarine research.

Estuarine carbonate system variability is affected by the mixing of riverine and oceanic endmembers as well as estuarine biogeochemical processes. Two end-member mixing models can be used to examine allochthonous and autochthonous dissolved constituents in order to analyze conservative/nonconservative behaviors (Bianchi 2012). Considering the relatively long residence times of these estuaries, especially in southern estuary MAE and NE (~360 d; Table 3.3), uncertainties for riverine DIC and TA were within range of 150~550 $\mu mol \cdot kg^{-1}$ for all estuaries (Table 3.3). By excluding that, DIC and TA still followed salinity change quite obviously (in variety of 1000—2000 $\mu mol \cdot kg^{-1}$; Fig. 3.4a—h), which reveals a clear mixing

scenario from river mouth to tidal inlet. Therefore we followed Jiang et al. (2008) method, DIC due to two endmembers (river and ocean) mixing at station *i* ($DIC^{r+o}_{mix/i}$) can be estimated as:

$$DIC^{r+o}_{mix/i} = \frac{(Sal_{ocean} - Sal_i) \times DIC_{river} + (Sal_i - Sal_{river}) \times DIC_{ocean}}{Sal_{ocean} - Sal_{river}} \quad (5)$$

where $DIC_{river}$ and $Sal_{river}$ are river end-member DIC and Salinity; $DIC_{ocean}$ and $Sal_{ocean}$ are ocean end-member DIC and Salinity; $Sal_i$$Sal_i$ is salinity at station *i*, $Sal_{i-1}$$Sal_{i-1}$ is salinity at station *i* from last field campaign. However, Eq. 5 is not applicable in estuaries under hypersaline conditions when evaporation effect exceeds limited riverine input. Therefore, an evaporation-based equation was derived only for hypersaline water (S>36.5):

$$DIC^{r+o}_{mix/i} = \frac{Sal_i}{Sal_{i-1}} \times DIC_{i-1} \quad (6)$$

$DIC_{i-1}$ also indicates surveyed data at station *i* from last field campaign, then produced/consumed DIC due to estuarine biogeochemical processes ($DIC_{estuarine}$) can be calculated as:

$$DIC_{estuarine} = DIC_i - DIC^{r+o}_{mix/i} \quad (7)$$

DIC due to ocean mixing at station *i* ($DIC^{o}_{mix/i}$$DIC^{o}_{mix}$) can be calculated from:

$$DIC^{o}_{mix/i} = \frac{Sal_i}{Sal_{ocean}} \times DIC_{ocean} \quad (8)$$

Similarly, $TA^{r+o}_{mix/i}$$TA^{r+o}_{mix}$$TA^{r+o}_{mix}$$TA^{r}_{mix}$, $TA^{o}_{mix/i}$$TA^{o}_{mix}$and $TA_{estuarine}$ can be estimated by simply replacing DIC with TA.

As a result of flood, elevated input of river-delivered organic matter would increase estuarine community respiration (CR), which can be followed by enhanced gross primary production (GPP) due to nutrients input (Bruesewitz et al. 2013). Stimulated NEM during wet periods contributed a large variation of $DIC_{estuarine}$ and $TA_{estuarine}$ (-500~1000 μmol·kg$^{-1}$, where positive values are net production and negative values are net consumption, Fig. 3.4d&h) especially in the upper estuaries. The positive $DIC_{estuarine}$ and $TA_{estuarine}$ values for most measurements in the wet period

represented heterotrophic water coupled with other biogeochemical processes. For example, ΔDIC vs. ΔTA (Fig. 3.5) provided the useful insights into drivers of DIC and TA dynamics (Liu et al. 2017; Sippo et al. 2016). The majority of ΔDIC/ΔTA ratios in wet period (Fig. 3.5) ranged between slopes that would be expected for a combination of aerobic respiration (-0.2), denitrification (0.9), and calcium dissolution (2). All three processes have been well studied in this area during wet period (Bruesewitz et al. 2013; Murgulet et al. 2018; Russell et al. 2006). This overall net heterotrophy also helps explain the calculated positive air-water $CO_2$ flux in wet condition (Fig. 3.4l). In addition, consistent with the riverine DIC and TA variations, few samples in LCE and MAE displayed strong dilution effect (1.2) leading ΔDIC/ΔTA change during large flood (S<5, Fig. 3.5).

By contrast, a small number of negative $DIC_{estuarine}$ and $TA_{estuarine}$ near river mouths (S<10, Fig. 3.4d and 3.4h) indicated a net consumption resulted from the transition to net autotrophy. Such resilience extended through the following relaxation of flood. Particularly near the river mouth, DIC and TA consumption could amount to a maximum of -2000 $\mu mol \cdot kg^{-1}$ in dry conditions (Fig. 3.4c and 3.4g). At this time ΔDIC/ΔTA (Fig 3.5) was mainly influenced by photosynthesis (-0.2), calcium precipitation (2), and nitrification (-∞). Sustained high levels of phytoplankton (Reyna et al. 2017) and particulate organic carbon (Mooney and McClelland 2012) in the region indicated that autotrophy is favored. An and Joye (2001) also reported convincing evidence of nitrification being stimulated (tenfold higher, up to 12.85 $mmol \cdot m^{-2} \cdot d^{-1}$) by benthic photosynthesis in adjacent shallow estuarine sediment. It is reasonable to expect such enhancement occurred in water column when phytoplankton accumulated after flood. On the other hand, as Texas estuaries support commercial oyster landings, calcium precipitation may be an important process that could decrease both $DIC_{estuarine}$ and $TA_{estuarine}$ in dry condition

(Murgulet et al. 2018). However, detailed explorations of C and N co-variation in response to hydrologic change are necessary to better understand the biogeochemistry at play, rather than solely relying on stoichiometry.

Hypersalinity occurred in upper MAE and NE during May 2014 and October 2014, when salinity exceeded average ocean end-member in our studied area (shown as S>36.5 in Fig. 3.4a, 3.4c, 3.4e, 3.4g, 3.4i, 3.4k). During the dry period, TA/DIC ratio increased along with salinity and exceeded the ocean end-member value (1.1), indicating that DIC decreased at higher rate than TA. Variable but higher $CO_2$ effluxes revealed a rising trend of $CO_2$ degassing at higher salinity (S>35, Fig. 3.4k). This is consistent with our previous study that evaporated water is less capable of holding dissolved $CO_2$, thus $CO_2$ efflux increased under high wind conditions (Yao and Hu 2017). This $CO_2$ efflux should contribute to DIC loss ($DIC_{estuarine}$<0; Fig. 3.4c). We also observed TA consumption with rising salinity under dry conditions (Fig. 3.4e&g), consistent with a previous study on the net alkalinity loss during hypersaline conditions (Hu et al. 2015; Murgulet et al. 2018). Negative $TA_{estuarine}$ was expected from increasing ammonium (up to 100 $\mu mol \cdot m^{-2} \cdot h^{-1}$) release and sulfide accumulation (~40 $\mu mol \cdot kg^{-1}$) at sediment-water interface, as a result of enhanced dissimilatory nitrate reduction to ammonium (DNRA) when the environment reached hypersalinity in NE (Gardner et al. 2006). Meanwhile, no hypoxia was observed throughout our entire study period, indicating the potentially nitrification and sulfide oxidation in water column. Therefore, $\Delta DIC/\Delta TA$ range in hypersalinity ($-\infty$ and 1.2 when S>36.5 in MAE and NE, Fig. 3.5) could be attributed to nitrification/sulfide oxidation ($-\infty$) and evaporation (1.2).

3.4.2. River-borne, ocean-borne, and estuarine generated $CO_2$

We categorized $[CO_2]_o$, $[CO_2]_r$, and $[CO_2]_e$ to represent ocean-borne $[CO_2]$, river-borne $[CO_2]$ and estuarine produced $[CO_2]$, respectively. Because aqueous $CO_2$ ($[CO_2]$) does not mix

conservatively, $[CO_2]_r$ is the difference between $[CO_2]_{mixing\ w/R}$ and $[CO_2]_{mixing\ w/o}$ (Jiang et al. 2008). In which $[CO_2]_{mixing\ w/R}$ was the aqueous $CO_2$ concentration if conservative mixing occurred between river and ocean end-members, calculated using $DIC^{r+o}_{mix/i}$ and $TA^{r+o}_{mix/i}$; $[CO_2]_{mixing\ w/o}$ was the aqueous $CO_2$ concentration if only ocean end-member was diluted by zero DIC freshwater, calculated by $DIC^{o}_{mix/i}$ and $TA^{o}_{mix/i}$. $[CO_2]_e$ ($CO_2$ change due to estuarine biogeochemical reactions) was calculated by the difference between actual $[CO_2]$ based on field data and $[CO_2]_{mixing\ w/R}$. Since $[CO_2]$ was subject to water temperature changes, all categorized $[CO_2]$ were normalized to the average temperature (23.9 °C) to eliminate the thermal effect (Jiang et al. 2008). TA in these estuarine waters contains non-carbonate species, which would lead to an underestimation of $CO_2$ concentration if using TA and DIC as input variables, for example, including 50 μmol·kg$^{-1}$ (an average ΔTA from our surveys) of non-carbonate alkalinity in the TA input would decrease calculated $[CO_2]$ by 3.0 μmol·kg$^{-1}$ at salinity 23.3 and temperature 24.1 (all average values). Nevertheless, this exercise would still be useful for qualitatively tracking the dynamic of $CO_2$ flux in aquatic system especially for $[CO_2]$ mixing from multiple sources (Jiang et al. 2008).

Area-weighted average $[CO_2]$ for each sampling trip was calculated (arithmetic mean of stations in each bay, then multiplied by bay area), the three $[CO_2]$ categories displayed significant temporal and spatial distributions (Fig. 3.6, Table 3.2). When $[CO_2]_r$ accounted for more than 50% of $[CO_2]$ the scenario was considered river-dominated, and when $[CO_2]_o$ accounted for more than 50% of $[CO_2]$ the scenario was considered ocean-dominated. These estuaries displayed scenarios between river-dominated and ocean-dominated, mostly depending on hydrologic conditions. For instance, river discharge was two orders of magnitude lower in NE and MAE than LCE and GE (Fig. 3.2a). This directly led to a $[CO_2]_r$ that was 89.2% higher in

GE (30.5±9.1 μmol·kg$^{-1}$) than NE (3.3±2.7 μmol·kg$^{-1}$) and a $[CO_2]_o$ 46.1% lower annually in GE (7.3±4.0 μmol·kg$^{-1}$) than NE (15.8±1.1 μmol·kg$^{-1}$) on the annual scale. As a result, GE was river-dominated throughout the entire study period (Fig. 3.6b). In contrast, NE was clearly an ocean-dominated estuary at all times (Fig. 3.6d), primarily due to anthropogenic disruptions (i.e. dam construction and river fragmentation; Murgulet et al. 2016) that limited freshwater inflow into this estuary resulting in a more negative freshwater balance (Montagna et al. 2012). LCE and MAE exhibited both river-dominated and ocean-dominated scenarios depending on hydrologic condition (Fig. 3.6a&c).

Interestingly, all four estuaries responded differently to hydrologic condition changes (Fig. 3.7). First, as expected, $CO_2$ flux was closely correlated to $[CO_2]_r$ in this region during flooding (Fig. 3.7a—d). $CO_2$ effluxes increased exponentially with more $[CO_2]_r$ flushing into LCE, GE and MAE at river-dominated state (wet condition of Fig. 3.7a—c). This agrees with previous studies that have suggested that river-borne $CO_2$ ventilation predominates $CO_2$ emission in river-dominated estuaries (Borges et al. 2006). However, Borges et al. (2006) also asserted that river-borne $CO_2$ ventilation will decrease exponentially with longer residence, but even in NE where ocean-dominated condition prevailed most of the time, $[CO_2]_r$ was still found important to $CO_2$ flux in wet condition ($R^2$=0.403, $p$=0.038, Fig. 3.7d). While Jiang et al. (2008) showed strong correlation between $[CO_2]_r$ and $CO_2$ flux in two river-dominated estuaries, it appears that ventilation of river-borne $CO_2$ was not the main control on $CO_2$ flux ($R^2$<0.403 for both dry and wet condition; Fig. 3.7a—d).

$[CO_2]_e$, an indication for estuarine biogeochemical processes, played a crucial role in determining $CO_2$ flux of this region (Fig. 3.7i—l). For example, $CO_2$ flux in MAE was controlled mainly by $[CO_2]_e$ both in drought and wet condition ($R^2$=0.801 and 0.960,

respectively; $p<0.001$ for both, Fig. 3.7k). Likewise, $[CO_2]_e$ contributed significantly in other studied estuaries ($p<0.05$ for all cases; Fig. 3.7i—j, l) especially in wet periods. Due to long residence time (40—360 d; Solis and Powell 1999), pulses of riverine inflows could generate profound influences in oligotrophic systems, i.e., surging of river inflows elevated $CO_2$ flux during flooding, by contrast $CO_2$ flux on annual scale fell, potentially as phytoplankton grew from increasing nutrients after floods. Particularly, both $DIC_{estuarine}$ and categorized $[CO_2]$ revealed a stronger autotrophy in mild drought after major storm (seen as $DIC_{estuarine}$ ranged -2000—-1000 $\mu mol \cdot kg^{-1}$ in salinity 10—20, Fig. 3.4c; area-weighted $[CO_2]_e$ in all estuaries ranged -15—-45 $\mu mol \cdot kg^{-1}$ in Fall 2015, Fig. 3.6). This dominating autotrophy in drought favored a similar $CO_2$ flux among LCE, MAE and NE (~18.0 $mmol \cdot C \cdot m^{-2} \cdot d^{-1}$). GE was found even as $CO_2$ sink (-0.7±42.5 $mmol \cdot C \cdot m^{-2} \cdot d^{-1}$), despite that its river discharge was one order magnitude greater than MAE and NE.

Even though ocean-dominated scenario was identified in LCE, MAE and NE (Fig. 3.6a, c—d), the lack of significant correlation between $[CO_2]_o$ and $CO_2$ flux suggested that $[CO_2]_o$ was the least strong control on $CO_2$ flux in this area (Fig. 3.7e—h). The only exception was LCE, in which $[CO_2]_o$ was significantly related to $CO_2$ flux ($p=0.014$ for drought and $p=0.002$ for wet period; Fig. 3.7e). LCE may be the exception because of less organic matter from decreasing riverine input (seen as lower $[CO_2]_r$; Fig. 3.6a), which further led to lower $[CO_2]_e$ (Fig. 3.6a). $[CO_2]_e$ was most important for $CO_2$ flux of LCE ($R^2=0.646$ and 0.952 for dry and wet condition, respectively; Fig. 3.7i).

3.4.3. Annual and seasonal $CO_2$ flux

Based on the past three years of data, our studied nwGOM estuaries acted as an overall $CO_2$ source (Table 3.4; Fig. 3.2). By applying area-weighted average method (Eq. 4), annual air-water

$CO_2$ flux from the entire system reached 16.6±17.1 $mol \cdot C \cdot m^{-2} \cdot y^{-1}$, with approximately an order of magnitude decline between northern estuaries and southern estuaries (i.e., from 25.6 $mol \cdot C \cdot m^{-2} \cdot yr^{-1}$ in LCE to 2.7 $mol \cdot C \cdot m^{-2} \cdot yr^{-1}$ in NE, Table 3.4). This value agreed with an earlier estimation on $CO_2$ flux in global lagoonal estuaries (17.3±16.6 $mol \cdot C \cdot m^{-2} \cdot y^{-1}$; Laruelle et al. 2010). On the other hand, Chen et al. (2013) summarized that average $CO_2$ flux in North American estuaries is 2.2 $mol \cdot C \cdot m^{-2} \cdot y^{-1}$, although they based their study mostly on estuaries on the east coast. Furthermore, annual $CO_2$ flux in MAE during this three years was 6.9±6.5 $mol \cdot C \cdot m^{-2} \cdot y^{-1}$, much lower than 12.4±3.3 $mol \cdot C \cdot m^{-2} \cdot y^{-1}$ from our previous study that sampled between May 2014 and April 2015, in which the drought condition was studied ahead of major storm in April 2015 (Yao and Hu 2017). In this longer time series, it is likely that increasing riverine input might have brought in nutrients, which enhanced autotrophic production and reduced $CO_2$ emission, especially in the period when flood influence dissipated and the estuary turned to an ocean-dominated condition. Moreover, wind condition has also played a crucial role on estuarine $CO_2$ flux. This windy and shallow environment favored air-water gas exchange even though average $pCO_2$ was not much greater than the atmospheric values (Table 3.1). However, gas transfer velocity was a wind dependent function (Eq. 3) that was originally derived from the open ocean (Wanninkhof 1992). So far no consensus has been reached on directly measured gas transfer velocity in rivers and estuaries, therefore a better gas transfer velocity measurement is crucial to developing more accurate $CO_2$ flux estimates in future estuarine research since quantifying turbulence is more complicated in such dynamic areas (Jiang et al. 2008; Raymond and Cole 2001; Rosentreter et al. 2017). Regardless, the comparison between the two data series with different temporal coverages highlighted the dynamic nature of estuarine environments and the hydrologic control exerted by connecting rivers.

Not only did estuarine $CO_2$ flux in the nwGOM vary spatially, it also exhibited strong seasonality (Table 3.4; Fig. 3.8a). In this study, strong $CO_2$ efflux in spring and summer weakened and turned to influx in fall and winter (Table 3.4; Fig. 3.8a). It was expected that large riverine inflows from three major storms in conjunction with high wind speeds (data not shown) resulted in strong seasonal $CO_2$ efflux in spring and summer. After the river flood influence subsided, net autotrophy (as demonstrated by widespread high pH, low $pCO_2$, and negative $[CO_2]_e$ (Table 3.1; Fig. 3.6) contributed to a significantly diminished $CO_2$ efflux in fall (Fig. 3.8a). Water temperature decreased from fall to winter along with $pCO_2$ and $CO_2$ flux. An approximately 10°C decline in temperature could result in ~200 μatm decrease in $pCO_2$ in MAE (Yao and Hu 2017). Together, the least windy condition in winter and low estuarine $pCO_2$ resulted in a moderate to weak $CO_2$ sink in these estuaries (Fig. 3.8a). Larger $pCO_2$ decline was expected in more fresh estuary LCE and GE (Table 3.1), since this thermal effect was also salinity-related, i.e. temperature-normalized $pCO_2$ would decrease in low salinity region with smaller coefficient ($\partial \ln pCO_2/\partial T$), (Joesoef et al. 2015). Therefore, the $CO_2$ flux reversal in winter appears to be controlled more by weather condition (temperature and wind) than biological activities. For example, $CO_2$ flux dropped ~20 mmol· $C \cdot m^{-2} \cdot d^{-1}$ in GE and MAE from fall to winter (Table 3.4), yet $[CO_2]_r$ and $[CO_2]_e$ remained similar levels (Fig. 3.8c&d). However, hydrologic change should be highlighted over thermal effect. To be more specific, as a result of raised river inflows ($[CO_2]_r$ increased from 8.3±3.1 to 14.3±6.5 $\mu mol \cdot kg^{-1}$; Fig. 3.8b), seasonal $CO_2$ efflux in LCE still doubled from fall to winter despite high variation (from 24.4±44.5 to 53.5±178.7 mmol· $C \cdot m^{-2} \cdot d^{-1}$, Table 3.4).

## 3.5. Conclusions

Our study covered a range of extreme hydrologic conditions from drought to flooding and estuarine types from river-dominated to ocean-dominated. In general, nwGOM estuaries LCE, GE, MAE and NE are a $CO_2$ source on the annual scale with large temporal and spatial variations. About an order of magnitude decline in annual average air-water $CO_2$ flux was observed from north to south. Prominent $CO_2$ degassing in spring and summer resulted from large freshwater inflow events and high wind conditions; whereas $CO_2$ flux reversed in fall and winter, from moderate $CO_2$ source to $CO_2$ sink. Hydrologic and climatic influences, such as river discharge, wind speed and water temperature played important roles. Both negatively varying estuarine DIC and [$CO_2$] implied overall autotrophy to largely offset nutrients and $CO_2$-riched water after summer flooding. In addition, $CO_2$ emission was elevated by evaporation and high wind speed, which further led to net DIC consumption in hypersaline water. Net TA consumption appears to be more associated with other elementary cycles such as nitrogen and sulfur. Overall, our findings indicate that estuarine carbon cycle variability is highly dependent on estuarine hydrologic condition, and more comprehensive studies should be done to further assess this effect in a broader context.

References

Abril, G. and others 2015. Technical Note: Large overestimation of $pCO_2$ calculated from pH and alkalinity in acidic, organic-rich freshwaters. Biogeosciences **12:** 67-78.

An, S., and S. B. Joye. 2001. Enhancement of coupled nitrification□denitrification by benthic photosynthesis in shallow estuarine sediments. Limnology and oceanography **46:** 62-74.

Bauer, J. E., W. J. Cai, P. A. Raymond, T. S. Bianchi, C. S. Hopkinson, and P. A. Regnier. 2013. The changing carbon cycle of the coastal ocean. Nature **504:** 61-70.

Bianchi, T. S. 2012. Estuarine chemistry, p. 39-83. Estuarine Ecology.

Borges, A. V., L. S. Schiettecatte, G. Abril, B. Delille, and F. Gazeau. 2006. Carbon dioxide in European coastal waters. Estuarine, Coastal and Shelf Science **70:** 375-387.

Boynton, W., L. Murray, J. Hagy, C. Stokes, and W. Kemp. 1996. A comparative analysis of eutrophication patterns in a temperate coastal lagoon. Estuaries **19:** 408-421.

Bruesewitz, D. A., W. S. Gardner, R. F. Mooney, L. Pollard, and E. J. Buskey. 2013. Estuarine ecosystem function response to flood and drought in a shallow, semiarid estuary: Nitrogen cycling and ecosystem metabolism. Limnology and Oceanography **58:** 2293-2309.

Butman, D., and P. A. Raymond. 2011. Significant efflux of carbon dioxide from streams and rivers in the United States. Nature Geoscience **4:** 839-842.

Carter, B. R., J. A. Radich, H. L. Doyle, and A. G. Dickson. 2013. An automated system for spectrophotometric seawater pH measurements. Limnology and Oceanography: Methods **11:** 16-27.

Chen, C. T. A., T. H. Huang, Y. C. Chen, Y. Bai, X. He, and Y. Kang. 2013. Air–sea exchanges of $CO_2$ in the world's coastal seas. Biogeosciences **10:** 6509-6544.

Cromwell, J. E. 1971. Barrier coast distribution: a world-wide survey. Abstracts, Second Coastal and Shallow Water Research Conference, US Office of Naval Research Geography Program, University Press, University of Southern California, Los Angeles, California.

Crosswell, J. R. and others 2017. Carbon budget of a shallow, lagoonal estuary: Transformations and source-sink dynamics along the river-estuary-ocean continuum. Limnology and Oceanography **62:** S29-S45.

Crosswell, J. R., M. S. Wetz, B. Hales, and H. W. Paerl. 2012. Air-water $CO_2$ fluxes in the microtidal Neuse River Estuary, North Carolina. Journal of Geophysical Research: Oceans **117:** doi:10.1029/2012jc007925.

Dickson, A. G. 1990. Standard potential of the reaction: $AgCl(s)+ 12H_2(g)= Ag(s)+ HCl(aq)$, and and the standard acidity constant of the ion $HSO_4^-$ in synthetic sea water from 273.15 to 318.15 K. The Journal of Chemical Thermodynamics **22:** 113-127.

Dickson, A. G., J. D. Afghan, and G. C. Anderson. 2003. Reference materials for oceanic $CO_2$ analysis: a method for the certification of total alkalinity. Marine Chemistry **80:** 185-197.

Dickson, A. G., C. L. Sabine, and J. R. Christian. 2007. Guide to Best Practices for Ocean $CO_2$ Measurements. North Pacific Marine Science Organization.

Dürr, H. H., G. G. Laruelle, C. M. van Kempen, C. P. Slomp, M. Meybeck, and H. Middelkoop. 2011. Worldwide typology of nearshore coastal systems: Defining the estuarine filter of river inputs to the oceans. Estuaries and Coasts **34:** 441-458.

Fagan, K. E., and F. T. Mackenzie. 2007. Air–sea $CO_2$ exchange in a subtropical estuarine-coral reef system, Kaneohe Bay, Oahu, Hawaii. Marine Chemistry **106:** 174-191.

Gardner, W. S., M. J. McCarthy, S. An, D. Sobolev, K. S. Sell, and D. Brock. 2006. Nitrogen fixation and dissimilatory nitrate reduction to ammonium (DNRA) support nitrogen dynamics in Texas estuaries. Limnology and Oceanography **51:** 558-568.

Gran, G. 1952. Determination of the equivalence point in potentiometric titrations. Part II. Analyst **77:** 661-671.

Ho, D. T., N. Coffineau, B. Hickman, N. Chow, T. Koffman, and P. Schlosser. 2016. Influence of current velocity and wind speed on air□water gas exchange in a mangrove estuary. Geophysical Research Letters **43:** 3813-3821.

Hsu, S. A., E. A. Meindl, and D. B. Gilhousen. 1994. Determining the power-law wind-profile exponent under near-neutral stability conditions at sea. Journal of Applied Meteorology **33:** 757-765.

Hu, X., J. B. Pollack, M. R. McCutcheon, P. A. Montagna, and Z. Ouyang. 2015. Long-term alkalinity decrease and acidification of estuaries in northwestern Gulf of Mexico. Environmental Science & Technology **49:** 3401-3409.

Hunt, C. W., J. E. Salisbury, D. Vandemark, and W. McGillis. 2010. Contrasting Carbon Dioxide Inputs and Exchange in Three Adjacent New England Estuaries. Estuaries and Coasts **34:** 68-77.

Jiang, L. Q., W. J. Cai, and Y. Wang. 2008. A comparative study of carbon dioxide degassing in river- and marine-dominated estuaries. Limnology and Oceanography **53:** 2603-2615.

Joesoef, A., W. J. Huang, Y. Gao, and W. J. Cai. 2015. Air–water fluxes and sources of carbon dioxide in the Delaware Estuary: spatial and seasonal variability. Biogeosciences **12:** 6085-6101.

Koné, Y.-M., and A. Borges. 2008. Dissolved inorganic carbon dynamics in the waters surrounding forested mangroves of the Ca Mau Province (Vietnam). Estuarine, Coastal and Shelf Science **77:** 409-421.

Laruelle, G. G., H. H. Dürr, C. P. Slomp, and A. V. Borges. 2010. Evaluation of sinks and sources of $CO_2$ in the global coastal ocean using a spatially-explicit typology of estuaries and continental shelves. Geophysical Research Letters **37**.

Lewis, E., D. Wallace, and L. J. Allison. 1998. Program Developed for $CO_2$ System Calculations. Carbon Dioxide Information Analysis Center, managed by Lockheed Martin Energy Research Corporation for the US Department of Energy Tennessee.

Liu, Q. and others 2017. Carbonate system biogeochemistry in a subterranean estuary – Waquoit Bay, USA. Geochimica et Cosmochimica Acta **203:** 422-439.

Longley, W. L. 1994. Freshwater Inflows to Texas Bays and Estuaries: Ecological Relationships and Methods for Determination of Needs. Texas Water Development Board and Texas Parks and Wildlife Department.

Millero, F. J. 2010. Carbonate constants for estuarine waters. Marine and Freshwater Research **61:** 139-142.

Millero, F. J., W. T. Hiscock, F. Huang, M. Roche, and J. Z. Zhang. 2001. Seasonal variation of the carbonate system in Florida Bay. Bulletin of Marine Science **68:** 101-123.

Milliman, J. D., K. L. Farnsworth, P. D. Jones, K. H. Xu, and L. C. Smith. 2008. Climatic and anthropogenic factors affecting river discharge to the global ocean, 1951–2000. Global and Planetary Change **62:** 187-194.

Montagna, P., T. A. Palmer, and J. Pollack. 2012. Hydrological Changes and Estuarine Dynamics Springer Science & Business Media.

Montagna, P. A., X. Hu, T. A. Palmer, and M. Wetz. 2018. Effect of hydrological variability on the biogeochemistry of estuaries across a regional climatic gradient. Limnology and Oceanography **63:** 2465-2478.

Mooney, R. F., and J. W. McClelland. 2012. Watershed Export Events and Ecosystem Responses in the Mission–Aransas National Estuarine Research Reserve, South Texas. Estuaries and Coasts **35:** 1468-1485.

Murgulet, D., V. Murgulet, N. Spalt, A. Douglas, and R. G. Hay. 2016. Impact of hydrological alterations on river-groundwater exchange and water quality in a semi-arid area: Nueces River, Texas. Science of the Total Environment **572:** 595-607.

Murgulet, D., M. Trevino, A. Douglas, N. Spalt, X. Hu, and V. Murgulet. 2018. Temporal and spatial fluctuations of groundwater-derived alkalinity fluxes to a semiarid coastal embayment. Science of the Total Environment **630:** 1343-1359.

Orr, J. C., J.-M. Epitalon, A. G. Dickson, and J.-P. Gattuso. 2018. Routine uncertainty propagation for the marine carbon dioxide system. Marine Chemistry **207:** 84-107.

Peterson, D. H. 1979. Sources and sinks of biologically reactive oxygen, carbon, nitrogen, and silica in northern San Francisco Bay, p. 175-194. San Francisco Bay - the urbanized estuary. American Association for the Advancement of Science- Pacific Division.

Raymond, P. A., J. E. Bauer, and J. J. Cole. 2000. Atmospheric $CO_2$ evasion, dissolved inorganic carbon production, and net heterotrophy in the York River estuary. Limnology and Oceanography **45:** 1707-1717.

Raymond, P. A., and J. J. Cole. 2001. Gas exchange in rivers and estuaries: Choosing a gas transfer velocity. Estuaries and Coasts **24:** 312-317.

Reyna, N. E., A. Hardison, and Z. Liu. 2017. Influence of major storm events on the quantity and composition of particulate organic matter and the phytoplankton community in a subtropical estuary, Texas. Frontiers in Marine Science **4:** doi:10.3389/fmars.2017.00043.

Rosentreter, J. A., D. T. Maher, D. T. Ho, M. Call, J. G. Barr, and B. D. Eyre. 2017. Spatial and temporal variability of $CO_2$ and $CH_4$ gas transfer velocities and quantification of the CH4 microbubble flux in mangrove dominated estuaries. Limnology and Oceanography **62:** 561-578.

Russell, M. J., and P. A. Montagna. 2007. Spatial and temporal variability and drivers of net ecosystem metabolism in western Gulf of Mexico estuaries. Estuaries and Coasts **30:** 137-153.

Russell, M. J., P. A. Montagna, and R. D. Kalke. 2006. The effect of freshwater inflow on net ecosystem metabolism in Lavaca Bay, Texas. Estuarine, Coastal and Shelf Science **68:** 231-244.

Sippo, J. Z., D. T. Maher, D. R. Tait, C. Holloway, and I. R. Santos. 2016. Are mangroves drivers or buffers of coastal acidification? Insights from alkalinity and dissolved inorganic carbon export estimates across a latitudinal transect. Global Biogeochemical Cycles **30:** 753-766.

Solis, R., and G. Powell. 1999. Hydrography, mixing characteristics, and residence times of Gulf of Mexico estuaries, p. 29-61. Biogeochemistry of Gulf of Mexico estuaries. John Wiley & Sons.

Stets, E. G., V. J. Kelly, and C. G. Crawford. 2014. Long-term trends in alkalinity in large rivers of the conterminous US in relation to acidification, agriculture, and hydrologic modification. The Science of the total environment **488-489:** 280-289.

Takahashi, T., S. Sutherland, and A. Kozyr. 2012. Global ocean surface water partial pressure of $CO_2$ database: Measurements performed during 1957–2011 (Version 2011). ORNL/CDIAC-160, NDP-088 (V2011), Carbon Dioxide Information Analysis Center, Oak Ridget National Laboratory, US Department of Energy, Oak Ridge, Tennessee.

Wanninkhof, R. 1992. Relationship between wind speed and gas exchange. Journal of Geophysical Research **97:** 7373-7382.

Weiss, R. F. 1974. Carbon dioxide in water and seawater: the solubility of a non-ideal gas. Marine Chemistry **2:** 203-215.

Weiss, R. F., and B. A. Price. 1980. Nitrous oxide solubility in water and seawater. Marine Chemistry **8:** 347-359.

Yao, H., and X. Hu. 2017. Responses of carbonate system and $CO_2$ flux to extended drought and intense flooding in a semiarid subtropical estuary. Limnology and Oceanography **62:** S112-S130.

Zeng, F.-W., C. A. Masiello, and W. C. Hockaday. 2011. Controls on the origin and cycling of riverine dissolved inorganic carbon in the Brazos River, Texas. Biogeochemistry **104:** 275-291.

Table 3.1. Hydrologic and carbonate system parameters in four nwGOM estuaries (April 2014-February 2017).

| Variable | Estuary | Spring | Summer | Fall | Winter | Annual | Dry | Wet |
|---|---|---|---|---|---|---|---|---|
| Temperature (°C) | LCE | 21.6±1.7 | 30.1±0.8 | 27.6±1.0 | 16.0±3.6 | 23.6±5.7 | 22.0±6.9 | 25.1±3.9 |
| | GE | 21.0±1.4 | 29.8±0.4 | 27.1±1.0 | 15.9±3.8 | 23.3±5.6 | 23.1±6.8 | 23.4±4.8 |
| | MAE | 23.1±3.6 | 29.2±1.2 | 25.3±4.5 | 16.0±3.2 | 24.4±5.5 | 23.6±5.5 | 26.8±4.6 |
| | NE | 22.8±1.4 | 30.0±0.7 | 27.2±1.9 | 15.3±4.4 | 23.7±5.9 | 22.9±5.5 | 25.0±6.3 |
| Salinity | LCE | 18.4±8.4 | 15.8±9.7 | 23.2±5.2 | 19.3±8.1 | 19.1±8.4 | 24.3±5.4 | 14.7±8.0 |
| | GE | 14.5±8.5 | 9.6±10.7 | 19.6±8.7 | 17.8±8.2 | 15.3±9.6 | 24.6±5.5 | 9.5±6.7 |
| | MAE | 23.3±7.5 | 24.3±12.6 | 26.1±9.0 | 24.6±7.0 | 24.6±9.6 | 26.9±8.3 | 18.4±10.4 |
| | NE | 31.0±1.9 | 30.1±7.2 | 32.5±4.3 | 31.1±2.5 | 31.2±4.3 | 32.9±3.4 | 28.4±4.2 |
| DO ($\mu mol \cdot kg^{-1}$) | LCE | 252.6±56.6 | 208.5±44.1 | 221.8±21.8 | 335.4±133.5 | 254.4±88.5 | 275.2±112.0 | 236.6±56.3 |
| | GE | 271.7±52.0 | 226.3±31.7 | 238.5±37.2 | 383.2±138.6 | 279.3±96.0 | 282.9±136.5 | 277.1±59.3 |
| | MAE | 229.4±22.9 | 200.8±24.1 | 222.6±37.1 | 261.4±33.9 | 224.0±35.6 | 225.5±37.5 | 219.8±29.6 |
| | NE | 220.5±15.7 | 190.9±31.0 | 207.5±27.8 | 270.2±30.5 | 222.5±38.8 | 223.1±33.9 | 221.5±45.7 |
| pH | LCE | 8.05±0.29 | 7.99±0.18 | 8.09±0.08 | 8.17±0.30 | 8.07±0.24 | 8.14±0.18 | 8.01±0.27 |
| | GE | 8.08±0.18 | 8.13±0.10 | 8.26±0.14 | 8.50±0.27 | 8.23±0.24 | 8.26±0.27 | 8.21±0.22 |
| | MAE | 8.00±0.11 | 8.10±0.11 | 8.10±0.11 | 8.03±0.10 | 8.06±0.12 | 8.06±0.10 | 8.07±0.16 |
| | NE | 8.04±0.09 | 8.06±0.08 | 8.14±0.06 | 8.14±0.08 | 8.09±0.09 | 8.09±0.07 | 8.10±0.12 |
| DIC ($\mu mol \cdot kg^{-1}$) | LCE | 2141.9±440.0 | 2156.7±354.8 | 2281.6±351.8 | 2146.6±374.8 | 2178.6±388.5 | 2271.0±349.9 | 2099.5±403.7 |
| | GE | 2764.4±313.7 | 2936.1±334.4 | 2557.1±341.5 | 2664.5±494.4 | 2733.1±391.7 | 2442.3±299.6 | 2914.9±328.6 |
| | MAE | 2250.7±294.4 | 2188.7±201.1 | 2268.6±207.5 | 2360.4±183.7 | 2254.5±234.5 | 2293.6±203.8 | 2147.0±276.8 |
| | NE | 2231.6±65.7 | 2341.1±229.6 | 2170.5±161.0 | 2269.5±87.5 | 2251.7±155.5 | 2270.3±119.1 | 2222.4±197.5 |
| TA ($\mu mol \cdot kg^{-1}$) | LCE | 2344.7±498.4 | 2384.7±424.4 | 2590.0±374.4 | 2378.5±418.3 | 2418.3±444.4 | 2557.8±356.5 | 2298.8±477.6 |
| | GE | 2998.6±338.0 | 3190.5±287.4 | 2952.6±363.3 | 3091.2±397.0 | 3053.6±354.3 | 2839.1±296.3 | 3187.7±321.5 |
| | MAE | 2481.8±331.9 | 2470.0±239.3 | 2570.9±213.6 | 2608.6±191.6 | 2523.4±259.3 | 2579.0±206.6 | 2370.9±321.7 |
| | NE | 2491.5±97.2 | 2735.3±285.2 | 2599.2±150.9 | 2544.4±87.9 | 2584.5±190.2 | 2603.0±164.8 | 2555.5±223.1 |
| $pCO_{2,water}$ (µatm) | LCE | 681.7±821.3 | 722.2±466.8 | 463.4±126.4 | 484.4±427.9 | 595.1±559.8 | 420.6±164.4 | 744.7±715.6 |
| | GE | 707.8±343.3 | 872.9±407.0 | 355.0±57.9 | 275.2±219.3 | 564.6±377.1 | 364.0±165.7 | 690.0±417.1 |
| | MAE | 527.7±192.3 | 525.8±121.9 | 434.2±80.6 | 381.7±85.0 | 477.6±142.5 | 452.8±98.3 | 546.0±208.3 |
| | NE | 475.2±111.2 | 471.8±76.7 | 351.8±74.4 | 363.9±86.1 | 419.8±106.5 | 419.1±88.6 | 421.0±130.8 |

Table 3.2. Two-way ANOVA tests for different variables in estuarine hydrology and the carbonate system. The factors include hydrological conditions (wet vs. dry) and locations.

| Parameter | df | *F* | *P* |
|---|---|---|---|
| Temperature | 3 | 2.079 | 0.101 |
| DO | 3 | 4.772 | 0.003 |
| Salinity | 3 | 8.657 | <0.001 |
| pH | 3 | 5.513 | <0.001 |
| DIC | 3 | 38.590 | <0.001 |
| TA | 3 | 28.480 | <0.001 |
| $pCO_{2,water}$ | 3 | 13.220 | <0.001 |
| Air-water $CO_2$ flux | 3 | 16.870 | <0.001 |
| $[CO_2]_r$ | 3 | 9.312 | <0.001 |
| $[CO_2]_o$ | 3 | 17.400 | <0.001 |
| $[CO_2]_e$ | 3 | 13.390 | <0.001 |

Table 3.3. Estuarine parameters and carbonate system end-members for each estuary at dry (D) and wet (W) conditions.

| Estuary | Mean Depth (m) | Open Water Area ($km^2$) | Residence Time (d) | Mean Annual Evaporation ($km^3 \cdot yr^{-1}$) | Watershed Area ($10^3$ $km^2$) | Mean Annual Freshwater inflow ($m^3 \cdot s^{-1}$) | Period | DIC ($\mu mol \cdot kg^{-1}$) | TA ($\mu mol \cdot kg^{-1}$) | Salinity | pH | TA/DIC |
|---|---|---|---|---|---|---|---|---|---|---|---|---|
| LCE | 1.1 | 1180.6 | 81 | 1.39 | 130.3 | 107.9 | D | 3174.5±340.6 | 3295.4±321.4 | 4.5±4.7 | 8.06±0.16 | 1.04 |
| | | | | | | | W | 1548.9±434.3 | 1546.5±424.4 | 0.5±0.7 | 7.51±0.22 | 1.00 |
| GE | 1.1 | 561.6 | 39 | 0.78 | 28.1 | 48.3 | D | 4401.4±570.5 | 4324.7±306.5 | 0.4±0.2 | 7.85±0.08 | 0.98 |
| | | | | | | | W | 2564.8±292.1 | 2541.2±291.9 | 0.2±0.0 | 7.50±0.06 | 0.99 |
| MAE | 1.1 | 575.7 | 360 | 0.72 | 7.2 | 7.3 | D | 4661.0±499.6 | 4705.4±491.0 | 0.7±0.1 | 7.87±0.13 | 1.01 |
| | | | | | | | W | 1885.8±255.5 | 1886.1±230.2 | 0.1±0.0 | 7.37±0.01 | 1.00 |
| NE | 1.2 | 536.6 | 356 | 0.83 | 45.6 | 8.6 | D | 3937.5±128.7 | 4061.9±193.6 | 1.7±1.6 | 7.99±0.18 | 1.03 |
| | | | | | | | W | 3729.4±383.7 | 3824.0±406.9 | 0.4±0.3 | 7.89±0.13 | 1.03 |
| Tidal inlet | 5.0 | — | — | — | — | — | D | 2232.4±69.6 | 2460.0±28.3 | 36.5±0.9 | 8.05±0.07 | 1.10 |
| | | | | | | | W | 2094.9±65.2 | 2290.0±70.7 | 29.5±0.2 | 8.14±0.09 | 1.09 |

Data is partially from Solis and Powell (1999) and TWDB (http://www.twdb.texas.gov/surfacewater/bays/coastal_hydrology/index.asp).
D = drought period, W = wet period, dashes "—" = no data.

Table 3.4. Annual and seasonal air-water $CO_2$ fluxes in U.S. estuaries.

| Estuary | Average air-water $CO_2$ flux (*unit*: mol·C·m$^{-2}$·y$^{-1}$ for annual; mmol· C·m$^{-2}$·d$^{-1}$ for seasonal) | | | | | Latitude (°N) | Reference |
|---|---|---|---|---|---|---|---|
| | Annual | Spring (Mar-May) | Summer (Jun-Aug) | Fall (Sep-Nov) | Winter (Dec-Feb) | | |
| [b]Altamaha Sound | 26.8 | 57.8 | 127.0 | 79.7 | 28.5 | 31.3 | (Jiang et al. 2008) |
| [a]Delaware | 2.4±4.8 | -13.7±16.4 | 13.4±22.2 | 2.7±6.6 | 15.6±5.2 | 38.9 | (Joesoef et al. 2015) |
| [b]Florida Bay | 1.7 | | | | | 25.0 | (Millero et al. 2001) |
| [a]Great Bay | 3.6 | | | | | 43.1 | (Hunt et al. 2010) |
| [b]Kaneohe Bay | 1.5 | | | | | 21.4 | (Fagan and Mackenzie 2007) |
| [a]Kennebec River | -0.5 | 22.5 | 22.0 | -0.2 | -49.6 | 43.8 | (Takahashi et al. 2012) LDEO database |
| [a]Little Bay Estuary | 4.0 | -5.1 | 33.0 | 3.9 | | 43.1 | (Hunt et al. 2010) |
| [a]New River Estuary | -0.2—2.0 | | | | | 34.6 | (Crosswell et al. 2017) |
| [a]Nuece River | 4.7 | 1.73 | -0.84 | 38.4 | 12.1 | 35.0 | (Crosswell et al. 2012) |
| [b]San Francisco Estuary | 0.4 | | 1.8 | | 0.5 | 37.7 | (Peterson 1979) |
| [a]Shark River | 16.0 | | | | | 25.2 | (Koné and Borges 2008) |
| [a]Shark River | 36.1 | | | | | | (Ho et al. 2016) |
| [b]York River | 5.6 | 10.0 | 29.0 | 16.7 | 6.5 | 37.2 | (Raymond et al. 2000) |
| [a]LCE | 25.6±28.8 | 118.5 ±390.0 | 190.6±317.6 | 24.4±44.5 | 53.5±178.7 | 27.8—28.1 | This study |
| [a]GE | 35.9±24.2 | 98.2±136.9 | 343.2±365.1 | -6.0±9.2 | -31.3±39.8 | | |
| [a]MAE | 6.9±6.5 | 33.8±66.1 | 42.1±47.2 | 11.5±22.2 | -9.4±23.8 | | |
| [a]NE | 2.7±8.1 | 55.3±101.2 | 26.6±24.0 | -12.7±24.7 | -6.4±21.4 | | |

*Superscripts a,b indicate different tidal types, a - microtidal estuary and b - macrotidal estuary.

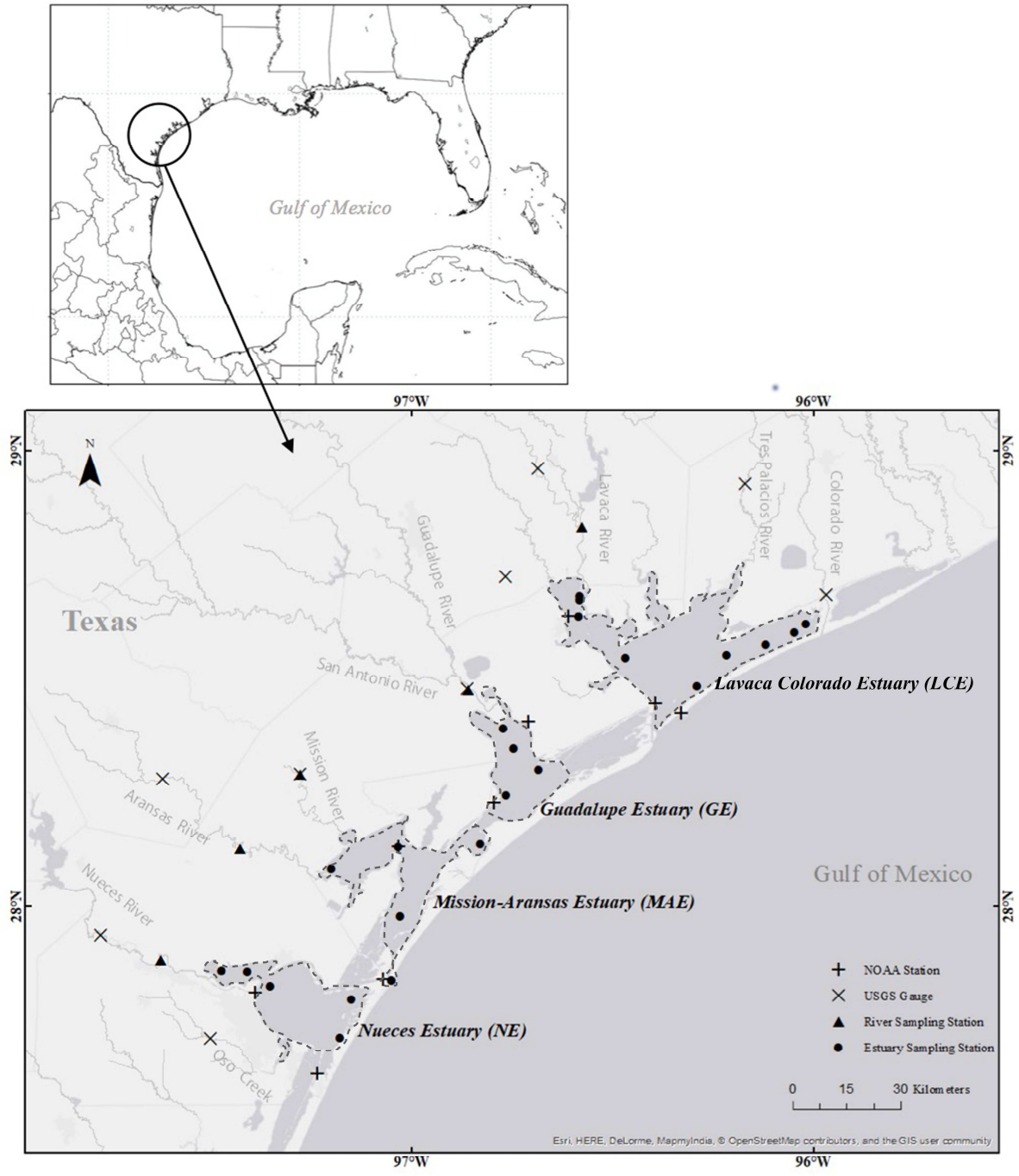


Figure 3.1. Map of sampling stations in the northwestern Gulf of Mexico estuaries and contributing rivers, "•"means estuary sampling stations; "▲" means river sampling stations; "×" means USGS monitoring gauges; "+" means NOAA monitoring stations. Estuary area is delineated with dashed lines on the map.

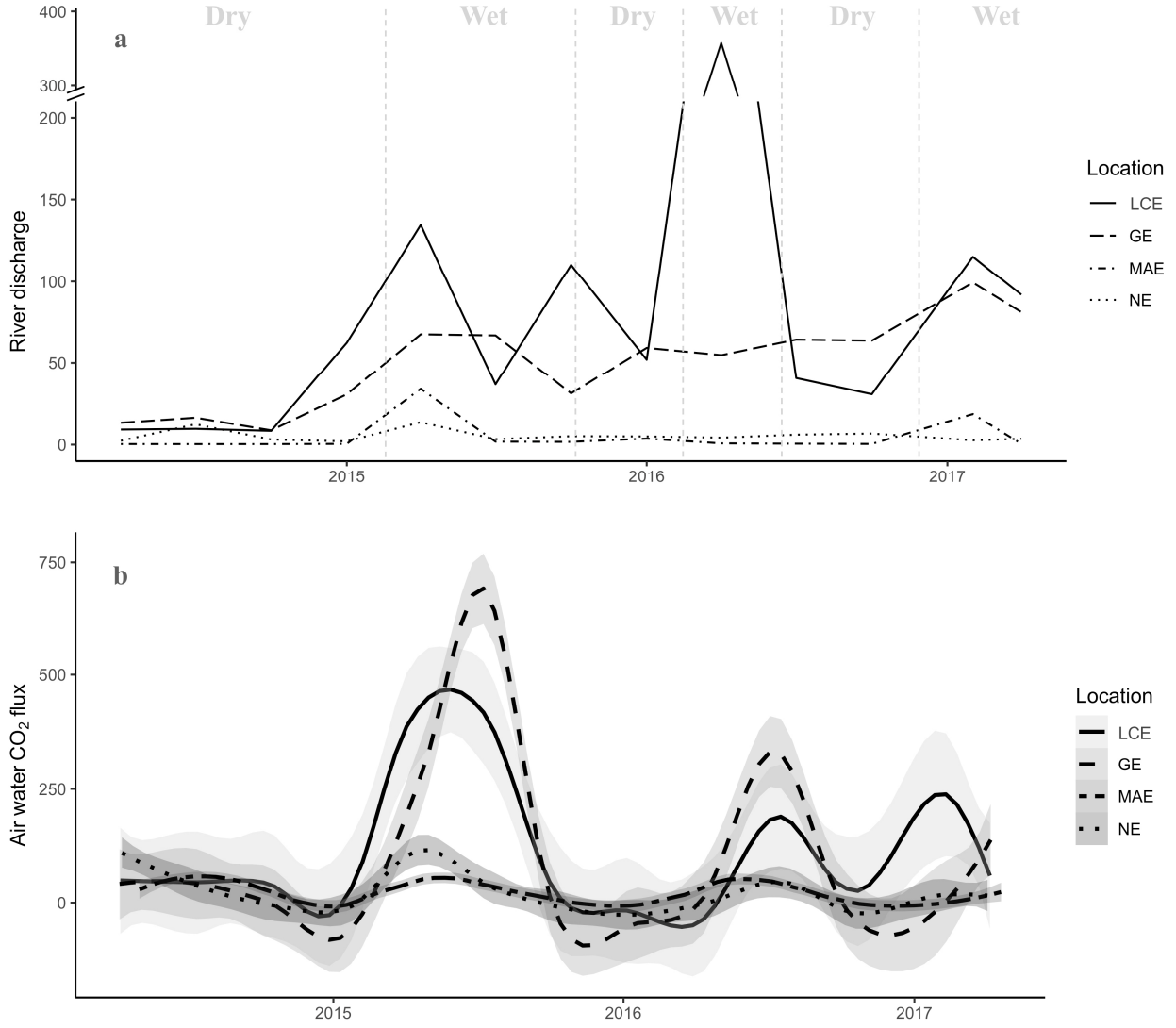


Figure 3.2. River discharge (a) and air-water $CO_2$ flux (b) in studied estuaries, shaded area means stand deviation within 95% confidence. (units: $m^3 \cdot s^{-1}$ for river discharge, $mmol \cdot C \cdot m^{-2} \cdot d^{-1}$ for air-water $CO_2$ flux)

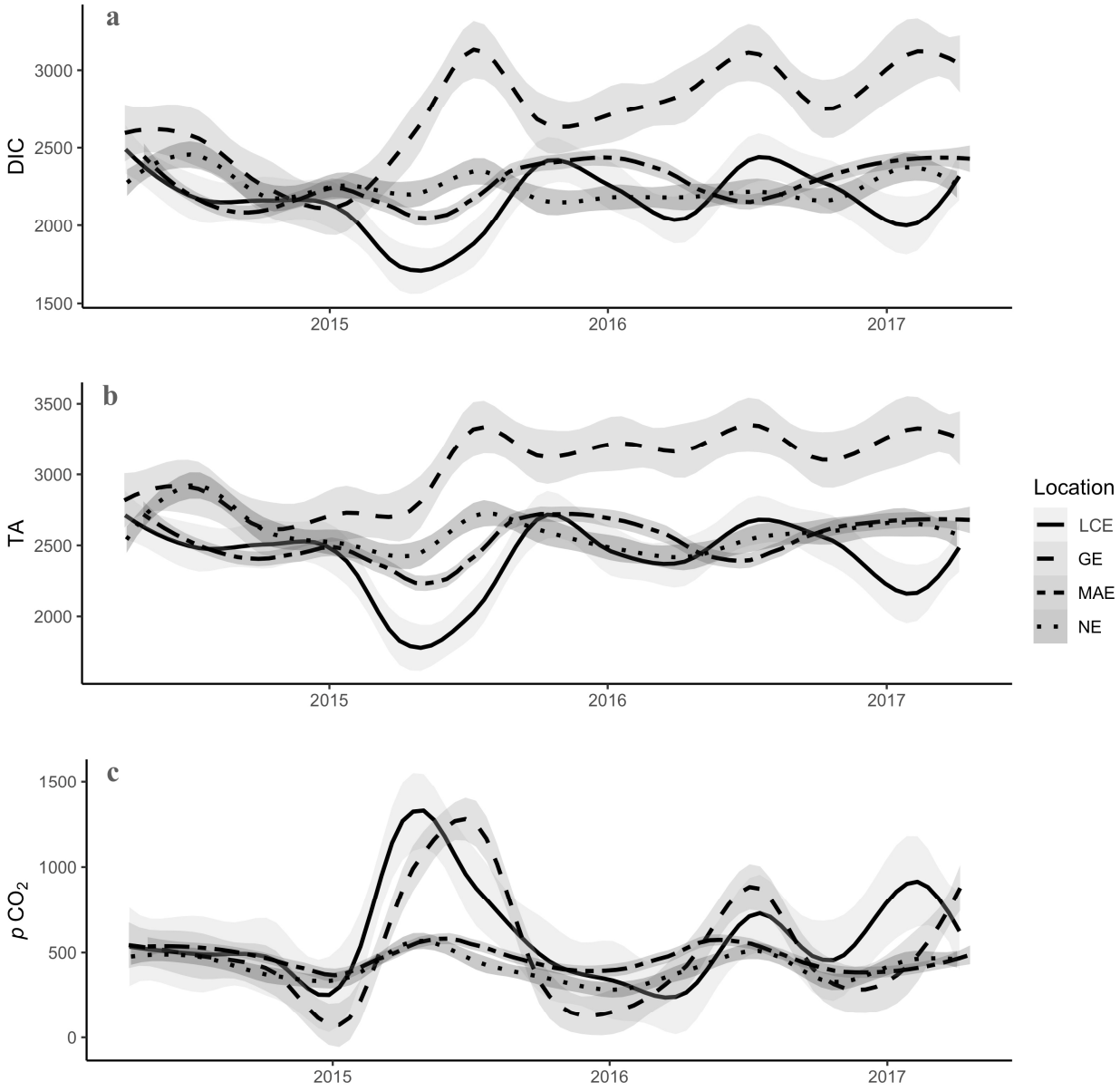


Figure 3.3. Average seasonal variations of carbonate system in studied estuaries, shaded area means standard deviation within 95% confidence. (units: $\mu mol \cdot kg^{-1}$ for DIC and TA, $\mu atm$ for $pCO_2$)

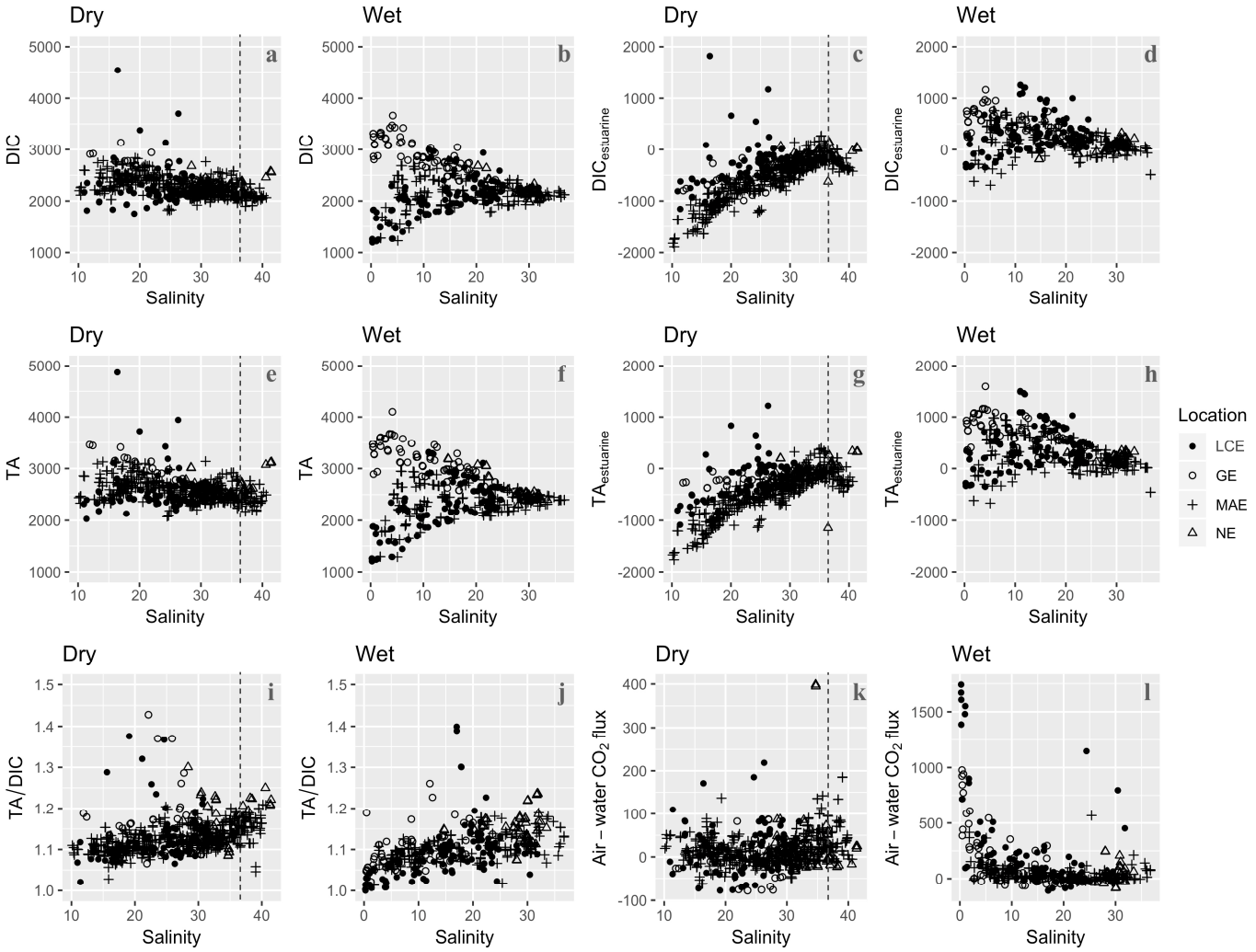


Figure 3.4. DIC, TA and $CO_2$ flux variations during hydrologic changes, a. observed DIC in dry condition; b. observed TA in dry condition; c. calculated extra produced/consumed DIC by estuarine process in dry condition; d. calculated TA by estuarine process in dry condition; e. observed DIC in wet condition; f. observed TA in wet condition; g. calculated extra produced/consumed DIC by estuarine process in wet condition; h. calculated TA by estuarine process in wet condition; i. TA/DIC ratios in dry condition; j. TA/DIC ratios in wet conditions; k. air-water $CO_2$ flux in dry condition; l. air-water $CO_2$ flux in wet condition. Vertical dashed lines in panel a, c, e, g, i, k indicate for hypersalinity. (units: $\mu mol \cdot kg^{-1}$ for DIC, TA, $DIC_{estuarine}$, $TA_{estuarine}$, $mmol \cdot C \cdot m^{-2} \cdot d^{-1}$ for air-water $CO_2$ flux)

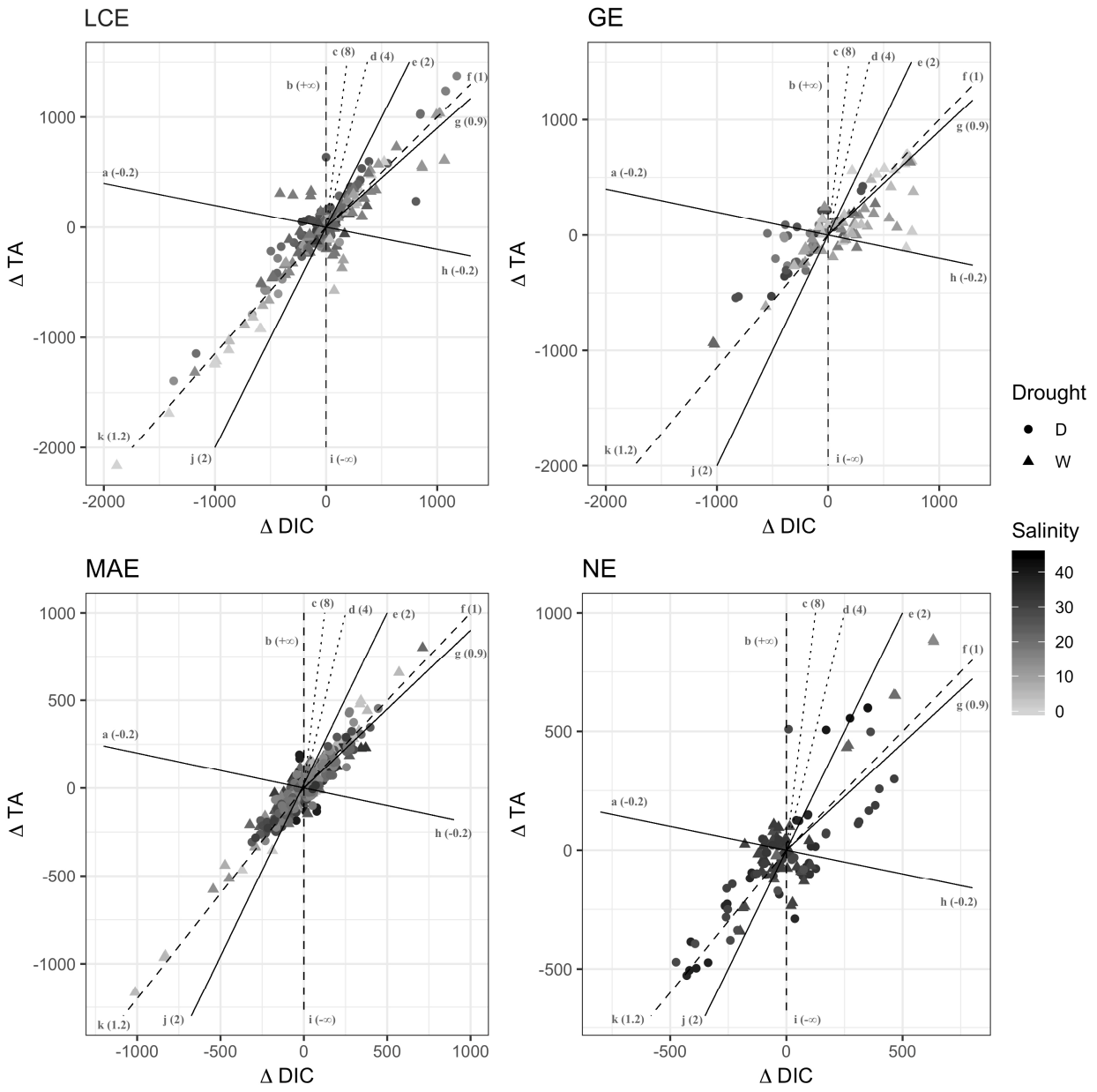


Figure 3.5. ΔDIC vs. ΔTA in each estuary. Lines indicate different biogeochemical processes that will direct DIC and TA changes in fixed ratios (numbers in bracket indicate the ratios/slopes, Liu et al. 2017; Sippo et al. 2016). a. photosynthesis; b. hydrolysis; c. iron reduction; d. manganese reduction; e. calcium dissolution; f. sulfate reduction; g. denitrification; h. aerobic respiration; i. nitrification/sulfide oxidation; j. calcium precipitation; k. pure water dilution/evaporation. (unit: $\mu mol \cdot kg^{-1}$)

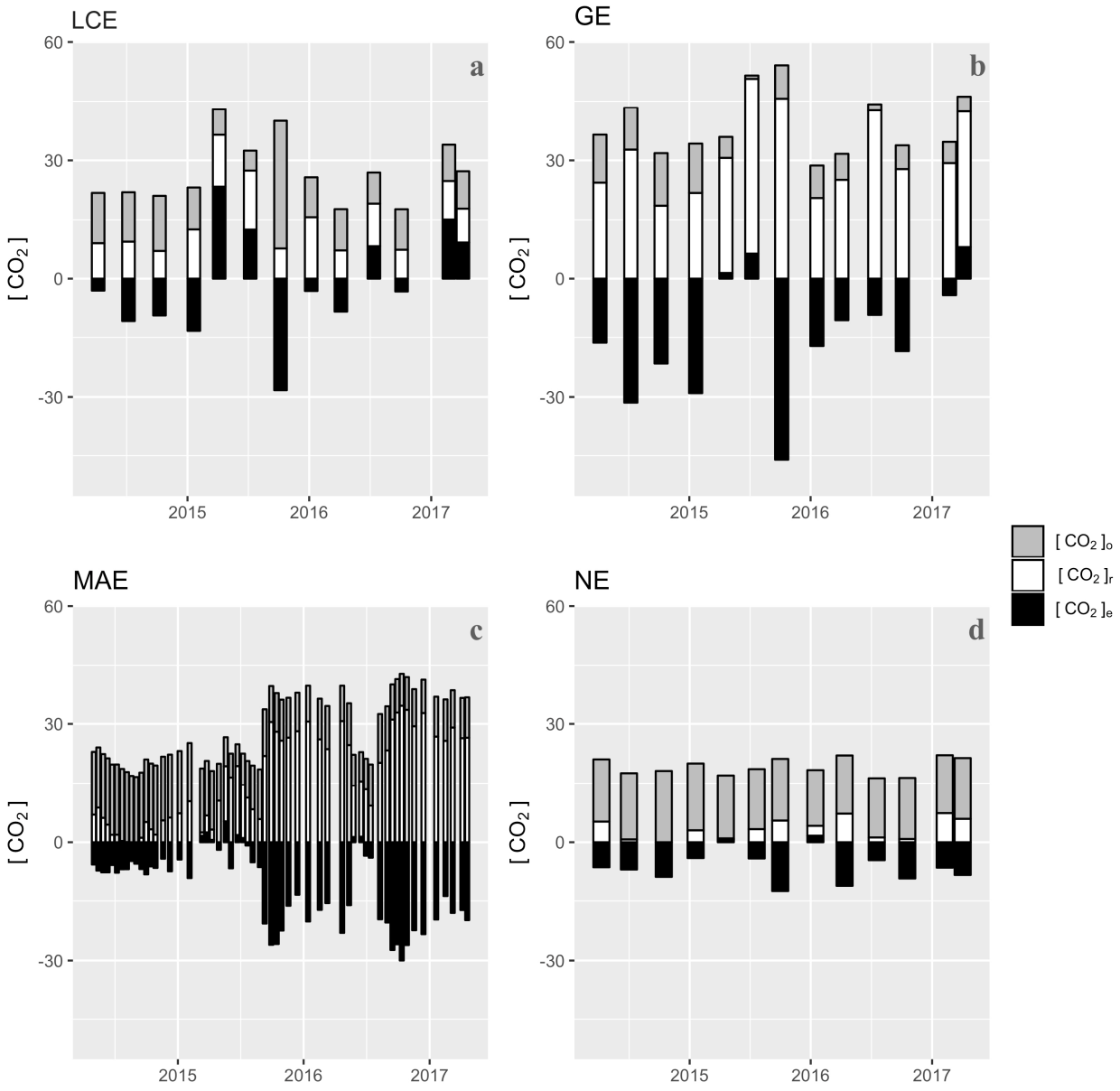


Figure 3.6. Area-weighted average categorized aqueous $CO_2$ concentrations ($[CO_2]_r$ ; $[CO_2]_o$ ; $[CO_2]_e$) in studied estuaries during sampling period. (unit: $\mu mol \cdot kg^{-1}$)

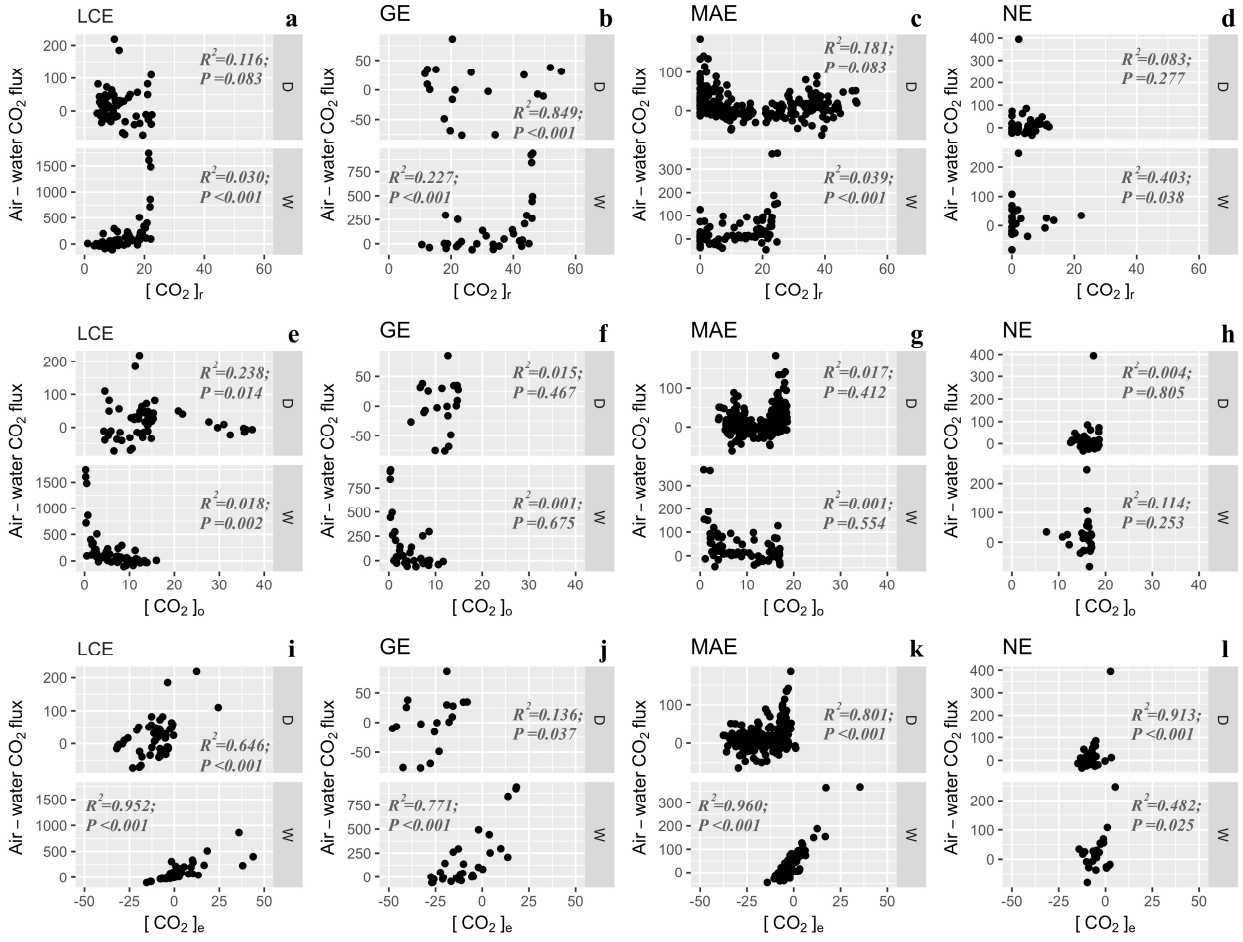


Figure 3.7. Linearity between categorized $[CO_2]_x$ and air-water $CO_2$ flux in studied estuaries during hydrologic changes. D = dry condition, W = wet condition. (units: $\mu mol \cdot kg^{-1}$ for $[CO_2]_x$ ; $mmol \cdot C \cdot m^{-2} \cdot d^{-1}$ for air-water $CO_2$ flux)

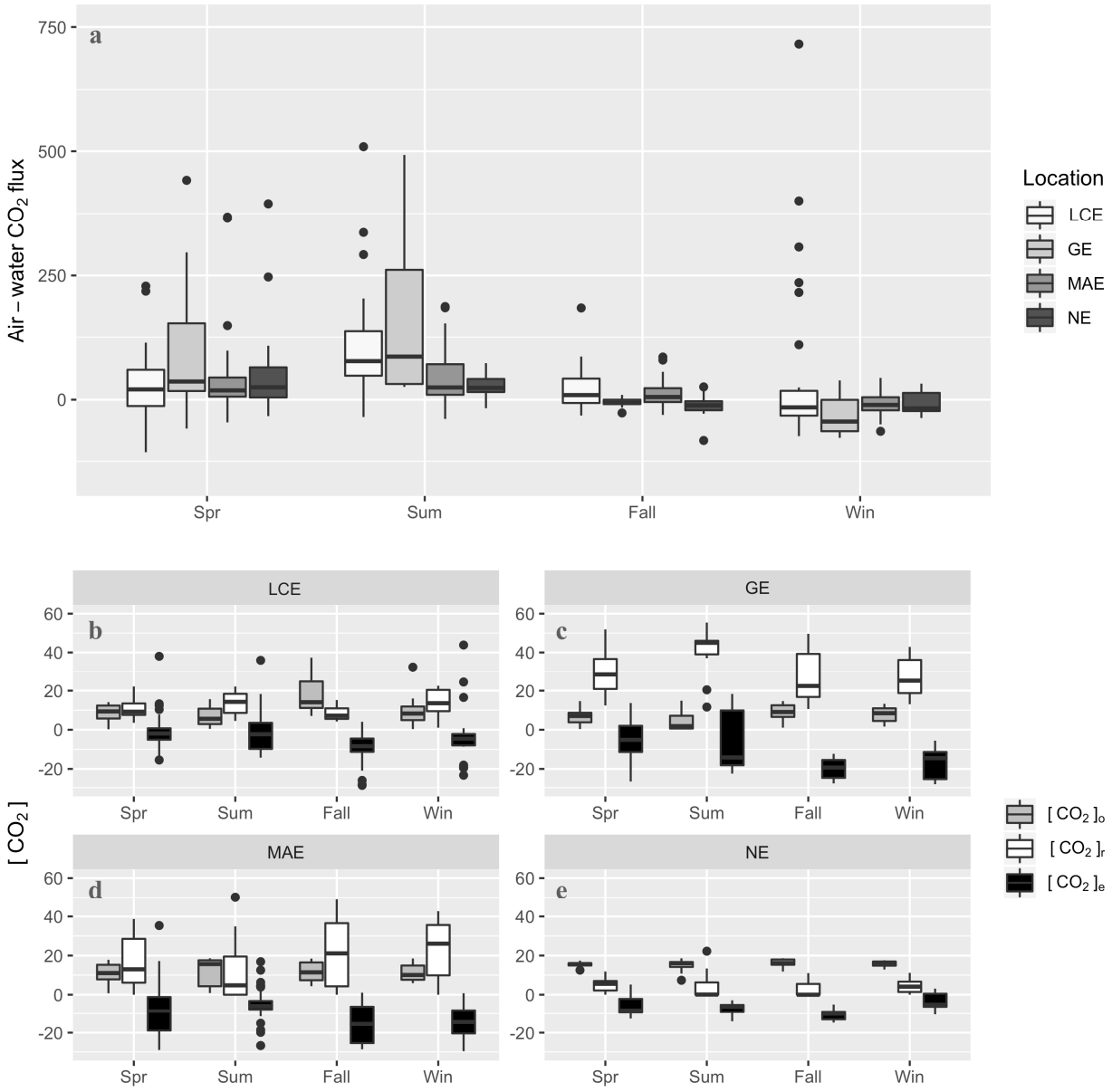


Figure 3.8. Seasonality of air-water $CO_2$ flux and categorized $[CO_2]_x$ in studied estuaries. (units: $\mu mol \cdot kg^{-1}$ for $[CO_2]_x$ ; $mmol \cdot C \cdot m^{-2} \cdot d^{-1}$ for air-water $CO_2$ flux)

# CHAPTER IV: CARBON BUDGETS IN NORTHWESTERN GULF OF MEXICO COASTAL ESTUARIES: IMPLICATIONS FOR LATERAL TRANSPORT AND CHALLENGES OF FLOODING AND SEA LEVEL RISE


## Abstract

Estuarine carbon cycle is more subject to climate change, as coastal areas are more prone to flooding and sea level rise. Based on a four-year dataset, a mass balance model was established to interpret carbon fluxes and their spatiotemporal variability in four coastal estuaries along the northwestern Gulf of Mexico (nwGOM) coast. Results demonstrate that annual lateral carbon transport from tidal marsh-mangrove to the estuaries account for ~95% and ~70% of total organic carbon (TOC) and dissolved inorganic carbon (DIC) inputs to estuarine open waters, respectively. This transport sustains a moderate to high level of air-water $CO_2$ flux (16.7±3.0 $mol \cdot C \cdot m^{-2} \cdot yr^{-1}$), which was greater than that in most estuaries in the east coast of North America. In addition, annual $CO_2$ efflux is threefold of the exported DIC to open ocean from these estuaries. Due to long water residence time, the majority of imported TOC is buried (~75%) into sediment, leaving ~20% for heterotrophic activities and ~5% exported to open ocean. Nevertheless, these carbon fluxes are highly variable because of hydrologic condition changes. For example, storm-driven flooding could dramatically elevate estuarine $CO_2$ evasion by 2—10 times. In addition, there are also substantial increases for lateral transport of both TOC (from 42.7±87.5 to 155.6±136.2 $mmol \cdot C \cdot m^{-2} \cdot d^{-1}$) and DIC (from -2.8±45.3 to 94.3±222.5 $mmol \cdot C \cdot m^{-2} \cdot d^{-1}$) from tidal wetland to estuary, because of the extreme weather events. Finally, sea level rise is estimated to result in ~0.9% and ~0.6% decline in lateral TOC and DIC transport from tidal wetland, which would decrease estuarine air-water $CO_2$ flux by ~1% each year for nwGOM estuaries.

## 4.1. Introduction

Coastal area, consisting of tidal wetlands, estuaries, and continental shelf waters, is a key component in the global carbon cycle. Estuaries, where terrestrial carbon is delivered by brackish water to the coastal ocean, is the most dynamic system. For example, estuaries account for only 0.3% ($1.05\times10^{12}$ $m^2$) surface area of the global ocean, their $CO_2$ emission (0.10—0.25 $Pg\cdot C\cdot yr^{-1}$; Cai 2011; Chen et al. 2013) is estimated to be equivalent to the magnitude of continental shelves $CO_2$ uptake (note the opposite direction) and 30% of riverine total carbon input (Bauer et al. 2013; Cai 2011). However, the uniqueness of each estuary from geomorphological, climatic, and hydrologic perspectives, results in tremendous spatiotemporal heterogeneity in carbon processing across the world (Bauer et al. 2013; Montagna et al. 2012). In addition, anthropogenic effects vary spatially (i.e. land-use change, wastewater discharge, etc.), and these effects have increased terrestrial total carbon influx to estuaries by 20% globally since pre-industrial times (from 0.8 to 1.0 Pg·C·yr-1; Regnier et al. 2013a). Attempts to synthesize estuarine carbon budget face several challenges, i.e., interpreting carbon-relevant biogeochemical processes (including ecosystem metabolism, riverine discharge and lateral transport, air-water $CO_2$ flux, export to the coastal ocean, and sediment burial), and determining sufficient resolution for a variety of research and management objectives (Swaney et al. 2012). As a reflection of estuarine trophodynamics, knowledge on net ecosystem metabolism (NEM, both in water column and sediment) and air-water $CO_2$ flux is critical for understanding the internal connections between organic and inorganic carbon in an estuary, both are widely used in estuarine biogeochemical and carbon cycle studies.

Carbon flows can be determined through different ways. Process-based models that couple estuarine hydrodynamics and biogeochemistry may solve the interactions between organic and

inorganic carbon cycles (Gordon et al. 1996; Laruelle et al. 2017). Detailed information at fine spatial and temporal scales, for example higher resolution data on river-delivered carbon, is required to constrain potential errors in process-based models (Bauer et al. 2013; Kemp et al. 1997). In comparison, mass balance approaches based on observations and stoichiometric relationships may potential amplify uncertainties because of the propagation of errors (Smith et al. 1991). However, mass balance models are capable of separating individual processes that significantly influence regional carbon cycle, and errors could be constrained or at least recognized if temporal and spatial patterns are chosen carefully (Maher and Eyre 2012).

There is a paucity of total carbon budget estimates in subtropical estuaries worldwide. Around the Gulf of Mexico (GOM) there is one of the world largest lagoonal systems (Dürr et al. 2011), i.e. estuaries that are separated from the coastal ocean by barrier islands, through which channels and waterways connect the water bodies. Despite the fact that rivers in this region are rich in inorganic carbon (Butman and Raymond 2011; Zeng et al. 2011), it is difficult to estimate the regional carbon flows due to large temporal and spatial variability. A clear decreasing trend in river inflows from northeast to southwest is one of the most distinctive features in this area (Montagna et al. 2012). In addition, a variety of anthropogenic (i.e. dam construction and river fragmentation; Murgulet et al. 2016) and climatic (i.e. interactions between drought and flood; Yao and Hu 2017) interventions could further complicate the hydrologic conditions.

The objectives of this study were to (1) construct detailed carbon budgets for nwGOM estuaries, using a mass balance model based on bi-weekly to quarterly observations, (2) examine different biogeochemical drivers and separate critical processes (riverine inflow, lateral transport, burial, air-water $CO_2$ flux, NEM, export to ocean), and (3) assess climatic impact on estuarine

carbon budget, including that from a severe flooding event (i.e., caused by a hurricane) and sea level rise.

## 4.2. Methods

### 4.2.1. Study sites

Four nwGOM estuaries (Fig. 4.1)—Lavaca-Colorado Estuary (LCE), Guadalupe Estuary (GE), Mission-Aransas Estuary (MAE), and Nueces Estuary (NE) from northeast to southwest along the nwGOM coast—were studied during April 2014 and April 2018. Average depth of these microtidal estuaries is approximately 1 m (Table 4.1), and these estuaries have restricted connections to the GOM due to the presence of a series of barrier islands (Fig. 4.1; Table 4.1). Each estuary connects to one or two dominant river-watershed(s). We designate the upper estuary as the area subject to more freshwater influence from rivers, whereas the lower estuary represents the area connected with the GOM through tidal inlet. The only exception is GE, which is river inflow-dominated due to its complete isolation from the GOM by barrier islands (Fig. 1; Montagna and Kalke 1992). The overall coastline, characterized by geomorphological similarity but contrast by remarkable hydrologic diversity (Table 4.1), is ideal to assess the effects of spatiotemporal factors (i.e. riverine inflow versus temperature) on estuarine carbon cycle.

### 4.2.2. Field campaign and laboratory analyses

Biweekly, monthly, or quarterly field campaigns were conducted between April 2014—April 2018 (see sampling stations in Fig. 4.1; both surface and bottom samples were taken). In LCE, GE and NE, water samples were collected quarterly, whereas MAE was sampled biweekly or monthly (biweekly in April—October, monthly in November—March). Additional biweekly trips were conducted in GE in May—September 2017; and another two monthly field campaigns were conducted in LCE, GE, and NE (November and December 2017) to explore the influence

of Hurricane Harvey in late August 2017. Moreover, bimonthly river end-members were also sampled during our study period, with additional sampling occurred in non-scheduled months (October 2015, January 2016, January 2017, June 2017).

*In-situ* data including temperature, depth, dissolved oxygen concentration were acquired by a calibrated YSI 6600 V2 data sonde; dissolved inorganic carbon (DIC) was determined by acidifying 0.5 mL samples with 10% phosphoric acid and the extracted $CO_2$ was quantified on an AS-C3 DIC analyzer (Apollo SciTech). pH was measured using spectrophotometric method (salinity >20, precision ±0.001; Carter et al. 2013) and Orion$^{TM}$ Ross pH electrode (salinity<20, precision of ±0.01). The pH electrode was calibrated using NBS buffers (4.01, 7.00, 10.01). All pH measurements were done at 25±0.1°C, and the lab measured pH values were converted to total scale at *in-situ* temperature for further analysis. Salinity was measured using a benchtop salinometer calibrated with MilliQ water and known salinity Certified Reference Material (Batch#142, 156, 159). $Ca^{2+}$ was titrated by egtazic acid (EGTA) on a Metrohm 888 Titrando automatic titrator using a calcium ion selective electrode to detect endpoint (Kanamori and Ikegami 1980), and the precision was ±0.2%.

4.2.3. Carbon mass balance

The major fluxes in an estuary may include multiple processes, including river discharge, lateral flux from tidal wetland, net ecosystem metabolism (NEM), air-water $CO_2$ flux, dry/wet deposition, evaporation, carbon export and calcium precipitation/dissolution (Crosswell et al. 2017; Laruelle et al. 2017; Maher and Eyre 2012; Najjar et al. 2018). Because these lagoons are a net $CO_2$ source (Yao et al. 2019; *in revision*), the mass balance equation for estuarine DIC is:

$$River\ inflow + Lateral\ transport - NEM = Atmospheric\ flux\ + Calcification + Export \quad (1)$$

For total organic carbon (TOC), which consists of dissolved organic carbon (DOC) and particulate organic carbon (POC), the equation can be written as:

$$River\ inflow + Lateral\ transport + Atmospheric\ flux = Burial - NEM + Export \quad (2)$$

4.2.4. River inflow

Riverine carbon fluxes were estimated from constituent concentrations and discharge data. Riverine DIC were derived from our river surveys between October 2015 and May 2018 (see stations in Fig. 4.1; average values in Table 4.2), riverine TOC were acquired from Texas Commission on Environmental Quality (TCEQ; https://www.tceq.texas.gov/). Average riverine DIC and TOC were applied to dry and wet periods, respectively. Monthly discharges were from U.S. Geological Survey (USGS; https://waterdata.usgs.gov/tx/nwis/rt) gauging stations (Fig. 4.1; Table 4.1). Annual average riverine DIC and TOC inflows were derived from monthly data.

4.2.5. Atmospheric flux

Here atmospheric DIC flux is separated into two components, i.e., rainfall could deposit DIC; while net evaporation will favor $CO_2$ evasion from water (Yao and Hu 2017); details of another important wind driven air-water $CO_2$ flux is listed below. Atmospheric TOC flux mainly depends on DOC deposition (regional atmospheric POC concentration ranges only 0.1—1.3×10-3 μmol·C·L-1; Benway and Coble 2014). Hereby we applied average concentrations (DOC 161 μmol·C·$L^{-1}$, DIC 17 μmol·C·$L^{-1}$; Willey et al. 2000) in global rainfall, and precipitation/evaporation rates (Texas Water Development Board, http://www.twdb.texas.gov/) to estimate rainfall input to these estuaries.

$pCO_{2,water}$ was calculated using measured DIC and pH as the input variables using CO2SYS (https://cdiac.ess-dive.lbl.gov/ftp/co2sys/CO2SYS_calc_MATLAB_v1.1/) for each sample.

Carbonic acid dissociation constants ($K_1$, $K_2$) were from Millero (2010), bisulfate dissociation constant was from Dickson (1990). Paired DIC/pH as the input variables in CO2SYS could introduce 2.6—3.2% uncertainty for calculated $pCO_2$ (Orr et al. 2018), which is approximately ±8-16 µatm error in this study (by applying annual average $pCO_2$ range from those estuaries). In addition, calculated $pCO_{2,water}$ values were in good agreement with *in-situ* monitored $pCO_{2,water}$ (±20 µatm; McCutcheon et al., in prep). Air-water $CO_2$ flux was then calculated:

$$F = k \cdot \mathrm{K}_0(pCO_{2,water} - pCO_{2,air}) \qquad (3)$$

where $K_0$ is solubility coefficient (Weiss 1974), $k$ is gas transfer velocity that was derived from wind speed (Jiang et al. 2008), $pCO_{2,air}$ is the partial pressure of $CO_2$ in atmosphere based on monitored dry air $xCO_{2,air}$ data in northern Gulf of Mexico (https://www.pmel.noaa.gov/co2/story/Coastal+MS). Positive flux indicates $CO_2$ emission from water, and negative value represents $CO_2$ uptake by water. Annual average $CO_2$ flux was obtained from area-weighted average $CO_2$ flux in each campaign and the time intervals in between the campaigns $F_{avg} = \frac{\Sigma F_i + d_i}{\Sigma d_i}$ (Yao and Hu 2017).

4.2.6. Net ecosystem metabolism (NEM)

Air-water $CO_2$ flux is driven by mixed layer metabolic processes (both pelagic and benthic; Borges et al. 2006). In this study, NEM was calculated following the equation (Eq. 4) from Maher et al. (2012), who found a strong significant inverse relationship between air-water $CO_2$ flux and mixed NEM from global estuaries.

$$Air - water\ CO_2\ flux\ = -0.4236 \cdot NEM + 11.991 \qquad (4)$$

However, Russell et al. (2006) integrated NEM from direct measurements in these estuaries and concluded that heterotrophic NEM in this region should not exceed -312.5 $mmol \cdot C \cdot m^{-2} \cdot d^{-1}$ (with the average depth in Table 4.1). Additionally, a previous study also found ventilation of

riverine $CO_2$ could significantly contribute to estuarine $CO_2$ emission during extremely flooding (Yao et al. 2019, *in revision*). Therefore, evaluated heterotrophic NEM (Eq. 4) in our study was assumed to have an upper limit of -312.5 $mmol \cdot C \cdot m^{-2} \cdot d^{-1}$.

4.2.7. Burial

Buried organic carbon was determined by sedimentation rates and sedimentary TOC content, assuming constant burial rates for dry and wet period. Sedimentation rates were obtained from previous studies (Bianchi et al. 2013a; Bronikowski 2004; Yeager et al. 2006) and TOC contents under dry and wet conditions were from TCEQ (Table 4.1).

4.2.8. Export to the coastal ocean

Due to long residence time, the estuarine water was assumed to be well mixed, a one-dimensional estuarine box-model approach was applied to estimate the net export to open ocean (Crosswell et al. 2017). More specifically, the net export was calculated from total freshwater inflow and the volume-weighted average DIC and TOC concentrations. Evaporation/rainfall effect was taken in consideration to adjust export water volume ($V_{discharge} - V_{exporation} + V_{rainfall} = V_{export}$) especially in dry condition. Estuarine TOC concentrations were obtained from Dr. Michael Wetz's Lab (TAMUCC) and TCEQ water quality survey. Because GE was not directly connected to GOM (Fig. 4.1), while its lower bay Espiritu Santo Bay displayed similarity in carbonate system (averaged differences on total alkalinity ~100 $\mu mol \cdot kg^{-1}$ and *in-situ* pH ~0.06 between our nearest sampling station and TCEQ station in Espiritu Bay). Herein we chose our nearest sampling station that representing final station for GE export to GOM.

4.2.9. Calcification

Daily calcification/dissolution was the difference of salinity-normalized $Ca^{2+}$ (Friis et al. 2003) between every two consecutive surveys divided by number of days. Annual average was then derived from cumulated daily calcification/dissolution divided by total days.

4.2.10. Lateral transport

The lateral carbon transport from tidal wetlands was the only missing part in the mass balance and was calculated using Eq. 1 and 2.

4.3. Results

4.3.1. Carbon budgets

Annual carbon budget in each estuary is represented by area-integrated DIC and TOC fluxes (Fig. 4.2). The largest DIC inflow and outflow are lateral transport and air-water $CO_2$ flux, respectively. Lateral DIC transport is ~threefold of riverine DIC input, $CO_2$ emission from these lagoons is more than twofold of DIC export to ocean. On the other hand, lateral transport accounts for ~96.7% of total TOC input, while riverine TOC input is small (3.3%). Moreover, ~85.4% of total TOC input has been buried, only a small portion is used to support heterotrophy (~9.5%) or exported to open ocean (~6.0%).

Because evaporation/rainfall and calcification are minor compared to those major fluxes (Fig. 4.2; Table 4.2), these contributions were omitted in the following discussion.

4.3.2. River inflow

Average annual river discharge ranged $8.6 \pm 16.9$ (NE)—$107.9 \pm 137.8$ $m^3 \cdot s^{-1}$ (LCE)in this area, consistent with the declining trend from north to south (LCE to NE, Table 4.2). In addition, distinct seasonality was observed: large river discharge in spring—summer in response to storm-driven flooding in 2015, 2016 and 2017; and fall—winter had much less discharge. As a result,

riverine DIC and TOC inflows followed such spatiotemporal trend (Fig. 4.3). During spring—summer flooding, maximum riverine DIC inputs in LCE and GE reached 84.4 and 59.5 $mmol \cdot C \cdot m^{-2} \cdot d^{-1}$, respectively, while those in in MAE and NE were substantially lower (27.8 and 16.7 $mmol \cdot C \cdot m^{-2} \cdot d^{-1}$, respectively). Similarly, maximum riverine TOC inflow was 8.6 and 14.1 $mmol \cdot C \cdot m^{-2} \cdot d^{-1}$ for LCE and GE, respectively; compared to 7.4 and 2.3 $mmol \cdot C \cdot m^{-2} \cdot d^{-1}$ for MAE and NE, respectively.

4.3.3. Air-water $CO_2$ flux

All four estuaries are net $CO_2$ source on an annual scale (Table 4.2), but with distinct spatiotemporal pattern (Fig. 4.3). Area-weighted average $CO_2$ fluxes ranged -50—500 $mmol \cdot C \cdot m^{-2} \cdot d^{-1}$ in the studied region (Fig. 4.3c). In spring and summer these estuaries tended to have stronger $CO_2$ emission (up to 500 $mmol \cdot C \cdot m^{-2} \cdot d^{-1}$) as a result of flooding. The peak of $CO_2$ emission in LCE and GE (~500 $mmol \cdot C \cdot m^{-2} \cdot d^{-1}$) was fourfold of MAE and NE (~100 $mmol \cdot C \cdot m^{-2} \cdot d^{-1}$). In contrast, $CO_2$ flux decreased significantly and even changed sign (-50—100 $mmol \cdot C \cdot m^{-2} \cdot d^{-1}$) in fall and winter, i.e., the estuaries can be a $CO_2$ sink. Overall, annual average $CO_2$ flux in LCE and GE was an order of magnitude higher than those in MAE and NE (Table 4.2).

4.3.4. NEM

Lowest NEM in spring and summer (-45.3±81.5 and -104.0±91.3 $mmol \cdot C \cdot m^{-2} \cdot d^{-1}$; respectively) indicated overall heterotrophy-dominant situation, increasing NEM in fall (-9.4±73.8 $mmol \cdot C \cdot m^{-2} \cdot d^{-1}$) suggested weakening heterotrophic activities, and positive NEM (66.4±53.9 $mmol \cdot C \cdot m^{-2} \cdot d^{-1}$) in winter accompanied autotrophic conditions. Annual NEM values suggest stronger heterotrophy in northern estuaries (i.e., LCE and GE), whereas weaker heterotrophy was found in MAE or even autotrophy dominated in NE (Table 4.2).

4.3.5. Lateral transport

Lateral DIC transport ranged from -180—540 mmol·C·$m^{-2}$·$d^{-1}$, and TOC transport ranged -130—415 mmol·C·$m^{-2}$·$d^{-1}$ (Fig. 4.3b&e). Positive values were indicative of lateral DIC and TOC input into the estuaries. GE had the largest annual lateral DIC input (Table 4.2) as well as the most intense variation (-181.4—539.3 mmol·C·$m^{-2}$·$d^{-1}$). On the other hand, lateral TOC transport was closely related to NEM and $CO_2$ flux (Fig. 4.3c&f). Lateral TOC inflow peaked in summer, with the maximum 412.7 mmol·C·$m^{-2}$·$d^{-1}$ estimated in LCE during the summer of 2015, a flooding period. In contrast, lateral TOC inflow appeared to reach minimum in winter (Fig. 4.3e).

4.3.6. Carbon burial in sediments

Area-weighted average organic carbon burial rates were 50.1 and 97.7 mmol·C·$m^{-2}$·$d^{-1}$ in LCE for dry and wet periods, respectively. These burial rates were lower in GE, i.e., 30.3 and 49.8 mmol·C·$m^{-2}$·$d^{-1}$ for dry and wet periods, respectively. This declining trend continued southward (3.6 and 28.5 mmol·C·$m^{-2}$·$d^{-1}$ for dry and wet in MAE; 5.1 and 5.4 mmol·C·$m^{-2}$·$d^{-1}$ for dry and wet in NE), consistent with decreasing river discharge.

4.3.7. Export to the coastal ocean

Ocean DIC export was between 0—90.5 mmol·C·$m^{-2}$·$d^{-1}$, and TOC export was 0—17.4 mmol·C·$m^{-2}$·$d^{-1}$ in all estuaries combined. The largest export was found in LCE at Apr 2016, but DIC export from NE was minimal throughout our study period. Consistent with river inflows, these estuaries exported most DIC and TOC to GOM in spring (22.6±20.0 and 2.5±4.0 mmol·C·$m^{-2}$·$d^{-1}$, respectively), lowest in NE (1.8±4.0 and 0.3±0.3 mmol·C·$m^{-2}$·$d^{-1}$ for DIC and TOC, respectively) and highest in GE (36.4±20.3 and 7.6±3.8 mmol·C·$m^{-2}$·$d^{-1}$). Minimum estuarine DIC and TOC exports were in fall (11.8±11.4 and 1.9±3.0 mmol·C·$m^{-2}$·$d^{-1}$), ranging

from lowest in NE (1.8±2.1 and 0.7±0.7 mmol·C·$m^{-2}$·$d^{-1}$) to highest in GE (25.8±13.0 and 6.3±3.0 mmol·C·$m^{-2}$·$d^{-1}$, respectively).

4.3.8. Uncertainties

Like all budgetary calculations, uncertainties could be amplified when integrating different processes from calculation and measurement-associated errors. Despite of relatively high-resolution sampling schedule for river end-members, still a range of uncertainty may have been introduced by assuming constant riverine DIC and TOC loading in dry and wet conditions. Air-water $CO_2$ flux calculation would incur 40—45% uncertainty due to the uncertainties associated with gas transfer velocity parameterization (20—25%; Ho et al. 2014) and limited spatial coverage (~20%). Further, evaluated NEM that is based on air-water $CO_2$ flux could generate ~5% error statistically (Maher and Eyre 2012). Our evaluated NEM range (-312.5—283.1 mmol·C·$m^{-2}$·$d^{-1}$) is slightly larger than previous estimate (-250—187.5 mmol·C·$m^{-2}$·$d^{-1}$; Russell and Montagna 2007; Russell et al. 2006), which is obtained from open-water oxygen monitoring. There is a bigger concern on uncertainty of carbon burial in these estuaries, due to the large variability for both sedimentation rate (Bronikowski 2004; Yeager et al. 2006) and sediment TOC concentration (uncertainty ~50%; measured by TCEQ). As a main influence on lateral TOC inflow quantification, more accurate carbon burial estimation is needed for future studies. Because the estimates were derived from imbalance of Eq. 1 and Eq. 2, lateral transport also suffered from the same orders of magnitude of uncertainty as other fluxes.

4.4. Discussion

4.4.1. Importance of lateral transport from tidal wetland

In the studied estuaries, annual riverine inflows only covered a small portion of total inputs (~3.5% for TOC and ~30.0% for DIC) (Fig. 4.2a&b). Given the imbalance between high carbon

outflows ($CO_2$ efflux and organic carbon burial) and relatively small riverine supplies, we predict that lateral exchange is crucial on carbon budgets in these estuaries. Tidal marsh and mangrove systems are among the most productive ecosystems on earth (Bouillon et al. 2008; Cai 2011; Hopkinson 1988). However, their role on estuarine carbon budget remains largely uncertain due to the complexity involved in direct assessment (Bouillon et al. 2008; Sippo et al. 2016; Wang et al. 2016). The nwGOM coastline has extensive distribution of saltmarshes and mangroves (Armitage et al. 2015; Saintilan et al. 2009), with the latter mostly in the south of N27˚ but with northward migration due to warming. Furthermore, our calculated lateral TOC and DIC transport are in concert with those in other tidal marsh and mangrove systems globally (Table 4.4). These results suggest that coastal saltmarshes and mangroves are important carbon sources to nwGOM estuaries as well. Tidal exchange was reported as major driver for TOC and DIC export from saltmarshes and mangroves (Sippo et al. 2016; Wang et al. 2017), and this tidal pump was observed to be more effective in shallower environment (Sippo et al. 2016). We speculate that the strongest lateral exchange should occur at the top layer of tidal wetland sediments. Bianchi et al. (2013a) pointed out a loss of carbon in surface layer of mangrove sediment from lower MAE area, based on an unusually low sediment C:N ratio. In addition, Murgulet et al. (2018) observed a strong signal of submarine groundwater discharge to DIC and total alkalinity in upper NE area (~4.1 and 4.9 $mol \cdot C \cdot m^{-2} \cdot d^{-1}$, respectively), which may be evidence of lateral exchange by tidal pumping (Maher et al. 2013).

Estuarine $CO_2$ flux was largely dependent on lateral transport ($R^2 = 0.504$ and 0.334 for TOC and DIC respectively, $p<0.001$ for both cases; Fig. 4.4a&b). While lateral TOC showed a strong correlation with $CO_2$ flux (Fig. 4.4a), the effect of lateral DIC transport appears to affect $CO_2$ flux differed spatially (Fig. 4.4b). For example, there was an inverse relationship between the

lateral DIC and $CO_2$ flux in MAE and NE, whereas an opposite correlation is present in LCE and GE (Fig. 4b). Considering that lateral DIC inflow increased air-water $CO_2$ flux in GE and LCE (Fig. 4b), a part of emitted estuarine $CO_2$ should directly come from lateral DIC during transport. Similarly, a highly significant relationship between lateral TOC transport and NEM ($R^2$=0.908, $p$<0.001; Fig. 4c) is observed, indicating that heterotrophic activities may strongly depend on lateral TOC transport from saltmarshes and mangroves. In contrast, lateral DIC transport appears to influence NEM differently in different estuaries (Fig. 4d), the poor correlation in LCE ($R^2$=0.092, $p$=0.207) and GE ($R^2$=0.004, $p$=0.756) suggested that [$CO_2$*] from tidal wetland respiration was less likely to be utilized by primary producers. By contrast, lateral DIC seemed to be more important for autotrophic activities in MAE and NE (Fig. 4d). Their rising lateral DIC inflows were associated with stronger autotrophic activities (increasing NEM), which was indicative of decreasing $CO_2$ emission or even atmospheric $CO_2$ uptake. In LCE and GE the river discharges are much greater, with shorter water residence time, hence $CO_2$ degassing correspond more to the "river-borne" $CO_2$ ventilation (Borges et al. 2006). On the other hand, in the smaller river-influenced MAB and NE, because of long water residence time, primary production may be stimulated based on the nutrient delivered by the rivers.

Consistent with other studies (Wang et al. 2017), lateral TOC and DIC exchanges in our study also showed large temporal variability (Fig. 3b&e). In general, lateral transport of different carbon sources followed a seasonal pattern, i.e., high TOC but low DIC transport in April—August while low TOC but high DIC transport in December—February. It is likely that drier winter prohibits plant photosynthesis on tidal wetland in December-February, thus organic carbon degradation caused DIC accumulation. Such lateral transport might support extensive winter autotrophy in these estuaries according to concurrent positive NEM and $CO_2$ uptake

(Russell and Montagna 2007; Yao et al. 2019, *in revision*). Conversely, increased production in marsh and mangrove yielded a high TOC/DIC ratio lateral flux through spring—summer flooding (April—August). In addition, floods could further increase lateral TOC transport by flushing more organic matter into the estuary.

4.4.2. Hydrologic control on estuarine carbon budget

During the period, the south Texas experienced extreme hydrologic changes from extremely dry (prior to April 2015) to wet, the latter also included a strong hurricane. We thus assigned the study period to four hydrologic conditions—drought, flood-relaxation, flood and hurricane (details in Table 4.3)—to further assess the estuarine carbon budget variability during this wide range of hydrologic conditions.

Air-water $CO_2$ flux, lateral exchange, organic carbon burial and NEM experienced most intense changes during the transitions between different hydrologic conditions (Fig. 4.5). Air-water $CO_2$ flux suggests that this area is an overall $CO_2$ source with moderate to strong emissions (22.2±81.0—184.7±256.6 $mmol \cdot C \cdot m^{-2} \cdot d^{-1}$) corresponding to hydrologic changes. It is worth noting that hurricane flooding lifted $CO_2$ flux by ~2—10 times compared to baseline values, with dramatic increase in northern estuary LCE (18.90±45.3 to 169.8±166.5 $mmol \cdot C \cdot m^{-2} \cdot d^{-1}$) and GE (40.1±83.2 to 403.0±424.1 $mmol \cdot C \cdot m^{-2} \cdot d^{-1}$), compared with mild increase in southern MAE (30.6±33.2 to 64.2±38.7 $mmol \cdot C \cdot m^{-2} \cdot d^{-1}$) and NE (15.6±27.9 to 45.8±68.3 $mmol \cdot C \cdot m^{-2} \cdot d^{-1}$), the latter two were on the "dry" side of the storm and riverine input did not substantially increase (seen as lower area-normalized riverine DIC and TOC inflows, Fig. 4.3a&d). This $CO_2$ flux increase in LCE and GE agreed with other similar studies that also found 5—9 times elevation of estuarine $CO_2$ fluxes due to storms or storm-induced flooding (Sarma et al. 2012; Van Dam et al. 2018). Such increase could be attributed to relevant biogeochemical processes changes, i.e.

enhanced aerobic respiration/mineralization, in response to hydrologic effort and riverine $CO_2$ ventilation (Yao et al. 2019, *in revision*).

Our study assessed the hydrologic impact on lateral transport in nwGOM estuaries. As expected, storm/hurricane-driven flooding accelerated lateral TOC transport from 42.7±87.5 $mmol \cdot C \cdot m^{-2} \cdot d^{-1}$ (dry) to 155.6±136.2 $mmol \cdot C \cdot m^{-2} \cdot d^{-1}$ (flooding, Fig. 4.5 from D to F), and averaged lateral DIC transport from -2.8±45.3 $mmol \cdot C \cdot m^{-2} \cdot d^{-1}$ (dry) to 94.3±222.5 $mmol \cdot C \cdot m^{-2} \cdot d^{-1}$ after the hurricane (Fig. 4.5 from D to H). We suspect that these transports were most likely caused by large surface runoff, as submarine groundwater discharge might actually decrease in their relative significance during flooding (Murgulet et al. 2018). This further confirmed the crucial role of lateral transport on the carbon budget. Because residence time has a key control on estuarine organic carbon degradation (Hopkinson et al. 1998), annual average long residence time in these four estuaries particularly in MAE and NE (Table 4.1), was presumably responsible for such organic carbon processing.

Despite the substantial TOC input, annually aggregated NEM in our study suggests a slight heterotrophy (-4.4±2.2 $mol \cdot C \cdot m^{-2} \cdot yr^{-1}$). The nearly balanced NEM was comparable to another lagoonal estuaries. For example, New River Estuary in North Carolina had NEM between -3.0—1.1 $mol \cdot C \cdot m^{-2} \cdot yr^{-1}$ (Crosswell et al. 2017). Nevertheless, the NEM also displayed spatiotemporal fluctuations similar to estuarine $CO_2$ flux pattern (Fig. 4.5), within range between -312.5—283.1 $mmol \cdot C \cdot m^{-2} \cdot d^{-1}$. Because previous incubation estimates pelagic NEM from -250—187.5 $mmol \cdot C \cdot m^{-2} \cdot d^{-1}$ during the 2004 flooding season (Russell and Montagna 2007), the difference suggests approximately 20—40% benthic contribution. Model simulation in adjacent Galveston Bay illustrated that oxygen concentration quickly decreases to zero in one hour without benthic

photosynthesis (An and Joye 2001). Wang et al. (2018) also suggested that 27—33% oxygen consumption occurs in sediment in two eutrophic estuaries in south Texas.

4.4.3. Integrated carbon budget and future climate influence

Global estuarine $CO_2$ emission offsets continental shelf $CO_2$ uptake despite their much smaller area (Bauer et al. 2013; Cai 2011). Our studied annual estuarine $CO_2$ emission at nwGOM coast was 16.8±3.0 $mol \cdot C \cdot m^{-2} \cdot yr^{-1}$, which was essentially threefold comparable to average $CO_2$ emission from East Coast estuaries (4.6±1.9 $mol \cdot C \cdot m^{-2} \cdot yr^{-1}$; Najjar et al. 2018). Given that North America has the world's largest estuarine surface area but lowest $CO_2$ flux emission (2.2 $mol \cdot C \cdot m^{-2} \cdot yr^{-1}$; Chen et al. 2013), which was mostly based on estuaries in the east coast, our findings highlighted the importance of greater coverage on studying estuarine $CO_2$ fluxes, particularly for those areas that still have large data gap (Fig. 4.6). We anticipate that a higher average estuarine $CO_2$ flux from North America (7.5±10.9 $mol \cdot C \cdot m^{-2} \cdot yr^{-1}$, more than three times higher) will result if more GOM coasts are included.

Based on this study and the literature (Ho et al. 2016; Jiang et al. 2008; Wang and Cai 2004), northwestern and eastern GOM coasts, together with the southeastern U.S. coast are among highest $CO_2$ emission level despite large variability (Fig. 4.6; Appendix 1). One important reason was due to highest riverine $CO_2$ in southern U.S. ($pCO_2$ ranged 4000—6000 μatm; Butman and Raymond 2011) and high wind speed despite relatively moderate water $pCO_2$ (this study, Yao and Hu). In addition, lateral carbon transport from saltmarshes and mangroves has not been adequately accounted for in explaining $CO_2$ flux. The ratio of marsh to mangrove was about 6.4:1 along the nwGOM coastline (240.4 and 37.9 $km^2$ in larger scale survey, respectively; Armitage et al. 2015). We applied this ratio to estimate regional total carbon fixation, sequestration and sediment $CO_2$ evasion based on previous studies (Fig. 4.7). For example, we

assumed total carbon fixation in this area was ~92.0 mol·C·m$^{-2}$·yr$^{-1}$, based on the 6.4:1 ratio, i.e. saltmarsh production rate is (89.4 mol·C·m$^{-2}$·yr$^{-1}$ from East Coast; Wang et al. 2016) and mangrove production rate is (109 mol·C·m$^{-2}$·yr$^{-1}$ globally; Bouillon et al. 2008) carbon fixation rates. In addition, high sedimentation rate in our studied estuaries held most of the lateral TOC transport (~75%), allowing only ~25% either respired/remineralized or exported to the coastal ocean. This carbon accumulation in estuarine sediment together with estimated wetland sequestration (Fig. 4.8) yields a high carbon burial rate of 26.8 mol·C·m$^{-2}$·yr$^{-1}$ in nwGOM estuaries. Therefore, our study highlights the necessity of re-evaluating coastal carbon sequestration (also known as "blue carbon"), which should have included buried carbon in estuaries/coastal shelves. Integrated sequestration from our study, for example, is about sevenfold higher than the global average, 4.8 mol·C·m$^{-2}$·yr$^{-1}$ of tidal wetland sequestration (Chmura et al. 2003). However, a possible large spatiotemporal variability is expected, depending on estuarine trophodynamics and residence time.

Unfortunately, nwGOM coast is recorded 77.8 km$^2$ of total saltmarsh loss from 1990 to 2010, a 24% net decrease under the influences of sea level rise and climate change (Armitage et al. 2015). Despite the northward mangrove expansion (16.1 km$^2$ increase totally; Armitage et al. 2015), there is still a 61.7 km$^2$ yr$^{-1}$ (~1% per year) net loss of marsh-mangrove ecotone in the last two decades. Consequently, we would estimate ~0.2 and ~0.1 mol·C·m$^{-2}$·yr$^{-1}$ decline of lateral TOC and DIC inflows respectively, amounting up to 0.9% and 0.6% of total TOC and DIC inputs that including riverine and lateral inflows. This decline is translated to ~0.14 mol·C·m$^{-2}$·yr$^{-1}$ (~1%) of decline in the annual estuarine $CO_2$ flux in this region ($CO_2$ flux ≈ 0.7×lateral TOC; Fig. 4.4a). In fact, this decline could be more dramatic if estuarine water contains more GOM seawater of lower $pCO_2$. Contrary to floods that dramatically elevate estuarine $CO_2$

evasion, sea level rise will decrease estuarine $CO_2$ flux by sinking tidal wetland and inducing more open ocean seawater. In this regard we could expect a scenario of gradually decreasing $CO_2$ flux in long-term but episodic flood-driven fluctuations.

4.5. Implications

Coastal carbon budget is important yet highly dynamic. Our mass balance model highlights the crucial lateral transport from saltmarsh and mangrove habitats. For example, lateral TOC inflow that exceeds riverine TOC inflow more than ten times, accounting for almost 95% of total TOC input to estuarine system. Given the extensive distribution of marsh-mangrove ecotone in the nwGOM coast, lateral carbon transport is not well studied. In addition, the high estuarine air-water $CO_2$ fluxes stresses the importance of sufficient spatial coverage in studying the GOM coast, by doing so we can better constrain the North American coastal carbon budget.

On the other hand, attempts to assess coastal carbon budget variability require better understanding of estuarine hydrology. Our four-year data that covered multiple dry-flooding cycles suggests as much as 2—10 times increase in estuarine $CO_2$ flux driven by floods compared with non-flood period. However, the magnitude of change itself suffers spatial variability as well, that is mainly depending on residence time and the amount of freshwater discharge that each estuary received. Other than hydrology, coastal saltmarsh-mangrove loss from sea level rise may eventually exert a decline of estuarine $CO_2$ emission. In our study, there is estimated ~1% per year decline due to sea level rise. At last, higher resolution spatiotemporal sampling and resulted interpretation of coastal carbon budget that integrating estuarine and tidal wetland systems, will enable us to better understand future challenge of climate change on coastal and ultimately global carbon cycle.

References

An, S., and S. B. Joye. 2001. Enhancement of coupled nitrification□denitrification by benthic photosynthesis in shallow estuarine sediments. Limnology and oceanography **46:** 62-74.

Armitage, A. R., W. E. Highfield, S. D. Brody, and P. Louchouarn. 2015. The contribution of mangrove expansion to salt marsh loss on the Texas Gulf Coast. PLoS One **10:** e0125404.

Bauer, J. E., W. J. Cai, P. A. Raymond, T. S. Bianchi, C. S. Hopkinson, and P. A. Regnier. 2013. The changing carbon cycle of the coastal ocean. Nature **504:** 61-70.

Benway, H., and P. Coble. 2014. Report of The US Gulf of Mexico Carbon Cycle Synthesis Workshop, March 27-28, 2013. Ocean Carbon and Biogeochemistry Program and North American Carbon Program.

Bianchi, T. S. and others 2013. Historical reconstruction of mangrove expansion in the Gulf of Mexico: linking climate change with carbon sequestration in coastal wetlands. Estuarine, Coastal and Shelf Science **119:** 7-16.

Borges, A. V., B. Delille, and M. Frankignoulle. 2005. Budgeting sinks and sources of $CO_2$ in the coastal ocean: Diversity of ecosystems counts. Geophysical Research Letters **32**.

Borges, A. V., L. S. Schiettecatte, G. Abril, B. Delille, and F. Gazeau. 2006. Carbon dioxide in European coastal waters. Estuarine, Coastal and Shelf Science **70:** 375-387.

Bouillon, S. and others 2008. Mangrove production and carbon sinks: a revision of global budget estimates. Global Biogeochemical Cycles **22**.

Bronikowski, J. L. 2004. Sedimentary environments and processes in a shallow, Gulf Coast Estuary-Lavaca Bay, Texas. Texas A&M University.

Butman, D., and P. A. Raymond. 2011. Significant efflux of carbon dioxide from streams and rivers in the United States. Nature Geoscience **4:** 839-842.

Cai, W. J. 2011. Estuarine and coastal ocean carbon paradox: $CO_2$ sinks or sites of terrestrial carbon incineration? Annual Review of Marine Science **3:** 123-145.

Carter, B. R., J. A. Radich, H. L. Doyle, and A. G. Dickson. 2013. An automated system for spectrophotometric seawater pH measurements. Limnology and Oceanography: Methods **11:** 16-27.

Chen, C. T. A., T. H. Huang, Y. C. Chen, Y. Bai, X. He, and Y. Kang. 2013. Air–sea exchanges of $CO_2$ in the world's coastal seas. Biogeosciences **10:** 6509-6544.

Chmura, G. L., S. C. Anisfeld, D. R. Cahoon, and J. C. Lynch. 2003. Global carbon sequestration in tidal, saline wetland soils. Global Biogeochemical Cycles **17**.

Crosswell, J. R. and others 2017. Carbon budget of a shallow, lagoonal estuary: Transformations and source-sink dynamics along the river-estuary-ocean continuum. Limnology and Oceanography **62:** S29-S45.

Dickson, A. G. 1990. Standard potential of the reaction: $AgCl(s)+ 12H_2(g)= Ag(s)+ HCl(aq)$, and and the standard acidity constant of the ion $HSO_4^-$ in synthetic sea water from 273.15 to 318.15 K. The Journal of Chemical Thermodynamics **22:** 113-127.

Dürr, H. H., G. G. Laruelle, C. M. van Kempen, C. P. Slomp, M. Meybeck, and H. Middelkoop. 2011. Worldwide typology of nearshore coastal systems: Defining the estuarine filter of river inputs to the oceans. Estuaries and Coasts **34:** 441-458.

Friis, K., A. Körtzinger, and D. W. R. Wallace. 2003. The salinity normalization of marine inorganic carbon chemistry data. Geophysical Research Letters **30**.

Gordon, D. and others 1996. LOICZ biogeochemical modelling guidelines. LOICZ Core Project, Netherlands Institute for Sea Research Yerseke.

Ho, D. T., N. Coffineau, B. Hickman, N. Chow, T. Koffman, and P. Schlosser. 2016. Influence of current velocity and wind speed on air□water gas exchange in a mangrove estuary. Geophysical Research Letters **43:** 3813-3821.

Ho, D. T., S. Ferrón, V. C. Engel, L. G. Larsen, and J. G. Barr. 2014. Air-water gas exchange and CO2 flux in a mangrove-dominated estuary. Geophysical Research Letters **41:** 108-113.

Hopkinson, C. S. 1988. Patterns of organic carbon exchange between coastal ecosystems, p. 122-154. Coastal-Offshore Ecosystem Interactions. Springer. Berlin, Heidelberg.

Hopkinson, C. S. and others 1998. Terrestrial inputs of organic matter to coastal ecosystems: an intercomparison of chemical characteristics and bioavailability. Biogeochemistry **43:** 211-234.

Jiang, L. Q., W. J. Cai, and Y. Wang. 2008. A comparative study of carbon dioxide degassing in river- and marine-dominated estuaries. Limnology and Oceanography **53:** 2603-2615.

Kanamori, S., and H. Ikegami. 1980. Computer-processed potentiometric titration for the determination of calcium and magnesium in sea water. Journal of the Oceanographical Society of Japan **36:** 177-184.

Kemp, W., E. Smith, M. Marvin-DiPasquale, and W. Boynton. 1997. Organic carbon balance and net ecosystem metabolism in Chesapeake Bay. Marine Ecology Progress Series**:** 229-248.

Laruelle, G. G., N. Goossens, S. Arndt, W.-J. Cai, and P. Regnier. 2017. Air–water CO2 evasion from US East Coast estuaries. Biogeosciences **14:** 2441-2468.

Maher, D. T., and B. D. Eyre. 2012. Carbon budgets for three autotrophic Australian estuaries: Implications for global estimates of the coastal air-water CO2 flux. Global Biogeochemical Cycles **26**.

Maher, D. T., I. R. Santos, L. Golsby-Smith, J. Gleeson, and B. D. Eyre. 2013. Groundwater-derived dissolved inorganic and organic carbon exports from a mangrove tidal creek: The missing mangrove carbon sink? Limnology and Oceanography **58:** 475-488.

Millero, F. J. 2010. Carbonate constants for estuarine waters. Marine and Freshwater Research **61:** 139-142.

Montagna, P., T. A. Palmer, and J. Pollack. 2012. Hydrological Changes and Estuarine Dynamics Springer Science & Business Media.

Montagna, P. A., and R. D. Kalke. 1992. The effect of freshwater inflow on meiofaunal and macrofaunal populations in the Guadalupe and Nueces estuaries, Texas. Estuaries **15:** 307-326.

Murgulet, D., V. Murgulet, N. Spalt, A. Douglas, and R. G. Hay. 2016. Impact of hydrological alterations on river-groundwater exchange and water quality in a semi-arid area: Nueces River, Texas. Science of the Total Environment **572:** 595-607.

Murgulet, D., M. Trevino, A. Douglas, N. Spalt, X. Hu, and V. Murgulet. 2018. Temporal and spatial fluctuations of groundwater-derived alkalinity fluxes to a semiarid coastal embayment. Science of the Total Environment **630:** 1343-1359.

Najjar, R. G. and others 2018. Carbon budget of tidal wetlands, estuaries, and shelf waters of eastern North America. Global Biogeochemical Cycles **32:** 389-416.

Orr, J. C., J.-M. Epitalon, A. G. Dickson, and J.-P. Gattuso. 2018. Routine uncertainty propagation for the marine carbon dioxide system. Marine Chemistry **207:** 84-107.

Regnier, P. and others 2013. Anthropogenic perturbation of the carbon fluxes from land to ocean. Nature geoscience **6:** 597–607.

Russell, M. J., and P. A. Montagna. 2007. Spatial and temporal variability and drivers of net ecosystem metabolism in western Gulf of Mexico estuaries. Estuaries and Coasts **30:** 137-153.

Russell, M. J., P. A. Montagna, and R. D. Kalke. 2006. The effect of freshwater inflow on net ecosystem metabolism in Lavaca Bay, Texas. Estuarine, Coastal and Shelf Science **68:** 231-244.

Saintilan, N., K. Rogers, and K. McKee. 2009. Salt marsh-mangrove interactions in Australasia and the Americas, p. 855-884. Coastal wetlands an integrated ecosystem approach. Elsevier.

Sarma, V. V. S. S. and others 2012. Carbon dioxide emissions from Indian monsoonal estuaries. Geophysical Research Letters **39**.

Sippo, J. Z., D. T. Maher, D. R. Tait, C. Holloway, and I. R. Santos. 2016. Are mangroves drivers or buffers of coastal acidification? Insights from alkalinity and dissolved inorganic carbon export estimates across a latitudinal transect. Global Biogeochemical Cycles **30:** 753-766.

Smith, S. V., J. T. Hollibaugh, S. J. Dollar, and S. Vink. 1991. Tomales Bay Metabolism: C-N-P Stoichiometry and Ecosystem Heterotrophy at the Land-Sea Interface. Estuarine, Coastal and Shelf Science **33:** 223-257.

Solis, R., and G. Powell. 1999. Hydrography, mixing characteristics, and residence times of Gulf of Mexico estuaries, p. 29-61. Biogeochemistry of Gulf of Mexico estuaries. John Wiley & Sons.

Swaney, D. P. and others 2012. Five critical questions of scale for the coastal zone. Estuarine, Coastal and Shelf Science **96:** 9-21.

Van Dam, B. R., J. R. Crosswell, and H. W. Paerl. 2018. Flood-driven $CO_2$ emissions from adjacent North Carolina estuaries during Hurricane Joaquin (2015). Marine Chemistry **207:** 1-12.

Wang, H., X. Hu, M. S. Wetz, and K. C. Hayes. 2018. Oxygen Consumption and Organic Matter Remineralization in Two Subtropical, Eutrophic Coastal Embayments. Environmental science & technology **52:** 13004-13014.

Wang, S. R., D. I. Daniela, W.-J. Cai, and C. S. Hopkinson. 2017. Inorganic carbon and oxygen dynamics in a marsh-dominated estuary. Limnology and Oceanography **63:** 47-71.

Wang, Z. A., and W. J. Cai. 2004. Carbon dioxide degassing and inorganic carbon export from a marsh□dominated estuary (the Duplin River): A marsh CO2 pump. Limnology and Oceanography **49:** 341-354.

Wang, Z. A., K. D. Kroeger, N. K. Ganju, M. E. Gonneea, and S. N. Chu. 2016. Intertidal salt marshes as an important source of inorganic carbon to the coastal ocean. Limnology and Oceanography **61:** 1916-1931.

Weiss, R. F. 1974. Carbon dioxide in water and seawater: the solubility of a non-ideal gas. Marine Chemistry **2:** 203-215.

Willey, J. D., R. J. Kieber, M. S. Eyman, and G. B. Avery. 2000. Rainwater dissolved organic carbon: concentrations and global flux. Global Biogeochemical Cycles **14:** 139-148.

Yao, H., and X. Hu. 2017. Responses of carbonate system and $CO_2$ flux to extended drought and intense flooding in a semiarid subtropical estuary. Limnology and Oceanography **62:** S112-S130.

Yeager, K. M., P. Santschi, K. Schindler, M. Andres, and E. Weaver. 2006. The relative importance of terrestrial versus marine sediment sources to the Nueces-Corpus Christi Estuary, Texas: An isotopic approach. Estuaries and coasts **29:** 443-454.

Zeng, F.-W., C. A. Masiello, and W. C. Hockaday. 2011. Controls on the origin and cycling of riverine dissolved inorganic carbon in the Brazos River, Texas. Biogeochemistry **104:** 275-291.

Table 4.1. Hydrologic information in four nwGOM lagoons

| | | Location | | | | Reference |
|---|---|---|---|---|---|---|
| | | LCE | GE | MAE | NE | |
| Mean Depth (m) | | 1.1 | 1.1 | 1.1 | 1.2 | (Solis and Powell 1999) |
| Open Water Area ($km^2$) | | 794.1 | 339.9 | 575.7 | 537.1 | (TCEQ) |
| Watershed Inflow ($km^3 \cdot yr^{-1}$) | | 4.17 | 2.95 | 0.55 | 0.75 | (TWDB) |
| Residence Time (d) | | 81 | 39 | 360 | 356 | (Bianchi et al. 1999) |
| Annual River Discharge ($m^3 \cdot s^{-1}$) | | 107.9 | 48.3 | 7.3 | 8.6 | (USGS) |
| Riverine DIC | D | 2941.9±569.6 | 4454.9±535.0 | 4948.4±994.4 | 4062.6±297.4 | (This study) |
| ($\mu mol \cdot kg^{-1}$) | W | 2061.2±879.6 | 2884.6±758.5 | 2925.7±957.4 | 3744.5±388.9 | |
| Riverine TOC | D | 558.4±204.9 | 371.5±151.4 | 300.7±31.1 | 619.3±72.9 | (TCEQ) |
| ($\mu mol \cdot kg^{-1}$) | W | 368.7±242.6 | 558.6±333.4 | 777.2±221.0 | 605.9±125.6 | |
| Sediment TOC Content | D | 5.4±3.7 | 6.0±0.8 | 2.8±0.7 | 4.2±1.8 | (TCEQ) |
| (‰) | W | 10.6±8.1 | 9.8±5.3 | 21.4±15.9 | 5.2±3.3 | |
| Sedimentation Rate ($cm \cdot yr^{-1}$) | | 0.92 | 0.84 | 0.22 | 0.26 | (Bianchi et al. 2013a; Bronikowski 2004; Yeager et al. 2006) |

D= dry and flood relaxation condition; W= flooding and hurricane condition;
TCEQ= Texas Commission of Environmental Quality, https://www.tceq.texas.gov/;
TWDB= Texas Water Development Board, http://www.twdb.texas.gov/

Table 4.2. Annual carbon fluxes (unit: $mol \cdot C \cdot m^{-2} \cdot yr^{-1}$) in four nwGOM lagoons.

| Location | Riverine Inflow | | Lateral Transport | | Export | | Evaporation/Rainfall | | Calcification | Air-water $CO_2$ Flux | NEM | Carbon Burial |
|---|---|---|---|---|---|---|---|---|---|---|---|---|
| | TOC | DIC | TOC | DIC | TOC | DIC | TOC | DIC | | | | |
| LCE | 0.8 (0.7) | 6.5 (6.8) | 41.2 (18.9) | 11.4 (13.1) | 1.2 (1.8) | 6.1 (8.3) | <0.01 | -0.01 (0.003) | <0.01 | 18.0 (22.5) | -5.9 (17.3) | 34.3 (9.2) |
| GE | 2.1 (1.2) | 13.5 (5.5) | 24.4 (19.9) | 19.1 (17.0) | 2.4 (1.1) | 10.1 (5.1) | <0.01 | -0.02 (0.01) | <0.01 | 31.6 (34.5) | -9.1 (18.7) | 15.1 (2.8) |
| MAE | 0.3 (1.1) | 1.3 (6.0) | 5.3 (3.8) | 3.3 (1.9) | 1.1 (1.0) | 5.8 (4.5) | <0.01 | -0.01 (0.005) | 0.014 (0.005) | 7.1 (2.4) | -1.9 (4.3) | 3.9 (0.8) |
| NE | 0.2 (0.03) | 1.4 (1.4) | -7.3 (11.1) | 12.1 (8.8) | 0.2 (0.1) | 0.4 (0.7) | <0.01 | -0.03 (0.02) | <0.01 | 3.8 (2.6) | 9.2 (11.2) | 1.9 (0.1) |

Values in bracket indicate the standard deviations.

Table 4.3. Estuarine carbonate system in different hydrologic periods. (unit: *μmol·kg$^{-1}$ for DIC*)

| Hydrologic condition and corresponding time period | | LCE | | | GE | | | MAE | | | NE | | |
|---|---|---|---|---|---|---|---|---|---|---|---|---|---|
| | | Sal | pH | DIC | Sal | pH | DIC | Sal | pH | DIC | Sal | pH | DIC |
| D | April 2014—March 2015; February—August 2017; January—April 2018 | 24.9 (4.7) | 8.103 (0.166) | 2314.7 (374.5) | 20.7 (7.1) | 8.224 (0.215) | 2369.3 (285.2) | 29.0 (7.3) | 8.057 (0.117) | 2279.2 (192.6) | 34.4 (3.3) | 8.031 (0.110) | 2264.0 (127.9) |
| FR | August 2015—May 2016; September 2016—January 2017; September—December 2017 | 19.9 (4.7) | 8.146 (0.114) | 2333.8 (345.6) | 13.3 (5.2) | 8.165 (0.995) | 2527.7 (419.0) | 20.6 (6.4) | 8.162 (0.143) | 2342.7 (208.9) | 29.9 (1.9) | 8.075 (0.102) | 2272.2 (120.4) |
| F | April—July 2015; June—August 2016; | 13.4 (8.7) | 8.097 (0.307) | 2020.7 (414.2) | 6.1 (5.4) | 8.189 (0.216) | 2967.7 (313.1) | 14.9 (9.7) | 8.210 (0.167) | 2110.3 (289.2) | 28.2 (4.7) | 8.149 (0.173) | 2232.9 (221.8) |
| H | September—October 2017 | 13.5 (6.2) | 8.000 (0.140) | 2468.9 (448.8) | 6.9 (6.5) | 7.896 (0.280) | 2293.6 (336.2) | 11.6 (5.7) | 8.165 (0.163) | 1998.4 (220.6) | 30.3 (2.3) | 8.123 (0.078) | 2059 (57.9) |

D=drought; FR=flood relaxation; F=flooding; H=hurricane;

Values in bracket indicate the standard deviations.

Table 4.4. Lateral TOC and DIC export (unit: $mol \cdot C \cdot m^{-2} \cdot yr^{-1}$) from saltmarsh and mangrove

| Site | Wetland System | Lateral TOC | Lateral DIC | Reference |
|---|---|---|---|---|
| Global | Mangrove | 21.0±23.1 | | (Bouillon et al. 2008) |
| Global | Mangrove | | 18.7 | (Borges et al. 2005) |
| US East Coast | Salt Marsh | 14.9 | 34.6 | (Wang et al. 2016) |
| Australia | Mangrove | | 21.5±10.6 | (Sippo et al. 2016) |
| Georgia (US) | Salt Marsh | | 13 | (Wang and Cai 2004) |
| Northwest GOM (US) | Salt Marsh and Mangrove | 17.9±7.1 | 12.4±1.3 | This study |

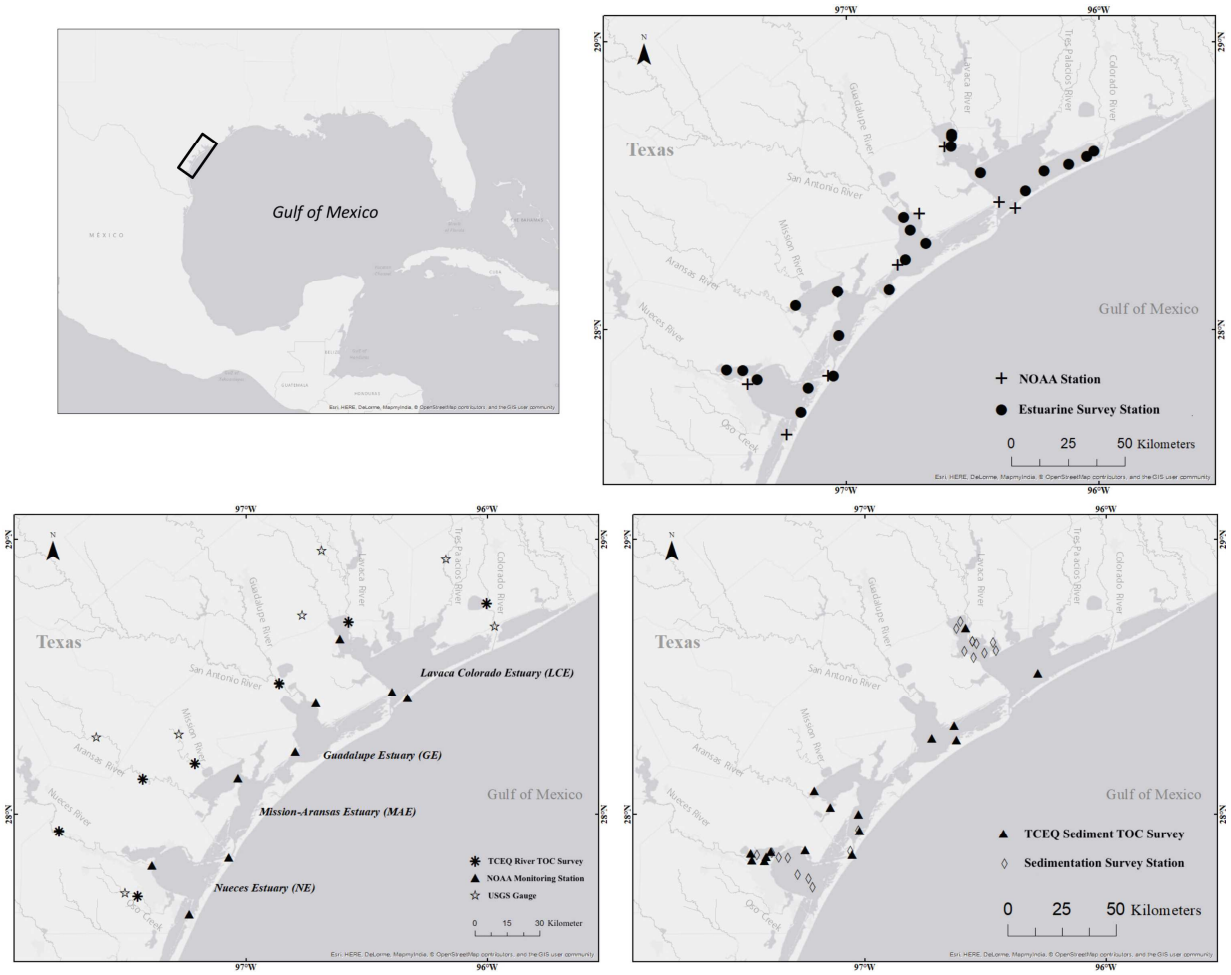


Figure 4.1. Sampling stations in northwestern GOM estuaries, a. estuary; b. river; c. sediment.

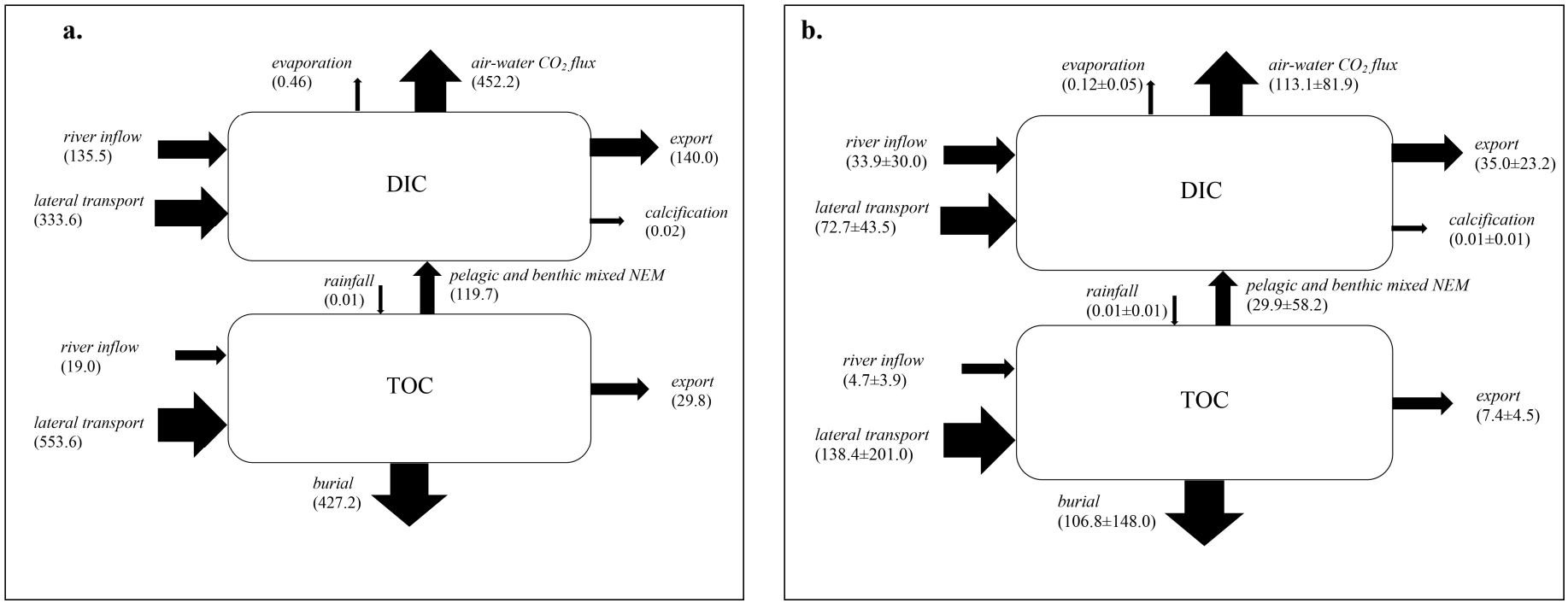


Figure 4.2. a. Integrated carbon fluxes (unit: $Gg{\cdot}C{\cdot}yr^{-1}$ *or* $10^{9}g{\cdot}C{\cdot}yr^{-1}$) for the four nwGOM estuaries; b. Averaged carbon fluxes among the four nwGOM estuaries.

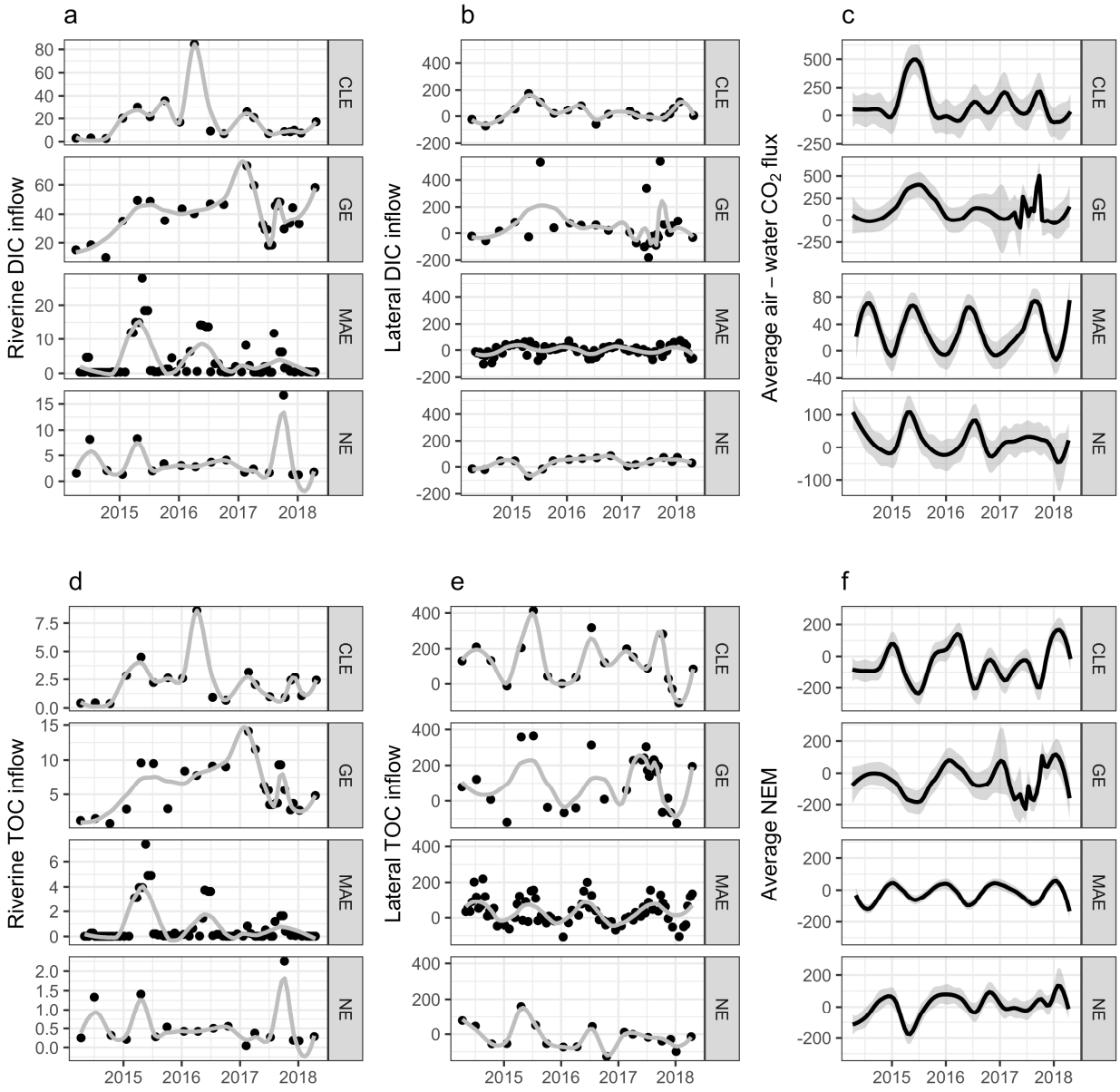


Figure 4.3. Carbon fluxes (unit: $mmol{\cdot}C{\cdot}m^{-2}{\cdot}d^{-1}$) in four studied estuaries. a. riverine DIC inflows; b. lateral DIC inflows; c. averaged air-water $CO_2$ flux; d. riverine TOC inflows; e. lateral TOC inflows; f. averaged NEM.

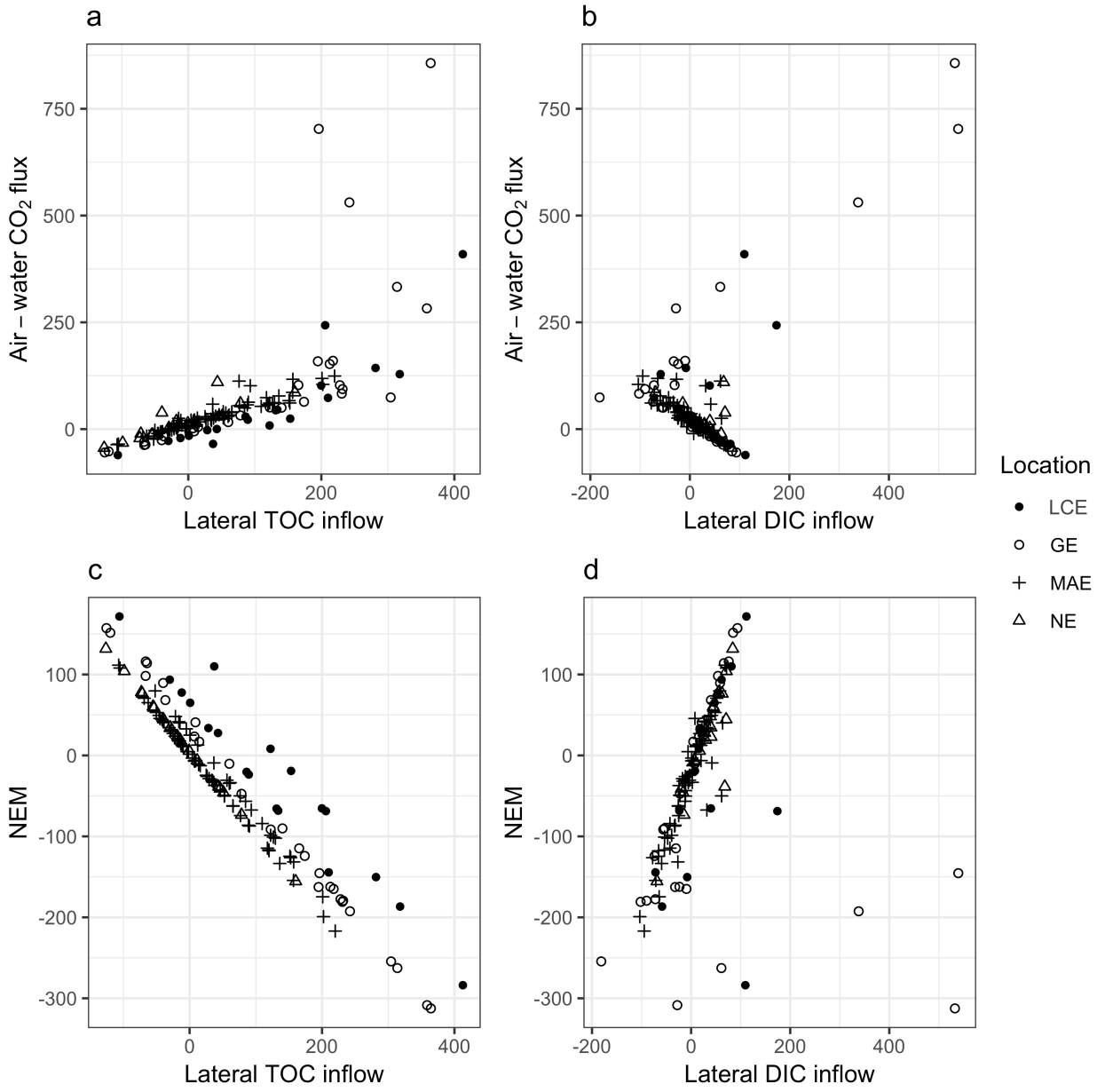


Figure 4.4. Correlations between different fluxes (unit: $mmol \cdot C \cdot m^{-2} \cdot d^{-1}$). a. lateral TOC vs. air-water $CO_2$ flux; b. lateral DIC vs. air-water $CO_2$ flux; c. lateral TOC vs. NEM; d. lateral DIC vs. NEM.

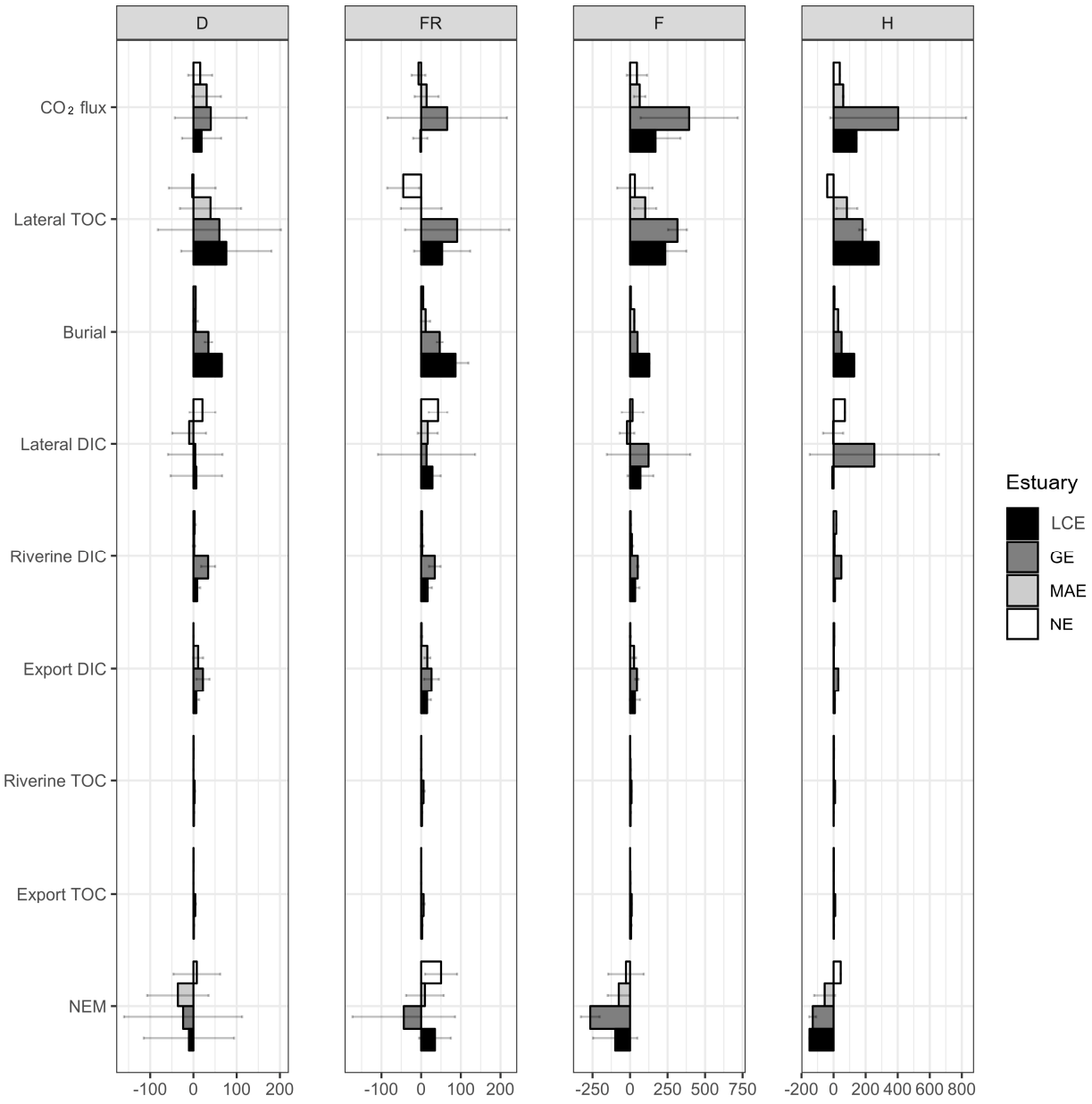


Figure 4.5. Carbon fluxes (unit: $mmol{\cdot}C{\cdot}m^{-2}{\cdot}d^{-1}$) under different hydrologic conditions. The headings are D—drought; FR—flooding relaxation; F—flooding; H—hurricane.

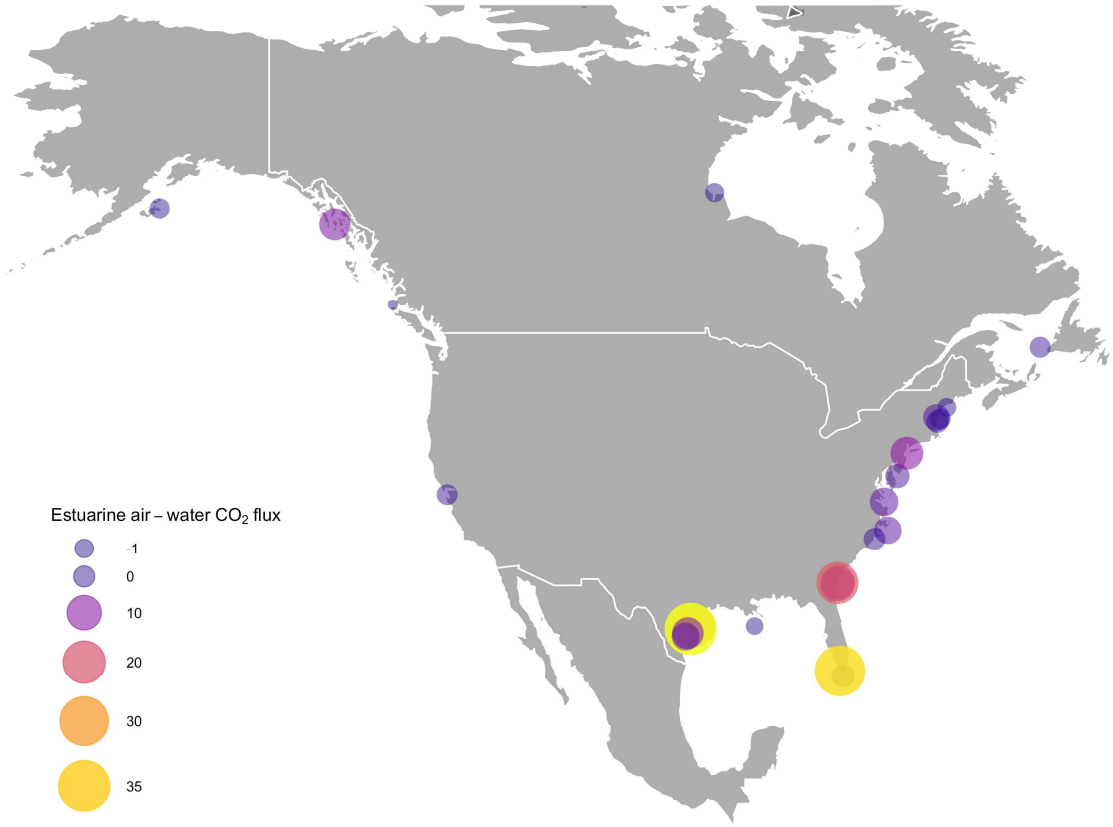


Figure 4.6. Estuarine air-water $CO_2$ fluxes (unit: $mol \cdot C \cdot m^{-2} \cdot yr^{-1}$, see more details in Appendix. 1) in North America's coast.

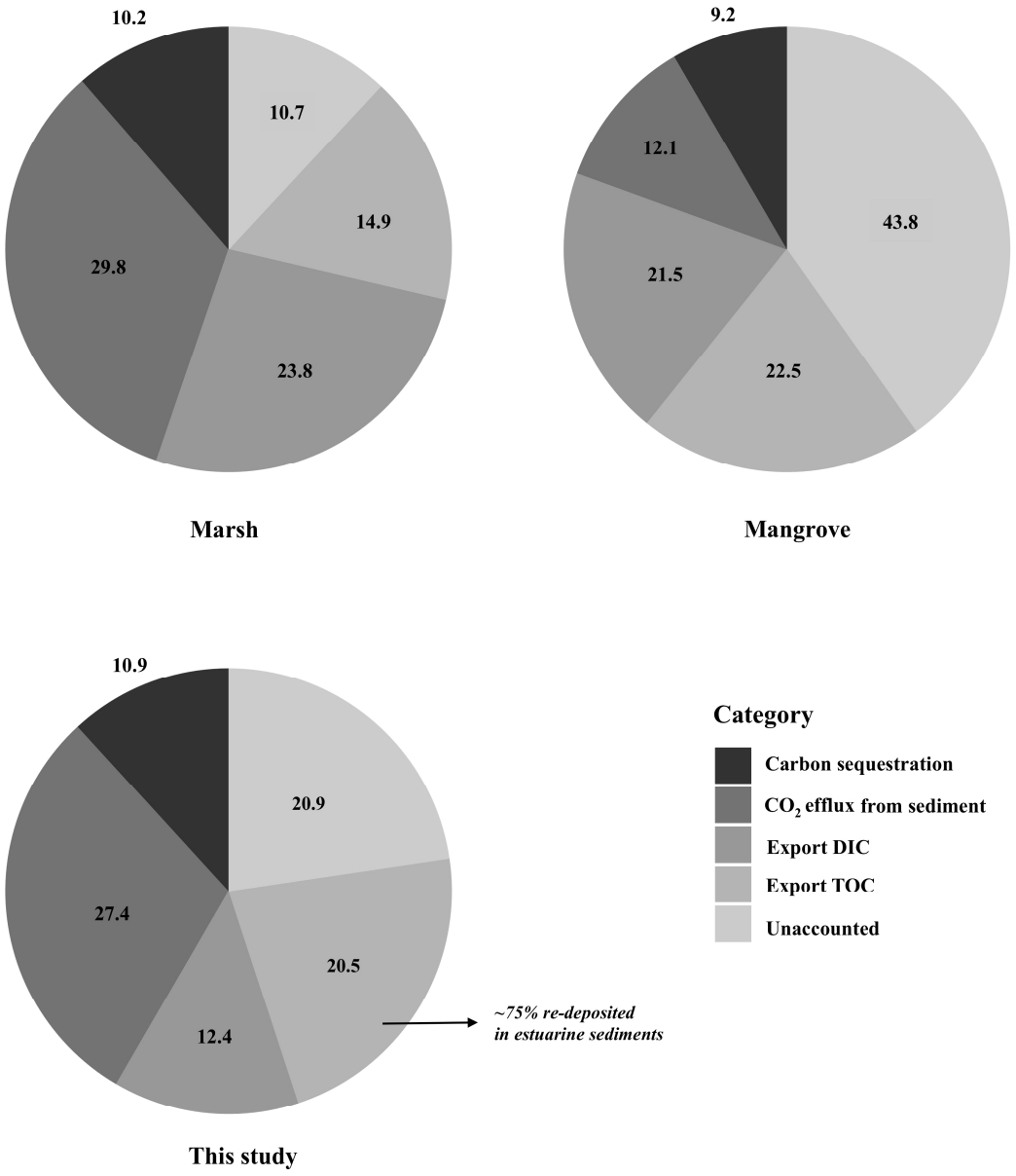


Figure 4.7. Carbon fluxes (unit: $mol{\cdot}C{\cdot}m^{-2}{\cdot}yr^{-1}$) from saltmarsh and mangrove, comparison between this study and other research (Borges et al. 2005; Bouillon et al. 2008; Sippo et al. 2016; Wang and Cai 2004; Wang et al. 2016).

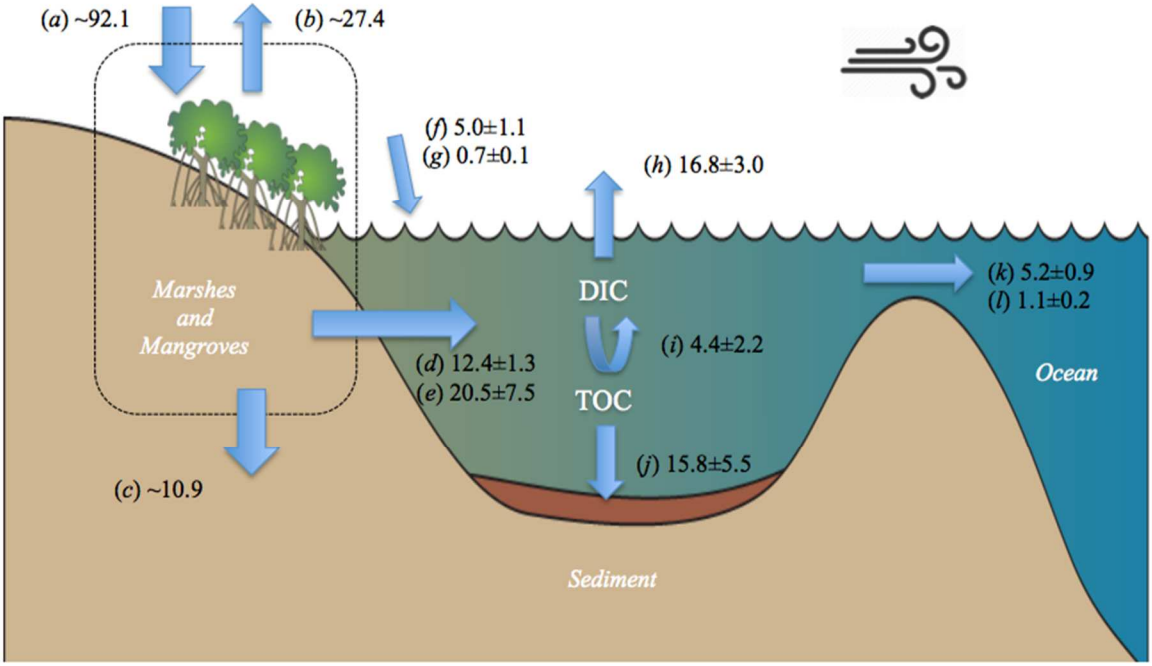


Figure 4.8. Schematic representation of integrated carbon fluxes (unit: $mol{\cdot}C{\cdot}m^{-2}{\cdot}yr^{-1}$) in the nwGOM estuaries. (a) carbon fixation by saltmarshes and mangroves; (b) $CO_2$ evasion from saltmarshes and mangroves; (c) carbon sequestration within the saltmarsh and mangrove habitats; (d) lateral DIC transport; (e) lateral TOC transport; (f) riverine DIC; (g) riverine TOC; (h) air-water $CO_2$ flux; (i) pelagic and benthic mixed NEM; (j) organic carbon burial; (k) DIC export; (l) TOC export.

# CHAPTER V: SUMMARY AND CONCLUSIONS

Through intensive observations of estuarine water carbonate system and air-water $CO_2$ flux calculations for four northwest Gulf of Mexico (nwGOM) estuaries that share geomorphologic similarity yet have hydrologic diversity, this dissertation revealed spatiotemporal variability of estuarine $CO_2$ flux and highlighted the hydrologic control in this land-ocean transition zone. In addition, with information on the riverine inflows and organic carbon burial (mostly rely on sedimentation and TOC content) in sediment, this study also evaluated the total carbon budget in this region and explored its controlling factors.

This study first investigated the carbonate system and estuarine $CO_2$ flux in Mission-Aransas Estuary during April 2014—April 2015 (Chapter II), which covered a large hydrologic range from hypersaline conditions in the beginning (May-October 2014) to a period after a spring flooding (March-April, 2015). During this period, the estuarine carbonate chemistry and $CO_2$ flux indicated an overall $CO_2$ source (12.4±3.3 $mol \cdot C \cdot m^{-2} \cdot y^{-1}$) but with high $CO_2$ emission under both hypersaline (74.5±41.1 $mmol \cdot m^{-2} \cdot d^{-1}$) and flooding (51.6±83.9 $mmol \cdot m^{-2} \cdot d^{-1}$) conditions. The former was due to high temperature-driven evaporation in conjunction with windy condition, while the later was attributed to enhanced biogeochemical process (i.e. organic matter respiration/mineralization) as a result of large increase in riverine inflows. In addition, thermal effect was highlighted under dry condition, especially when the entire estuary was turned to a $CO_2$ sink (-8.9±5.1 $mmol \cdot m^{-2} \cdot d^{-1}$) as water $pCO_2$ declined ~100 µatm due to cooling temperature in winter.

Second, the study incorporated three adjacent estuaries — Lavaca-Colorado- Estuary (LCE), Guadalupe Estuary (GE) and Nueces Estuary (NE)—and put all four estuaries in a longer study timeframe from April 2014—April 2017 (Chapter III), during which there was an extreme

hydrologic condition range from drought to completed flooding. All these estuaries were net $CO_2$ sources with annual emission ranged 2.7—35.9 $mol \cdot C \cdot m^{-2} \cdot y^{-1}$. Under the larger spatial coverage, a clear gradient, approximately one order of magnitude decline on annual $CO_2$ flux from north to south (35.9±24.2—2.7±8.1 $mol \cdot C \cdot m^{-2} \cdot y^{-1}$), was identified. This gradient corresponded to riverine inflows decrease. Hydrologic and climatic influences, such as river discharge, wind speed, and water temperature all played important roles in controlling estuarine $CO_2$ flux. Episodic flooding made the entire regional $CO_2$ fluxes differ significantly between dry (-0.7—20.9 $mmol \cdot C \cdot m^{-2} \cdot d^{-1}$) and wet (11.6—170.0 $mmol \cdot C \cdot m^{-2} \cdot d^{-1}$) conditions. Because of larger river discharge, hydrologic condition change tended to have larger influence on the northern estuaries (LCE and GE). Ventilation of river-borne $CO_2$ further strengthened the $CO_2$ emission when LCE and GE became overwhelmingly river-dominated. During flood relaxation, enhanced primary productivity as a result of riverine nutrient input compensated previous $CO_2$ emission from floods and resulted in smaller $CO_2$ efflux on an annual scale.

Based on the four-year data, a mass balance model was applied to evaluate the carbon budgets for both the entire nwGOM region and each individual estuary as studied above (Chapter IV). Based on my calculations, estuarine $CO_2$ emission in this region was from moderate to high compared with all other North American estuaries in the literature. In addition to the large spatial variability, the data that covered multiple dry-flooding cycles suggested as much as a 2—10 times increase in estuarine $CO_2$ flux driven by floods compared with non-flood period. The mass balance model also highlighted the crucial role of lateral carbon transport from saltmarsh and mangrove habitats. It is worth noting that lateral transport of total organic carbon (TOC) and dissolved inorganic carbon (DIC) exceeded riverine TOC and DIC by more than ten and two times respectively, accounted for almost 95% and 70% of total TOC and DIC input to the

estuarine open waters. However, the loss of coastal saltmarsh-mangrove habitats due to sea level rise could decrease estuarine $CO_2$ emission as a result of lateral transport decrease. It was estimated that ~1% per year decline in estuarine $CO_2$ emission will occur as a result of tidal wetland loss because of sea level rise.

The global estuarine carbon cycle still remains understudied due to large data gaps. Through intensive data interpretations, my dissertation will contribute to estuarine organic/inorganic carbon flux quantifications and understanding their controlling factor(s). Under the context of climate change, this study indicated that estuarine carbon cycle variability was highly dependent on estuarine hydrologic conditions. More comprehensive studies should be done to further assess this effect in a broader context.

# APPENDICES

## Appendix 1. Estuarine air-water $CO_2$ fluxes along North America's Coast

| Estuary | Type | Latitude (°) | Longitude (°) | Air-water $CO_2$ flux ($mol \cdot C \cdot m^{-2} \cdot y^{-1}$) | Reference |
|---|---|---|---|---|---|
| Sapelo Sound | B | 31.5 | -81.22 | 10.5 | (Jiang et al. 2008) |
| Doboy Sound | B | 31.4 | -81.3 | 10.7 | (Jiang et al. 2008) |
| Delaware | A | 39.0 | -75.0 | 2.4 | (Joesoef et al. 2015) |
| Florida Bay | B | 25.0 | -80.7 | 1.7 | (Millero et al. 2001) |
| Kennebec River | A | 43.8 | -69.8 | -0.5 | (Takahashi et al. 2012a) |
| Alaska fjord | B | 57.7 | -152.5 | 0.001 | (Takahashi et al. 2012a) |
| Cross Sound | B | 56.6 | -134.1 | 8.2 | (Takahashi et al. 2012a) |
| Little Bay Estuary | A | 43.1 | -70.9 | 4.0 | (Hunt et al. 2011) |
| Park River Estuary | A | 42.8 | -70.8 | 1.1 | (Raymond and Hopkinson 2003) |
| St. Lawernce Estuary | B | 48.0 | -60.0 | 0.5 | (Dinauer and Mucci 2017) |
| Nuece River Estuary | A | 35.2 | -76.0 | 4.7 | (Crosswell et al. 2012) |
| New River Estuary | A | 34.6 | -77.4 | 0.9 | (Crosswell et al. 2017) |
| Duplin River | A | 31.5 | -81.3 | 21.3 | (Wang and Cai 2004) |
| San Francisco Estuary | B | 37.7 | -122.3 | 0.4 | (Peterson 1979) |
| Mississippi Delta | B | 28.5 | -90.0 | -1.0 | (Huang et al. 2015) |
| Churchill River | A | 58.8 | -94.2 | -0.4 | (Stainton 2009) |
| Shark River | A | 25.4 | -81.0 | 36.1 | (Ho et al. 2016) |
| Gulf of Maine | B | 43.0 | -70.5 | 0.4 | (Vandemark et al. 2011) |
| Western Canadian Coast | B | 51.0 | -128.0 | -2.2 | (Evans et al. 2012) |

| | | | | | |
|---|---|---|---|---|---|
| York River | B | 37.2 | -76.4 | 5.6 | (Raymond et al. 2000) |
| Hudson River | A | 40.6 | -74.0 | 9.6 | (Raymond et al. 1997) |
| LCE | A | 28.5 | -96.3 | 21.6 | This study |
| GE | A | 28.3 | -96.7 | 38.5 | This study |
| MAE | A | 28.0 | -97.0 | 8.4 | This study |
| NE | A | 27.8 | -97.3 | 4.9 | This study |

Type: A= microtidal estuary; B= macrotidal estuary.

Appendix 2. Copyright of Chapter II